AD-A225 678

Potential Application of Magnetohydrodynamic Acceleration to Hypersonic Environmental Testing

R. A. Crawford, J. N. Chapman, and R. P. Rhodes
The University of Tennessee Space Institute
Tullahoma, Tennessee

August 1990

Final Report for Period March 1, 1988 through December 31, 1989

DTIC
ELECTE
AUG 1 4 1990
S E
D

**ARNOLD ENGINEERING DEVELOPMENT CENTER
ARNOLD AIR FORCE BASE, TENNESSEE
AIR FORCE SYSTEMS COMMAND
UNITED STATES AIR FORCE**

APPROVAL STATEMENT

This report has been reviewed and approved.

MARION L. LASTER
Deputy Director, Corporate Planning

Approved for publication:

FOR THE COMMANDER

LUTHER NEAL, JR.
Director of Corporate Planning

REPORT DOCUMENTATION PAGE

1. AGENCY USE ONLY (Leave blank)	2. REPORT DATE August 1990	3. REPORT TYPE AND DATES COVERED Final -- March 1, 1988 - December 31, 1989

4. TITLE AND SUBTITLE

Potential Application of Magnetohydrodynamic Acceleration to Hypersonic Environmental Testing

6. AUTHOR(S)

Crawford, R.A., Chapman, J.N., and Rhodes, R.P.

5. FUNDING NUMBERS

PE - 65807F

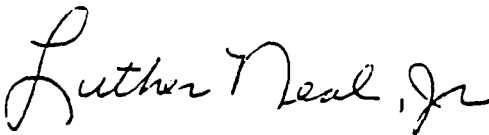**7. PERFORMING ORGANIZATION NAME(S) AND ADDRESS(ES)**

The University of Tennessee Space Institute
Tullahoma, TN 37388

8. PERFORMING ORGANIZATION REPORT NUMBER

AEDC-TR-90-6

9. SPONSORING/MONITORING AGENCY NAMES(S) AND ADDRESS(ES)

Arnold Engineering Development Center
Air Force Systems Command
Arnold Air Force Base, TN 37389-5000

10. SPONSORING/MONITORING AGENCY REPORT NUMBER

11. SUPPLEMENTARY NOTES
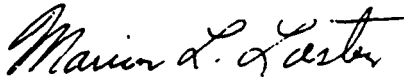
Available in Defense Technical Information Center (DTIC).

12a. DISTRIBUTION/AVAILABILITY STATEMENT

Approved for public release; distribution is unlimited.

12b. DISTRIBUTION CODE

13. ABSTRACT (Maximum 200 words)

This investigation reviews the technical results from previous MHD accelerator research and conducts a theoretical analysis of the simulation capabilities of an MHD-augmented hypersonic flow facility. This investigation identified the performance potential of MHD accelerator and hot gas generator combinations subject to reasonable constraints from available technology. The performance goal was to extend the hypersonic flight simulation limits from Mach 10 to Mach 25. The results of this investigation identified the critical technology issues which must be addressed in the design of an MHD-driven hypersonic test facility. The design trade study conclusions from the one-dimensional MHD accelerator model calculations were very encouraging and support the technical feasibility of the concept. A single-channel geometry accelerator supplied by an arc-heated airstream with 1-percent potassium seed, a magnetic field strength of 6 Tesla, and variable power segmented electrodes can simulate Mach 15 - 25 flow conditions. Combustor inlet conditions for hypersonic flight vehicles can be simulated with nearly exact properties. Free-stream flight condition simulations are more strongly influenced by accelerator magnetic field strength and initial conductivity. Acceptable transient simulation capability can be obtained from a reflected shock tunnel operating as a gas generator for the MHD accelerator. Hypersonic similarity parameters, as well as standard aerodynamic similarity parameters, were used to evaluate the quality of resulting hypersonic flow fields.

14. SUBJECT TERMS

magnetohydrodynamics, hot gas generator, hypersonic flow, flight simulation, arc-heated airstreams

15. NUMBER OF PAGES 99

16. PRICE CODE

17. SECURITY CLASSIFICATION OF REPORT UNCLASSIFIED	18. SECURITY CLASSIFICATION OF THIS PAGE UNCLASSIFIED	19. SECURITY CLASSIFICATION OF ABSTRACT UNCLASSIFIED	20. LIMITATION OF ABSTRACT SAME AS REPORT

PREFACE

CONTENTS

ILLUSTRATIONS

Figure   **Page**

TABLES

Tables   **Page**

APPENDIXES

1.0 INTRODUCTION

This report documents an investigation conducted by The University of Tennessee Space Institute (UTSI) which revisits the concept of hypersonic flow simulation through magnetohydrodynamic (MHD) acceleration. The technology advances of the last 25 years have provided new capability to address the critical technology issues associated with the development of an MHD-augmented hypersonic test facility.

1.1 BACKGROUND

The development of hypersonic flight vehicles has been handicapped and frustrated by a continuing long-term lack of experimental simulation facilities. This national shortage of hypersonic test capability includes the range of test facilities from small, basic flow physics research tunnels to large environmental simulation facilities for testing scaled airframe and propulsion systems. The recent renewal of national interest in development of hypersonic flight vehicles for both military and civilian application has directed attention to the critical simulation limitations of test facilities in this flight regime. Facilities based on heating a gas to stagnation conditions in a reservoir by combustion or electrical resistance techniques and expansion in a nozzle to hypersonic Mach number, are limited to true temperature simulation in the Mach 7 to 8 range. Advances in arc heater technology hold promise for air-breathing propulsion simulation to Mach 12 and higher Mach numbers for low-density flows. Shock-driven tunnels are capable of simulation to Mach 25 for millisecond durations. The most promising technology for simulation of flight Mach numbers in the 10 to 25 range utilizes magnetohydrodynamic forces to accelerate the test gas to the required stagnation enthalpies.

The MHD accelerator utilizes the Lorentz force, J × B body force, to increase gas velocity and thus the total pressure and temperature. Since the energy is added to a supersonic flow, the operating static pressures and temperatures in the accelerator are lower than the corresponding stagnation conditions, which should result in reduced wall heat transfer and test gas dissociation. The MHD acceleration requires that the gas have sufficient conductivity to allow current flow (J) at reasonable electrode voltages which requires that the air be seeded with an easily ionized material. The magnetic field (B) is provided by an electromagnet external to the flow channel. Although the principle of MHD acceleration is well understood and has been demonstrated in small facilities, the technology base is not sufficiently developed for a large-scale hypersonic facility development. Section 2.0 will summarize the published literature and the existing theoretical and experimental technology base for MHD accelerators.

1.2 INVESTIGATION GOALS

This investigation reviews previous MHD accelerator work, conducts a theoretical analysis of performance potential, and identifies critical technology issues. The primary goal of this

investigation is to identify, by theoretical analysis, the performance potential of MHD accelerator and hot gas generator combinations for which satisfactory and credible design, construction, and operating characteristics can be predicted. The minimum performance goal will be to extend the hypersonic flight simulation limits from current arc-driven gas generator capability into the Mach 10 to 25 range. A summary of hypersonic simulation requirements is presented in Section 3.0 for direct-connect propulsion testing, aerothermal testing, and free-stream simulation.

The second goal of this investigation is the identification of the critical technology issues which must be addressed in the design of an MHD-driven hypersonic test facility. The most important technology issues will be identified and analyzed during the accelerator design trade studies. The extensive literature survey documented in Sec. 2.0 also aided in identification of the critical technologies. The final goal is development of a technology road map and research plan to address the critical technology advances necessary to develop a large-scale hypersonic facility with MHD acceleration.

1.3 APPROACH

The approach to this study is comprised of an extensive literature search to establish the state of the art of MHD accelerator technology, and a theoretical analysis of hot gas generator and accelerator channel combinations. The literature search was complicated by the 25-year time gap between the early investigations and current interest. A large technology base was developed for MHD generators during this time period and is applicable in general to the accelerators. A one-dimensional MHD code was utilized to conduct the theoretical performance analysis, and the code is described in detail in Sec. 4.0. The math model has been modified and used extensively at UTSI in the evaluation of MHD generator designs and for accelerator design studies. Performance characteristics of current and projected arc heaters will be used to define entrance conditions to the accelerator for the baseline performance calculations and design trade studies. The results of these efforts will be evaluated to determine the critical technology issues which must be addressed during development of this unique simulation capability.

2.0 STATE OF THE ART LITERATURE SURVEY

A literature review of MHD papers and reports relevant to accelerator research and development revealed a peak in accelerator research during the period 1960 to 1970. This period of MHD accelerator research coincided with a peak in hypersonic flight vehicle research. The U.S. Air Force, NASA, universities, and several aerospace industries were earnestly involved in the investigation of MHD accelerator application to hypersonic simulation. The published research results show that the major programs were conducted by the USAF Arnold

Engineering Development Center and the NASA Langley Research Center. Although feasibility of MHD augmentation of arc-heated and shock tube-driven facilities was established by limited theoretical analysis and small-scale experiments, the efforts were terminated before prototype facilities were developed. Fortunately, this period of MHD accelerator interest was well documented and the technical conclusions and technical concerns remain nearly unchanged today.

Reentry vehicle development during the 1970's maintained a modest interest in MHD-augmented, high-enthalpy test facilities. Fortunately, the 1970's concern for energy resulted in major new programs in the application of MHD power generation for the utility industry. Thus a large research and development program into MHD generator technology was conducted. The great majority of technical information published on MHD has related to electrical power generators. Although the accelerator environment, current density, and wall heat loads are more severe than the generator operating conditions, the extensive generator technology base will contribute significantly to accelerator development. Reference 1 contains an extensive list of references from generator technology programs which document a technology base available for application to accelerator development. Super-conducting magnet technology, high-temperature materials, high-current electrical power generation and control, advanced cooling technology, and computational fluid dynamics and heat-transfer codes are some of the critical technology areas which have seen significant advances since the first look at MHD accelerators in the 1960's. Appendix A contains a bibliography of applicable references, which are not cited, to guide the new researchers to the historical technology base.

The renewal of hypersonic flight vehicle research in the mid-1980's, along with hypersonic air-breathing propulsion development brought new interest to MHD-augmented simulation facilities. The AEDC efforts in the HIRHO and LORHO programs established a major portion of the technical base unique to MHD accelerator development. The AEDC reports were considered the key historical references for this study. Reference 2 contains a good summary of AEDC accelerator research.

3.0 SIMULATION REQUIREMENTS

The hypersonic flight envelope contains a very large variation of altitude and flight velocity/Mach number; thus, definition of a flight corridor is required to restrict and identify the range of simulation parameters. In this section the hypersonic flight vehicle envelope will be defined in terms of the simulation parameters required to evaluate the MHD-augmented, high-enthalpy, facility performance. It is recognized that a reentry vehicle envelope is significantly different than the powered hypersonic flight vehicle envelope selected for this study.

3.1 HYPERSONIC FLIGHT VEHICLE ENVELOPE

Figure 1 shows a typical hypersonic flight vehicle corridor plotted on the altitude vs velocity map as the region between the 500 (psf) and 2,000 constant dynamic pressure lines. This envelope is determined by lift or propulsion limits along the 500 q line and dynamic pressure or heating limits along the 2,000 q line. The flight envelope for an air-breathing powered vehicle may be restricted by combustion and heat-transfer limits to a smaller region between the 500 q and 1,000 q lines. For this investigation all performance calculations were arbitrarily limited to velocity and altitude simulation along the 1,000 q line.

Simulation of the higher velocity flight environment in a ground test facility has been restricted by the structural and thermal limits on stagnation pressure and temperature in air heaters. Real gas effects and finite rate chemical reactions also impose serious constraints on simulation fidelity in hypersonic flows expanded from stagnation reservior condtions. MHD acceleration offers both higher total enthalpy and improved gas chemistry simulation. In the following section the simulation parameters will be defined which best describe the performance and quality of an MHD-augmented flow simulation.

3.2 SIMULATION PARAMETERS

The altitude vs flight velocity corridor can be converted into the following simulation and nondimensional parameters: total enthalpy, static temperature, static pressure, entropy, Mach number, Reynolds number, Prandtl number, and associated thermodynamic properties. The gas species concentration can be determined from the thermodynamic properties assuming equilibrium or finite rate gas kinetics. Total enthalpy is a measure of flow energy and at hypersonic speeds is dominated by the flow kinetic energy. Total enthalpy is the primary simulation parameter and assures that total temperature effects are duplicated (Ref. 3). The part of total enthalpy that depends on static temperature is partially a measure of inefficiency and losses in the acceleration process. Entropy, which is a function of pressure and temperature, is a better parameter for evaluating the efficiency of the acceleration process. Species concentrations from equilibrium or finite rate calculations are also important properties for evaluating simulation quality. With total enthalpy and entropy defined, the specification of static temperature or pressure will define Mach number and all other thermodynamic properties if equilibrium gas chemistry is assumed.

This study evaluates MHD accelerator performance on the total enthalpy vs entropy map which also contains three hypersonic flight vehicle simulation conditions: free stream, cowl lip, and combustor inlet. Figure 2 shows these three simulation requirements for the q = 1,000 lbf/ft^2 flight path. The cowl lip envelope and combustor inlet envelope on the enthalpy/entropy map are dependent upon vechicle forebody compression and inlet external
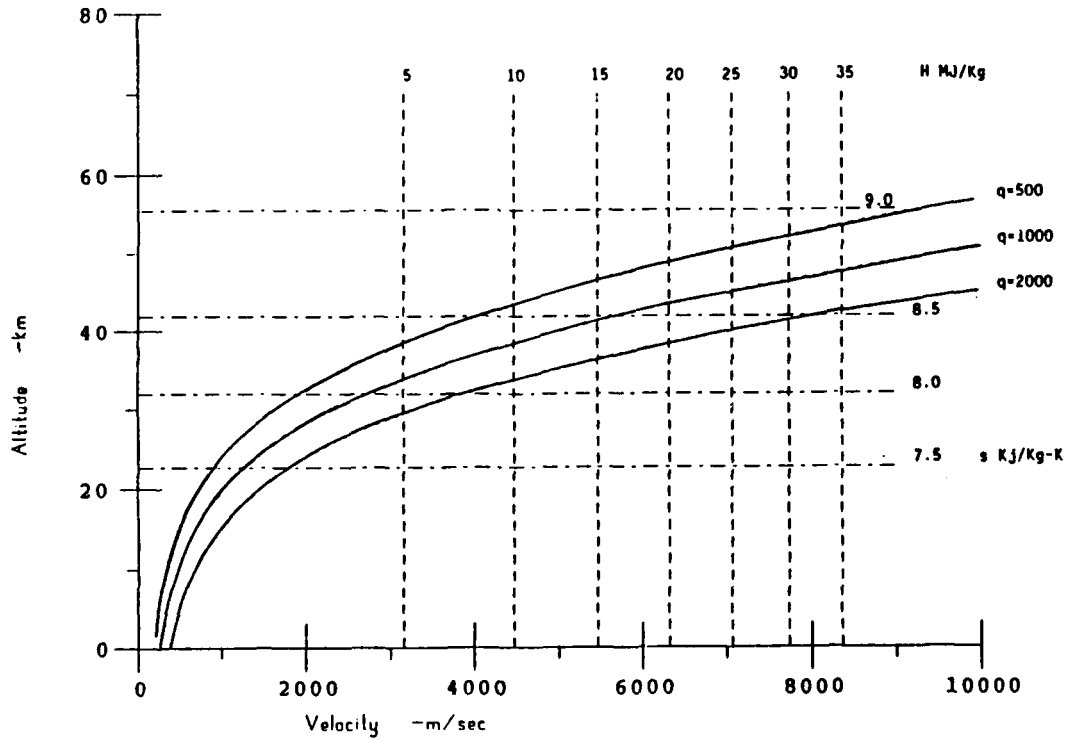
Figure 1. Flight envelope, q = 500 - 2,000 psf.
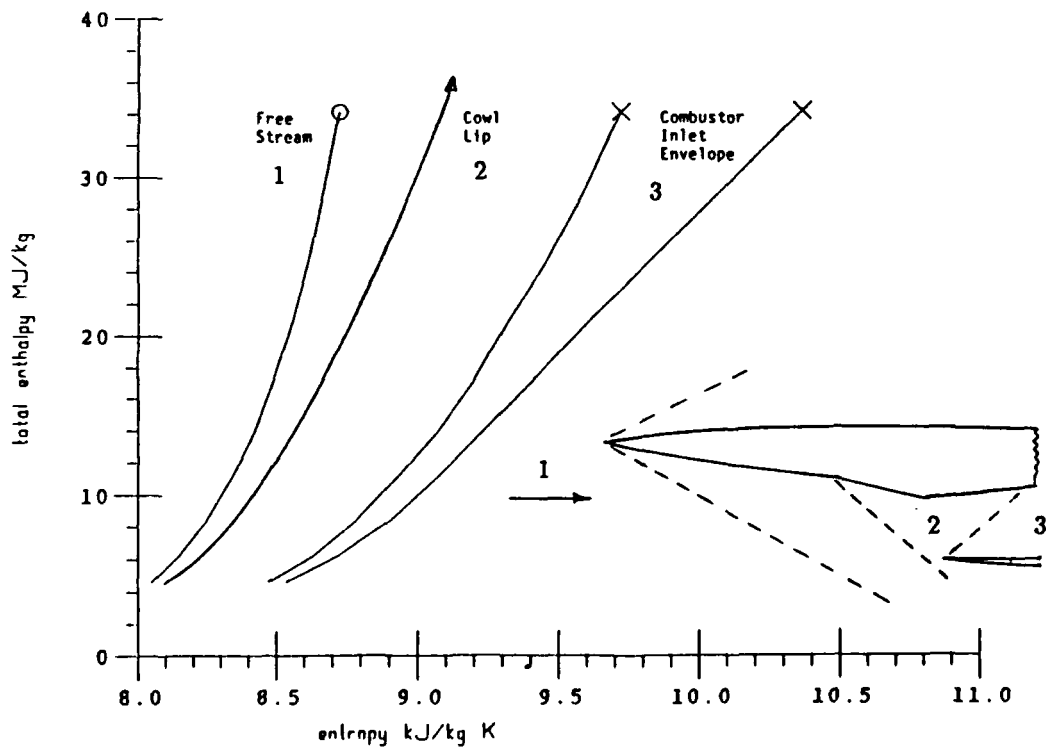
Figure 2. Scramjet test conditions, q = 1,000 psf.

compression. Typical values of NASP-type inlet losses were used to estimate these envelopes (Ref. 4). A similar figure from the AEDC white paper (Ref. 2) presents a combustor inlet envelope with more compression and larger shock losses and thus higher entropy at the same total enthalpy. Since real hypersonic inlet performance is unknown at these Mach numbers, the Fig. 2 values for cowl lip and combustor inlet should be considered simulation goals. Only the free-stream values are fixed numbers. The following modes of testing will be presented in terms of simulation requirements or critical simulation parameters. The direct-connect propulsion testing mode is presented first because the simulation requirements are most compatible with the MHD accelerator characteristics.

3.3 DIRECT-CONNECT PROPULSION TESTING

The air-breathing hypersonic propulsion system is integrated into the airframe to efficiently utilize the vehicle external compression of the capture airflow. Thus at the cowl lip, the start of internal compression, the flow has been compressed by oblique shock waves reducing the Mach number and raising the static temperature and pressure. Figure 2 shows the relation between free-stream, cowl lip, and combustor inlet enthalpy and entropy. The higher entropies and lower Mach numbers downstream of the inlet shock structure are easier to simulate than the free-stream conditions. The only simulation properties that will not be exactly duplicated are species concentration. The levels of atomic oxygen, oxides of nitrogen, and potassium seed must be evaluated for possible impact on propulsion testing. Section 5.0 results will show that the MHD-augmented facility will provide a good flow simulation for direct-connect propulsion testing.

3.4 AEROTHERMAL TESTING

Simulation of aerothermal heating at hypersonic Mach numbers has been limited by arc heater stagnation temperature and pressure limits. Existing arc heater facilities do not permit a simultaneous simulation of reentry conditions, Mach number, total pressure, and total enthalpy (Ref. 5). Since total enthalpy and total pressure are the primary simulation parameters for correct heat transfer with Mach number and species concentration providing secondary effects, the MHD-augmented facility will increase the aerothermal simulation envelope over current arc-heated facility limits. MHD augmentation of arc or combustion heaters should provide total enthalpy simulation beyond Mach 25. Although free-stream Mach number simulation will be low because of static temperature increases resulting from acceleration inefficiencies, the aerothermal simulation should be very good, due to the high flow kinetic energies. Species concentration to dissociation will be important if wall recombination is a significant contribution to the heat-transfer rate.

3.5 FREE-STREAM SIMULATION

The following discussion of hypersonic flight simulation requirements was presented by Ring (Ref. 3). Since real gas effects are very important in this flight regime, dissociation and recombination reaction rates must be considered. The simulation of correct finite rate chemistry may be the best measure of performance for an MHD-augmented facility. Free-stream velocity must be simulated to provide correct total enthalpy without excessive static temperatures. Free-stream dissociation should be a small fraction of the maximum dissociation in the flow over the body. Binary scaling requires keeping ϱ = constant, where L is a characteristic body length. Scaled test articles require corresponding high-density flows to duplicate binary scaling, which is difficult to obtain in a hypersonic facility. Since three-body recombination becomes important in the lower altitude portion of the hypersonic flight envelope, binary scaling is not applicable.

Free-stream simulation requirements include correct free-stream velocity, density, hypersonic Mach number, and low dissociation level. Mach number and density can be traded in the nozzle expansion; thus, the total enthalpy and entropy are the better simulation parameters for comparison. The MHD-augmented facility can be expected to provide correct total enthalpy, and the entropy will be determined by the required accelerator inlet conductivity and accelerator inefficiencies. The influence of accelerator exit entropy on Mach number, Prandtl number, Reynolds number, and hypersonic scaling parameters associated with boundary-layer scaling and finite rate reaction simulation must be evaluated. The MHD-augmented facility may provide significant environmental test capability without complete duplication of free-stream conditions.

4.0 MHD MATH MODEL DESCRIPTION

The performance of the MHD accelerator channel was computed by a series of codes which are routinely used by the UTSI MHD group. The primary code is a one-dimensional accelerator model which accounts for wall heat flux, wall friction, and variable thermodynamic properties. A brief description of the codes utilized and the calculational methodology is presented to aid in understanding the predicted accelerator performance.

4.1 CHEMICAL EQUILIBRIUM CODE

A chemical equilibrium code originated by NASA (Ref. 6) is used to calculate the thermodynamic properties of air seeded with either potassium or cesium. The basic code has been modified and updated to apply to specific requirements. It uses a file of thermodynamic data for each compound and element under consideration. These thermodynamic data are declared to be valid up to 5,000 K. In some accelerator cases, we have used this data for

higher temperatures, a possible source of error of unknown significance. This thermodynamic equilibrium code has been modified to include the calculation of electrical transport properties, specifically free electron density, electron mobility, collision frequency, and electrical conductivity. (See Figs. 3a and 3b). These calculations are made by the method of Frost (Ref. 7). For the electrical transport property calculation, an additional data file containing collision cross section data for each chemical specie in the flow has been added. These calculations have been well validated by experimental measurements, but at conductivities more characteristic of commercial MHD power conditions, e.g., around 10 Siemens/meter. The code has also been carefully compared with transport property calculations by AVCO, STD, ANL, AERODYNE, MIT, and others in a workshop program sponsored by the Department of Energy (Ref. 8).

This code is used to prepare a table of thermodynamic and electrical transport properties as a function of temperature and pressure. Typically, in the calculations in this report, an array of 70 temperatures and 70 pressures was used. The temperatures and pressures do not need to be equally spaced, so they are chosen closer together in the principal regions of interest. The accelerator code interpolates between the two pressures and temperatures spanning the pressure and temperature of interest to get the other thermodynamic properties and electrical transport properties. This table is used essentially to replace an equation of state for the gas.

4.2 MOLECULAR TRANSPORT PROPERTIES

Molecular transport properties, specifically viscosity and Prandtl number, were calculated by another NASA-originated computer code commonly called TRAN 72 (Ref. 9). These properties were curve fit as a function of temperature in the accelerator code.

4.3 QUASI ONE-DIMENSIONAL ACCELERATOR CODE

A quasi one-dimensional accelerator code was used to make the parametric accelerator calculations. The theory and assumptions used in this code are outlined below. The one-dimensional equations are:

Momentum Equation:

$$\varrho u \frac{du}{dx} + \frac{dP}{dx} = -J_y B - 4 \frac{\tau_w}{D} \tag{1}$$
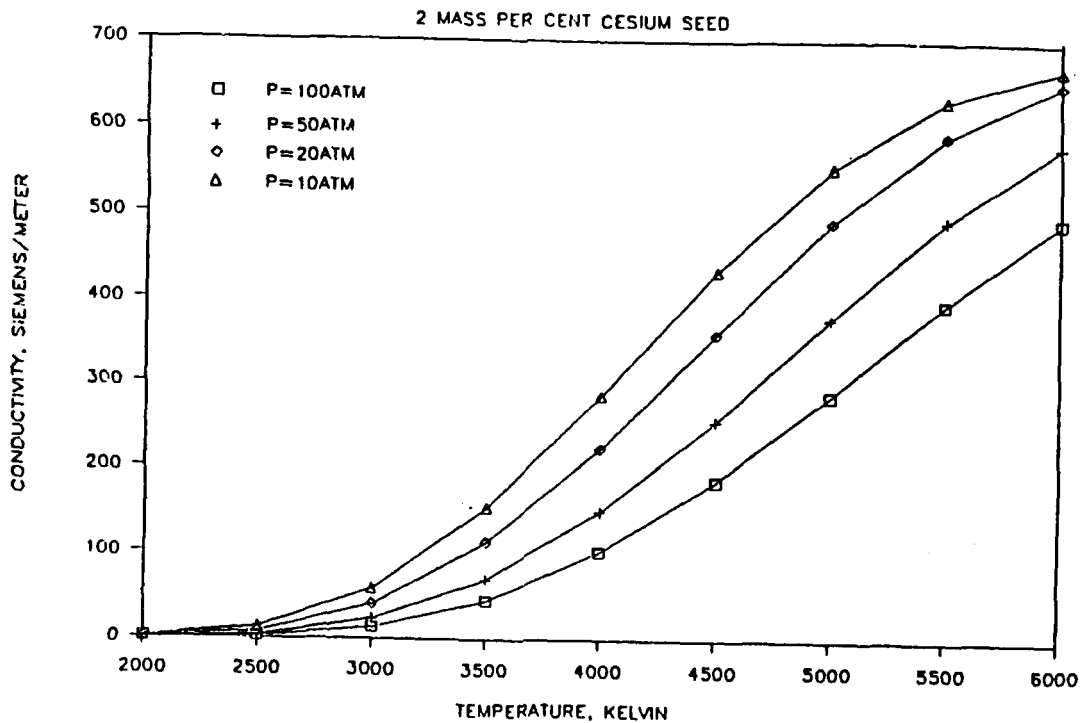
Figure 3a. Conductivity of air seeded with 2-percent cesium.
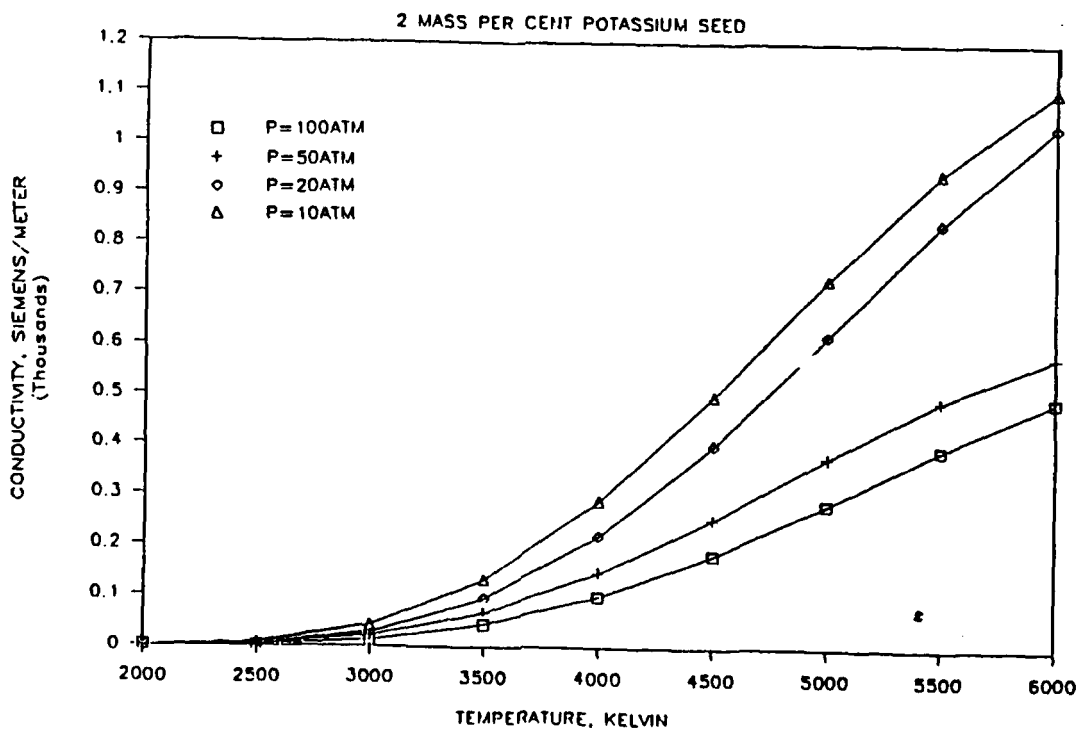
Figure 3b. Conductivity of air seeded with 2-percent potassium.

15

where

x,y,z	=	right-hand orthogonal coordinate system, x in flow direction
P	=	static pressure
τ_w	=	sheer stress
D	=	hydraulic diameter
B	=	magnetic field flux density magnitude
J_y	=	current density
u	=	velocity

Energy Equation:

$$\varrho u \frac{dh}{dx} + \varrho u^2 \frac{du}{dx} = J_y E_y + 4 \frac{q_w}{D} \tag{2}$$

where

E_y	= net electrical field in y-direction
q_w	= heat flux to walls
h	= enthalpy

Continuity Equation:

$$\varrho u A = \dot{m} \tag{3}$$

where

ϱ	=	density of gas
A	=	cross-sectional area of duct
$\dot{m}$	=	total mass flow

Ohm's Law

$$\bar{J} = \sigma(\bar{E} + \bar{u} \times \bar{B} + \bar{E}_d) - \frac{\Omega}{B} (\bar{J} \times \bar{B}) \tag{4}$$

E_d	=	electric field corresponding to plasma to electrode voltage drop
Ω	=	Hall parameter
σ	=	conductivity

From Ohm's Law, with Hall parameter assumed negligible

$$J^2 = \bar{J} \cdot \bar{J} = \sigma [\bar{J} \cdot \bar{E} + \bar{J} \cdot (\bar{u} \times \bar{B}) + \bar{J} \cdot \bar{E}_d] \tag{5}$$

or

$$\bar{J} \cdot \bar{E} = \frac{J^2}{\sigma} - J_y uB(1 - \Delta)$$

where

$$\Delta = \frac{E_d}{uB}$$

Equation of State

$$P = \varrho RT \tag{6}$$

where R = gas constant

Thermodynamic State

It is assumed that all the thermodynamic properties are expressed as functions of temperature and pressure, e.g.,

$$h = h(P, T) \tag{7}$$

$$R = R(P, T) \tag{8}$$

By differentiation and algebraic manipulation of Eqs. (1) through (8), the following equations are derived:

$$\left(\frac{1}{R} \frac{\partial R}{\partial T} + \frac{1}{T}\right) \frac{dT}{dx} + \left(\frac{1}{R} \frac{\partial R}{\partial P} - \frac{1}{P} - \frac{1}{\varrho u^2}\right) \frac{dP}{dx} = \frac{1}{A} \frac{dA}{dx} - \frac{J_y B}{\varrho u^2} - \frac{4\tau_w}{\varrho u^2 D} \tag{9}$$

$$\left[\frac{1}{u^2} \frac{\partial h}{\partial T} + \frac{1}{R} \frac{\partial R}{\partial T} + \frac{1}{T}\right] \frac{dT}{dx} + \left[\frac{1}{u^2} \frac{\partial h}{\partial P} + \frac{1}{R} \frac{\partial R}{\partial P} - \frac{1}{P}\right] \frac{dP}{dx}$$

$$= \frac{1}{A} \frac{dA}{dx} + \frac{\bar{J} \cdot \bar{E}}{\varrho u^3} + \frac{4q_w}{\varrho u^3 D} \tag{10}$$

The Eqs. (3), (9), and (10) constitute a set of three equations in four unknowns, u, P, T, A. Any two thermodynamic variables specify the state. If P and T are known, the other thermodynamic variables are determined from equations of the type (7), (8). In the code, they are determined from the table of thermodynamic properties.

If any one of the variables u, P, T, A are specified, the equations can be solved numerically for the other three.

In the application of the code to accelerator calculations in this study, two modes have been used. The area or the temperature is specified with respect to accelerator length.

Assumptions used in the calculation include:

- The gas is homogenous in species concentration and thermodynamic properties.

- The flow is uniform in a plane perpendicular to the flow.

- Induced magnetic fields are negligible.

- The gas is in chemical and thermodynamical equilibrium.

- Plasma-to-electrode voltage drops are proportional to generated voltage (uBd).

Input data required by the code:

- Entrance temperature and pressure

- Wall temperature

- Mass flow rate

- Entrance area and axial profile if running area mode

- Temperature profile if running temperature mode

- Maximum magnetic field and profile

- Wall roughness height (average $\cong 0.1$ mm)

18

- Delta, the electrical boundary layer loss factor defined as

$$\Delta = \frac{V_d}{uBd}$$

- Channel length and computational step size

- Channel loading, specified as $K = K_0 + K_1X + K_2X^2$ where $K = \dfrac{\text{voltage applied}}{uBd(1 - \Delta)}$, and maximum J_y if desired.

4.4 NONEQUILIBRIUM NOZZLE CALCULATIONS

The computer code is derived from the LAPP (Ref. 10) code which was originally written to calculate the properties of rocket exhaust plumes. The modifications include reducing the computational domain to a single stream tube without mixing and changing the boundary conditions from a prescribed pressure to a prescribed area for the flow. The axial momentum, energy, and species continuity equations are solved by an explicit forward marching technique with the chemical production terms which are numerically stiff being calculated using a linearized implicit technique. In addition, electromagnetic terms were added to the momentum and energy equation so that the effect of finite rate chemical reactions could be evaluated in an MHD channel.

The one-dimensional gas dynamic equations for channel flow with the MHD terms included are the same as presented in Sec. 4.3.

In addition the species continuity relation is required.

$$\frac{d}{dx} (\varrho uAc) = \text{chem production} \tag{11}$$

The chemical production terms are of the form:

$$dc/dx = \Sigma \ [a(f \cdot \Pi \ (\text{reactant species}) - b \cdot \Pi \ (\text{product species}))] \tag{12}$$

where Σ is the sum over all reactions, Π is the product of the concentrations of the species on one side of a single chemical reaction, and α is the stoichiometric coefficient of the species in the reaction whose rate is being determined ($-$ for a reactant and $+$ for a product). The forward and backward rates (f) and (b) of the reaction are in an Arrhenius form and related by the equilibrium constant.

19

These equations along with the equation of state for a thermally perfect gas (ϱ = pm/RT) were solved to provide a coupled set of equations for du/dx, dp/dx, dH/dx (total enthalpy), and dc/dx. The parameters A, J $\times$ B, and q are input to the program either as cubic equations in x or as tabular functions of x. The thermodynamic properties which provide the relationship between h and T and c, and the equilibrium constants are input as curve fits in T (Ref. 9).

The coupled set of nonlinear species equations is solved by a stiff equation solver which linearizes the equations and solves the resulting matrix for the change in each species (Ref. 11). The remaining equations are solved by an explicit Euler integration procedure with accuracy assured by limiting the step size.

With the electromagnetic terms set to zero, this program is used to calculate the gas properties during the expansion through the nozzle which follows the MHD channel (Sec. 5.5). It is also used to estimate the departure from equilibrium in an MHD channel by using the J $\times$ B force, the ohmic heating, and the area from the equilibrium acceleration code calculation of the baseline case (Sec. 5.6).

4.5 THREE-DIMENSIONAL MODELING CONSIDERATIONS

The flow field of an MHD accelerator which is of a size and capacity that is typical of that required for hypersonic flow simulation will exhibit features which require that an ultimate multidimensional evaluation be pursued. For conventional internal flows a myriad of experience and experimental data exists. This fact implies that established techniques for modeling turbulent flows using spatially integrated governing equations in one and two dimensions can be used with acceptable accuracy. Unfortunately, this is not necessarily the case for the MHD accelerator. Specifically, when the MHD interaction is strong, plasma and electrical nonuniformities that develop cannot confidently be modeled with spatially integrated techniques. Although these techniques do have value in fundamental engineering studies, (e.g., to roughly size the accelerator, map its operational regimes, and review its operational and performance characteristics) detailed specifications for the system design and precision evaluations of its performance can only be achieved through multidimensional analyses using primitive plasma and electrical variables.

Over the past 15 years with the advent of advanced computer resources, a significant amount of applied research has been directed at the development of multidimensional modeling techniques for simulation of the MHD devices. Most of this work has been directed at MHD generator studies, whereas the accelerator has received less attention. It is not known if there exists a comprehensive and proven model that is currently available in the public domain specifically for accelerator modeling. In contrast to this, there are several generator models in use which vary in dimensionality and mathematical/numerical sophistication. Since the

same physics principles apply to either the generator or the accelerator regime, it is reasonable to conclude that the modeling principles and techniques developed for the MHD generator are applicable to the MHD accelerator. Consequently, a sound multidimensional model for the accelerator is readily achievable, and the most expedient approach to realizing this is through adaptation of existing generator computer models.

In the following discussions a brief description of the MHD flow field is given. It is intended here to accentuate those dominant characteristics of the accelerator plasma dynamics and electrodynamics that are unique and demand multidimensional consideration to be fully understood.

4.5.1 The MHD Flow Field

The flow field within an MHD accelerator can be quite complex when it is compared to that of conventional aerodynamic internal flows. These complexities arise from electromagnetic phenomena. The degree of this influence is termed "MHD interaction." A plasma flow which develops in the presence of strong MHD interaction exhibits spatial nonuniformities and temporal variations of gas dynamic properties and electrical parameters. These nonuniformities are three dimensional in character and their effects on system operation and performance must be understood and adequately modeled for both system design as well as for interpretation of results.

As a means of viewing the MHD flow field, Eqs. (13) through (15) are presented. These equations are the time-dependent conservation equations which govern the MHD accelerator/generator flow field, i.e., mass, momentum, and enthalpy.

$$\frac{\partial \varrho}{\partial t} + \nabla \cdot \left(\varrho \vec{V} \right) = 0 \tag{13}$$

$$\varrho \frac{\partial \vec{V}}{\partial t} + \varrho \vec{V} \nabla \cdot \vec{V} = - \nabla P - \nabla T + \vec{J} \times \vec{B} \tag{14}$$

$$\varrho \frac{\partial}{\partial t}\left(h + \frac{V^2}{2} \right) + \varrho \vec{V} \cdot \nabla \left(h + \frac{V^2}{2} \right) - \frac{\partial P}{\partial t} = - \nabla \cdot \left(T \cdot \vec{V} \right) - \nabla \cdot \vec{q} + \vec{J} \cdot \vec{E} \tag{15}$$

As evident in these equations, a coupling exists between the plasma dynamics and the electrodynamics. This coupling is through the presence of the Lorentz body force term (J x B) in the momentum equation and the MHD power term (J • E) in the energy equation. A high interaction MHD device (generator/accelerator) is one in which the magnitude of these terms is large, leading to a significant influence on the spatial and temporal development of the flow field.

21

The stationary MHD accelerator process is summarized by the Eqs. (16) through (22). These equations describe both the gas dynamics and electrodynamics for a steady process subject to standard approximations applicable to the accelerator regime envisioned for hypersonic flow simulation.

$$\nabla \cdot \left(\varrho \vec{V} \right) = 0 \tag{16}$$

$$\varrho \vec{V} \nabla \cdot \vec{V} = -\nabla P + \nabla \cdot T + \vec{J} \times \vec{B} \tag{17}$$

$$\varrho \vec{V} \cdot \nabla \left(h + \frac{V^2}{2} \right) = \nabla \cdot \left(T \cdot \vec{V} \right) - \nabla \cdot \vec{q} + \vec{J} \cdot \vec{E} \tag{18}$$

$$\nabla \times \vec{E} = 0 \tag{19}$$

$$\nabla \cdot \vec{J} = 0 \tag{20}$$

$$\vec{E}_{\text{induced}} = \vec{V} \times \vec{B} \tag{21}$$

$$\vec{J} = \sigma \left(\vec{E} + \vec{V} \times \vec{B} \right) - w\tau \left(\vec{J} \times \vec{B} \right) \tag{22}$$

The first three of these equations are time-averaged turbulent flow equations for mass, momentum, and energy conservation for the plasma. Equations (19) through (22) describe the electrodynamics being Maxwell's conservation equations, Faraday's law for electromagnetic induction, and the generalized form of Ohm's law. Closure of this system of equations requires the appropriate equations of state for both the thermodynamic and electrical transport properties (conductivity and electron mobility), i.e.,

$$\varrho = f(P,h), \quad \sigma = g(P,h), \quad w\tau = h(P,h) \tag{23}$$

Nonuniformities that develop within the MHD flow field are driven by gradients of thermodynamic and electrical transport properties. These gradients are in part attributable to the same phenomena which exist in aerodynamic duct flows, i.e., wall losses (viscous effects and heat transfer). However, in MHD these are very strongly coupled to spatial variations in the plasma impedance and the MHD electrical processes. For example, flow-field boundary layers, which describe the velocity and temperature distributions near the duct walls, give rise to exaggerated gradients in the plasma electrical conductivity, electrical fields, and current densities. These electrical nonuniformities are in turn coupled to the plasma dynamics through the Lorentz force and Joulean heat dissipation. Consequently, the MHD interaction is distributed in intensity through the plasma over the cross plane and along the length of the accelerator duct. This distribution is a function not only of the gradients but also of the

accelerator configuration (Faraday, diagonal, etc.). The nonuniformity of MHD interaction along with constraints imposed on the accelerator by its configuration (electrical boundary conditions) lead to the development of unconventional profiles of electrical and plasma dynamic properties.

The complex nature of MHD interaction in the accelerator duct produces a three-dimensional, asymmetric flow field. The degree of these nonuniformities is effected by accelerator size and length. A measure of this interaction is given by the magnetic force number, S, which is defined as follows (Ref. 11),

$$S_u = \frac{x}{L_u} \tag{24}$$

where S_u is the interaction parameter based on velocity, x is a characteristic distance of the problem, and L_u is the velocity interaction length.

$$L_u = \frac{\varrho u}{\sigma B^2} \tag{25}$$

So, for x = L,

$$S_u = \frac{\sigma B^2 L}{eV} \tag{26}$$

The magnetic force number (MHD interaction parameter) represents the ratio of the magnetic body force to the fluid inertia force. When this quantity is large (>1), large perturbations in the flow field will arise due to the MHD interaction. It can be seen by the form of Eq. (25) that the degree of flow-field nonuniformity which develops may be dependent upon system size (throughput and volume) and operation (magnetic field intensity and applied power).

Along with the effects of nominal MHD interaction as highlighted above, further complexities which influence the accelerator flow and its stability arise from near electrode phenomena. Foremost among these are finite electrode segmentation and arcing.

Finite sized accelerator electrodes are necessary from a practical construction point of view. Depending upon the magnitude of the Hall effect and the span of the electrodes, equipotential surfaces within the plasma will be skewed from the normal between anode and cathode. This warping of the electrical potential produces an axial current component and leads to concentrations of current discharge toward the electrode leading and trailing edges. Axial (Hall) currents are detrimental to accelerator performance. First of all, they represent a loss since no axial acceleration is produced by Hall currents. Secondly, the Lorentz force

associated with axial current flow produces a vertical pressure gradient which leads to secondary flows. That is, the $J_x \times B$ component of the Lorentz force drives plasma mass vertically across the accelerator channel. This action, combined with nonuniformities in plasma impedance, produces secondary flows, i.e., strong cross plane, paired vortices.

Arcing discharge to the electrodes will occur when sufficient potential is developed across the wall boundary layers. This phenomenon is driven by the presence of cold electrode walls and the local increase in plasma impedance near these walls. Arcing is a statistical phenomenon which will occur randomly in both space and time. Also, an arc plasma discharge is not stationary - the action of Lorentz force on the high current in the arc causes it to move along the electrode surface.

4.5.2 Velocity and Temperature Profiles

A visualization of some of the three-dimensional characteristics of the MHD flow field as discussed above is provided by the illustrations presented in Fig. 4. These figures show the results of past MHD generator calculations performed at UTSI. The MHD generator analyzed was configured in the Faraday mode and is subject to moderate level of MHD interaction, $S \sim 2.0$. Although these are computations for an MHD generator, the accelerator flow field can be visualized by consideration of the fundamental difference between these two devices, that is, the direction of the Lorentz force. Whereas the generator flow is decelerated due to the upstream direction of these forces, in the MHD accelerator these forces are directed downstream and accelerate the flow.

Figures 4a and b show velocity and temperature profiles of an MHD generator channel flow. Features apparent in these profiles include an asymmetry which develops between the electrodes. This asymmetry is due to the MHD-induced secondary flows which pump high-temperature core plasma toward the center of the anode surface. The vector plot of Fig. 4c illustrates the paired vorticity, secondary flow patterns typical to the MHD generator. Also given in Fig. 4d is the resulting potential and current distribution in the channel cross plane.

The action of secondary flows leads to the development of a substantial pressure gradient across the generator channel. The anode side velocity profile in the generator can be driven towards flow separation. In the MHD accelerator the same type of behavior is anticipated. That is, strong secondary flows will develop for high interaction operation and the same general asymmetry as depicted for the generator will arise in the accelerator. However, since the direction of current is opposite, the accelerator asymmetry and secondary flow patterns will develop in a mirror image fashion to that illustrated for the generator.
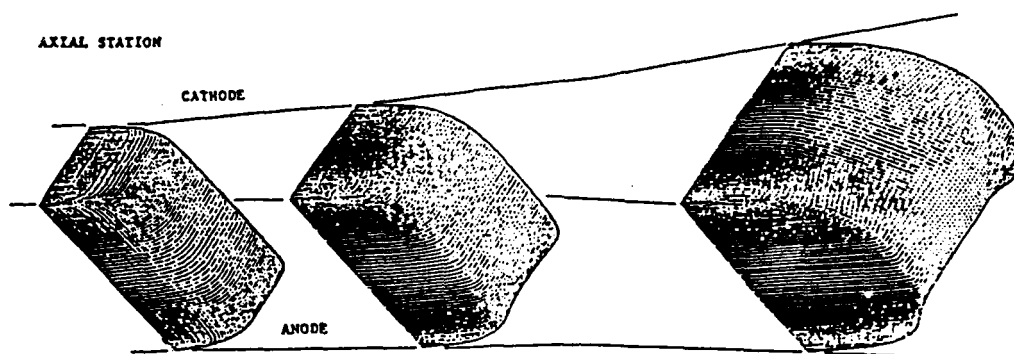
a. Cross-plane velocity profiles
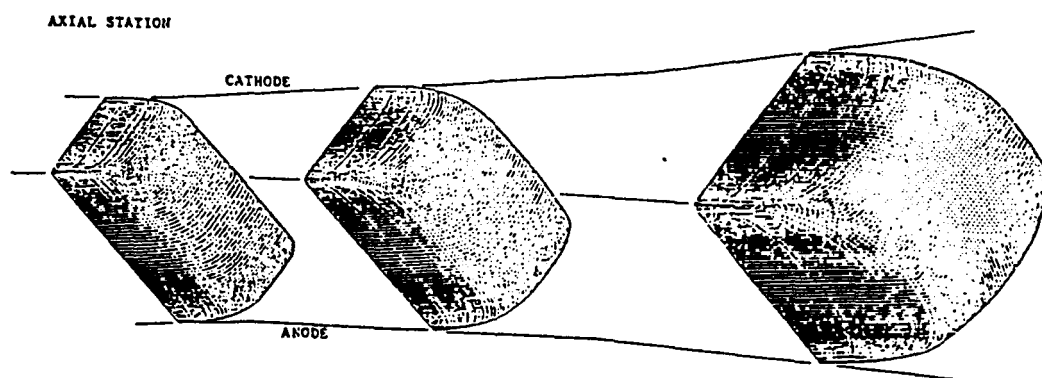
b. Cross-plane temperature profiles
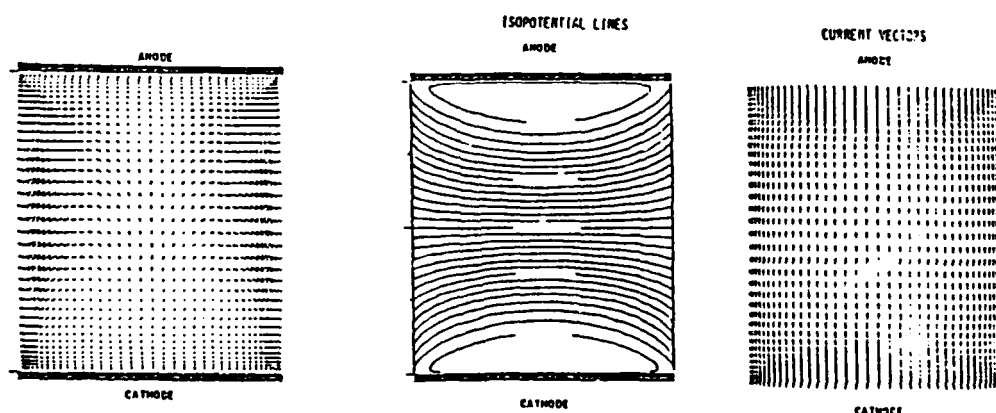
c. Cross-plane secondary flows
at generator exit

d. Cross-plane electrical patterns
at generator exit

Figure 4. Typical flow-field and electrical nonuniformities that develop in MHD generators.

25

A noticeable deceleration of the core region occurs in the MHD generator. This character is attributable to the fact that the Lorentz braking force is a maximum in the core region. As the flow traverses the duct length, flow in the core region is retarded more than that adjacent to the walls. Near the insulating walls of the Faraday generator, both the velocity and Faraday current minimize and therefore the Lorentz braking force is much weaker in the cold insulating wall region. Near the walls, shear forces dominate which leads to a nominal retardation of the flow due to viscous actions. These combined actions of the distributed Lorentz and the viscous forces lead to a deceleration near the insulating walls which is markedly less than that in the core. As a result, the velocity peaks in the profiles occur near the insulating walls. This phenomenon is known as the "velocity overshoots."

In the MHD accelerator the direction of Faraday current and Lorentz force is reversed from that of the generator, which gives rise to flow acceleration. However, in the accelerator the current producing potential is applied externally and forces current against the internally generated electric field u × B. Thus, the net field producing the current in the y-direction is (E − uB). For the regime considered in this study, the one- dimensional calculations (i.e., values are averaged across the y-z plane), show the magnitudes of E and uB are very close. Thus, one would expect that for a nonuniform velocity profile across the accelerator, current densities would be much higher in the region of lower velocity. This is a condition that would tend toward a more uniform velocity distribution as the J × B force would be higher in the lower velocity regions. One must consider the wall shear stress, however, which is extremely high for the high velocity flows considered and would tend to reduce the velocity near the walls. Previous experimental results for Faraday accelerators have shown a highly peaked profile (Refs. 12 - 13). Additional experimental work and multi-dimensional calculations for the accelerator are needed to provide more detailed performance predictions in this regard.

5.0 SUMMARY OF ACCELERATOR PERFORMANCE CALCULATIONS AND TRADE STUDIES

During this investigation the one-dimensional MHD accelerator model was first run in a design mode to determine the sensitivity of the design variables. Several acceptable accelerator channel operating configurations were evaluated and general performance analyzed. A baseline channel geometry and operating conditions were selected from the results of the initial calculations. An extensive series of performance calculations and design trade studies were then conducted around the baseline design. In the following sections the baseline channel and operating conditions will be described in detail, and the following trade studies will be presented: heater performance, magnetic field strength, seed concentration, wall friction loss, inlet pressure, channel length, and current density. Understanding of the potential performance of an MHD accelerator in combination with a gas generator requires a logical variation of the design variables with the goal of optimizing selected performance characteristics.

5.1 BASELINE CHANNEL DESIGN AND PERFORMANCE

A single gas generator was selected for the baseline channel design calculations and trade studies. The candidates for supplying inlet air to the MHD accelerator are high-pressure arc heaters, carbon-fueled combustors, and reflected shock tube drivers. Combustion heaters were not evaluated in this study because of the emphasis on propulsion testing and aerodynamic testing in "clean air." Impulse facilities utilizing shock drivers with MHD augmentation will be presented in Section 5.3. Only the arc heater was considered for the baseline design because of the existing data base on arc heater performance and the potential for growth in arc heater performance. Significant research at AEDC on high-pressure arc heaters has shown that hypersonic flight corridor simulation is improved by increasing the stagnation pressure in the heater to the limits defined by throat heat-transfer limits. Figure 5 from the AEDC white paper (Ref. 2) contains a performance limit for arc heaters as a function of total enthalpy and entropy. For the baseline definition of arc heater performance, the 200-atm point on the limit line H P $\frac{1}{2}$ = 40,000 (Btu/lbm $\sqrt{P_t}$) was selected resulting in the following arc heater exit conditions:

$$H = 6.65 MJ/kg, \ T = 4751 \ K, \ P = 200 \ atm, \ S = 8.86 kJ/kg - K$$

Accelerator performance calculations were based on these heater exit conditions except where noted.

The arc heater is connected to the accelerator channel by a convergent-divergent nozzle which is designed to provide a supersonic flow with uniform properties. The technology issues associated with the inlet nozzle will be discussed in Section 6.3. For the baseline calculations the nozzle is assumed isentropic and provides the selected accelerator inlet pressure at the corresponding Mach number. A primary requirement for the inlet flow to the accelerator is that the gas have sufficient conductivity so that it can be accelerated to overcome friction effeᴄᴛs and avoid deceleration and choking.

The baseline simulation design point was selected at Mach 20 along the q = 1,000 psf flight envelope line. A design mass flow of 22.10 kg/sec was selected based on projected requirements for a single hypersonic propulsion module. A baseline magnetic field strength of 8 Tesla was considered current state of the art. Two-percent potassium seed by weight was selected as the baseline seeding condition. Electrode current density was constrained to 50 amps/cm^2, and the channel cross section was assumed square with 0.32 deg divergence angle on each wall. Twenty atmospheres static inlet pressure was selected as the baseline operating pressure,which yielded an inlet Mach number of 2.161. The one-dimensional MHD math model was run in the design mode to determine channel length required to produce the design point total enthalpy of 22.65 MJ/kg. The resulting baseline channel length was
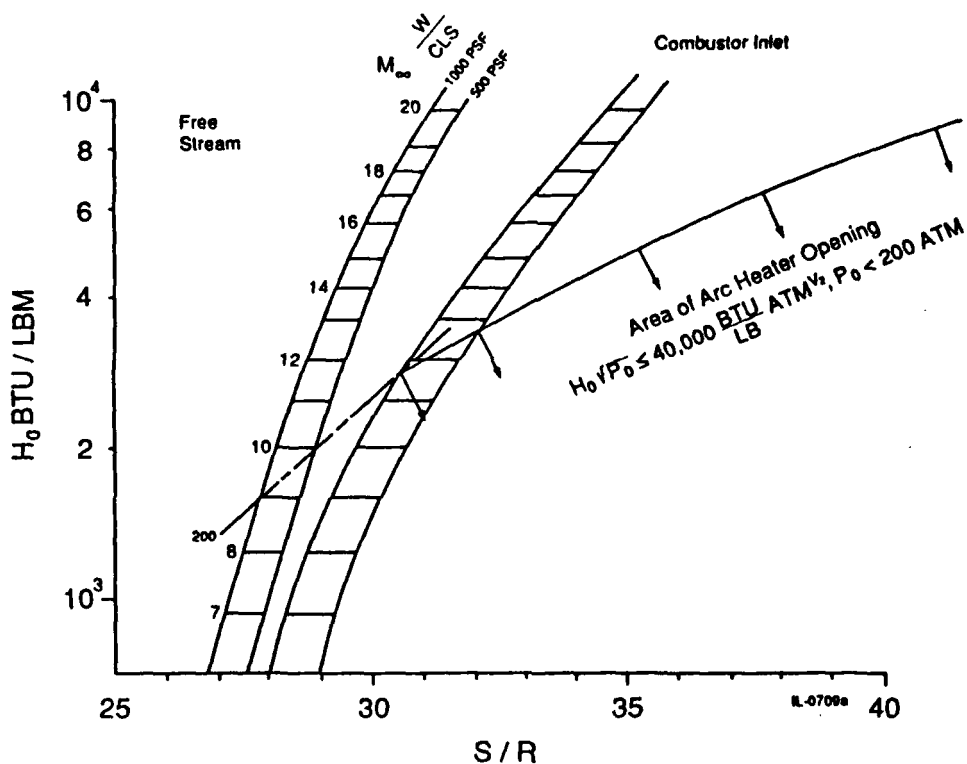
Figure 5. Hypersonic flight conditions versus arc facility capability.
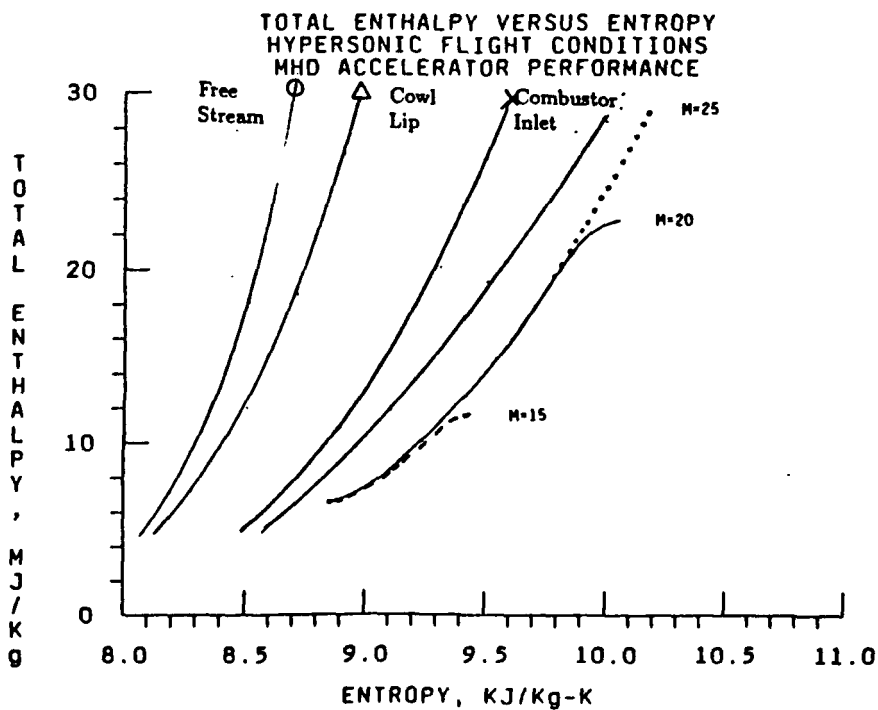
Figure 6. Total enthalpy versus entropy, MHD accelerator performance.

28

3.59 m, with an inlet area of 44.75 cm^2 and an exit area of 118 cm^2. The resulting baseline channel operating envelope was investigated by running the math model at various electrode current density limits. It was found that the channel would simulate Mach 15 conditions at 25 amps/cm^2 and Mach 25 at 70 amps/cm^2. Figure 6 shows the three accelerator simulation results on the enthalpy versus entropy plot, and Table 1 presents the baseline channel definition and resulting operating conditions.

Table 1. Baseline Faraday Accelerator Performance and Design Parameters

Baseline Design

Mach Number = 20
q = 1,000-psf Flight Profile
Magnetic Field Strength = 8 Tesla
Potassium Seed = 2 percent by weight
Mass Flow = 22.10 Kg/sec
Inlet Area = 44.75 cm^2
Exit Area = 118 cm^2
Length = 359 cm

Baseline Performance Results

Parameter	Inlet	Exit M = 15	M = 20	M = 25
P, atm	20.00	5.02	4.19	4.07
T, K	3266	3406	4025	4689
U, m/sec	2306.3	3721.9	5648.5	7168.4
h, MJ/kg	3.996	4.569	6.694	8.748
ϱ, kg/m^3	2.141	0.504	0.332	0.262
γ	1.203	1.180	1.189	1.229
σ, mhos/m	57.95	149.73	392.79	704.89
s, kJ/kg K	8.87	9.43	10.06	10.54
H, MJ/kg	6.67	11.50	22.65	34.44
P_t, atm	199.3	552.0	4068.8	7290.9
Mach	2.161	3.412	4.585	5.151
J, amps/cm^2	____	25	50	70
Q, kw/cm^2	____	5.07	10.37	16.10
Total Power, MW	____	175	458	755

The significant result from the baseline performance calculations was that a single channel geometry could produce a large simulation envelope by only varying electrode current. In the following section the key design variables are evaluated utilizing the one-dimensional MHD model.

5.2 ACCELERATOR DESIGN TRADE STUDIES

The Mach 20 baseline channel performance was selected as the comparison case for the design trade studies. The purpose of the trade studies was to identify performance sensitivities to each of the key design variables and identify improved accelerator designs.

5.2.1 Arc Heater Performance

Earlier studies at AEDC, (Refs. 2, 5, and 14), concluded that efficient MHD augmentation required high-pressure arc heaters operating at 200 atm so that the accelerator channel must operate at relatively high static pressures. This conclusion is derived from the enthalpy versus entropy performance curves for arc heaters, which show lower entropies for the higher pressure arc heaters. Thus it was considered very important to evaluate the influence of arc heater performance on accelerator performance. The baseline arc heater is a very high performance heater based on projected state-of-the-art technology and would require extensive technology development. The first trade study considered a lower technology arc heater with $H\,P^{1/2} = 30,000$ Btu/lbm atm$^{1/2}$ at $P = 160$ atm in comparison with the, $H\,P^{1/2} = 40,000$ Btu/lbm atm$^{1/2}$ at $P = 200$ atm baseline. Magnetic field strength and seed density were held constant at baseline values. The comparison results are presented in Table 2 and Fig. 7. The results were very encouraging and showed almost identical performance. The reduced arc heater case required more energy input in the accelerator to obtain the simulation enthalpy, but the resulting overall efficiency was nearly identical. This trade study result relaxes the arc heater requirements for an MHD-augmented facility. The implications of reducing total pressure on simulation entropy will be discussed in detail in Section 5.2.3.

Table 2. Baseline and Relaxed Arc Heater Performance Trade Study Results for Mach 20 Simulation

Parameter	Entrance Conditions Baseline	Relaxed	Exit Conditions Baseline	Relaxed
Mass flow, kg/sec	22.10	22.10	22.10	22.10
P, atm	20	20	4.19	4.16
T, K	3266	2941	4025	3990
U, m/sec	2306.3	2060.8	5648.5	5620.8
h, MJ/kg	3.996	3.393	6.694	____
ϱ, kg/m^3	2.141	2.396	0.332	0.334
γ	1.203	1.222	1.189	1.188
σ, mhos/m	57.95	23.37	392.79	378.25
s, kJ/kg K	8.87	8.67	10.06	10.03
H, MJ/kg	6.67	5.52	22.65	22.38
P_t, atm	199.3	158.2	4068.8	4173.8
Mach	2.161	2.027	4.585	4.594
J max, amps/cm^2	____	____	50	52
Q max, kw/cm^2	____	____	10.37	10.23
Total Power, MW	____	____	458	469

30

The math model was also utilized to calculate the Mach 10, 15, and 25 accelerator simulations for the relaxed arc heater, and the the results were nearly identical to the baseline calculations. The Mach 25 simulation required a current density of 75 amps/cm^2 which is not a significant increase. The Mach 10 simulation represents the lower simulation limit for the reduced arc heater/MHD accelerator facility due to the small augmentation required.

5.2.2 Magnetic Field Strength

The Lorentz accelerating force in an MHD augmentor is proportional to J × B, and one of the two primary loss mechanisms is the heating due to the current flow through the plasma resistance which is proportional to J^2/σ. Thus to reach high velocity without excessive heating of the driven gas, a high B-field is required. Subject to the limit that the resulting electric fields do not arc across insulators, increasing the B-field will yield improved efficiency of acceleration with less current flow and less increase in flow entropy. The baseline magnetic field strength of 8 Tesla was selected as representing the current state of the art for super-conducting magnets of this size. Since the estimated cost of the magnet is proportional to B^2, it was necessary to determine the sensitivity of accelerator performance to magnetic field strength. The baseline channel design with 2-percent potassium seed was evaluated at the Mach 20 simulation for magnetic field strengths of 6, 7, 8, 9 and 10 Tesla. The results are presented in Fig. 8, which shows a 1-percent increase in entropy for the 6-Tesla field and a 1-percent decrease in entropy for the 10-Tesla field. Figure 9 presents the changes in accelerator exit temperature resulting from the inefficiency associated with reduced magnetic field strength. The exit temperature for the 6-Tesla case is about 150 K higher than the baseline, and the exit temperature for the 10-Tesla case is about 100 K lower than the baseline. Clearly, the MHD accelerator will provide a better simulation, closer to free-stream entropy, at the highest affordable magnetic field strength. The performance, however, of the 6-Tesla magnet was very good and would provide acceptable flow simulation for direct-connect propulsion testing. Note that this trade study was conducted with 2-percent seed, and the results will show a larger influence of field strength for reduced seed densities.

5.2.3 Seed Concentration and Conductivity

Gas conductivity is the critical gas property controlling the efficiency and performance of the MHD accelerator. The accelerator entrance flow must be seeded with an easily ionized material (cesium or potassium) to provide the necessary conductivity at the lowest possible temperature to minimize the production of atomic oxygen and NO. This trade study was conducted to determine the influence of seed concentration on the baseline accelerator performance. To better understand the results of the trade study and to accept the limits of the MHD-augmented flow simulation envelope, the following conductivity analysis is presented. For a selected mixture of air and seed, 2-percent potassium in this study, the

31
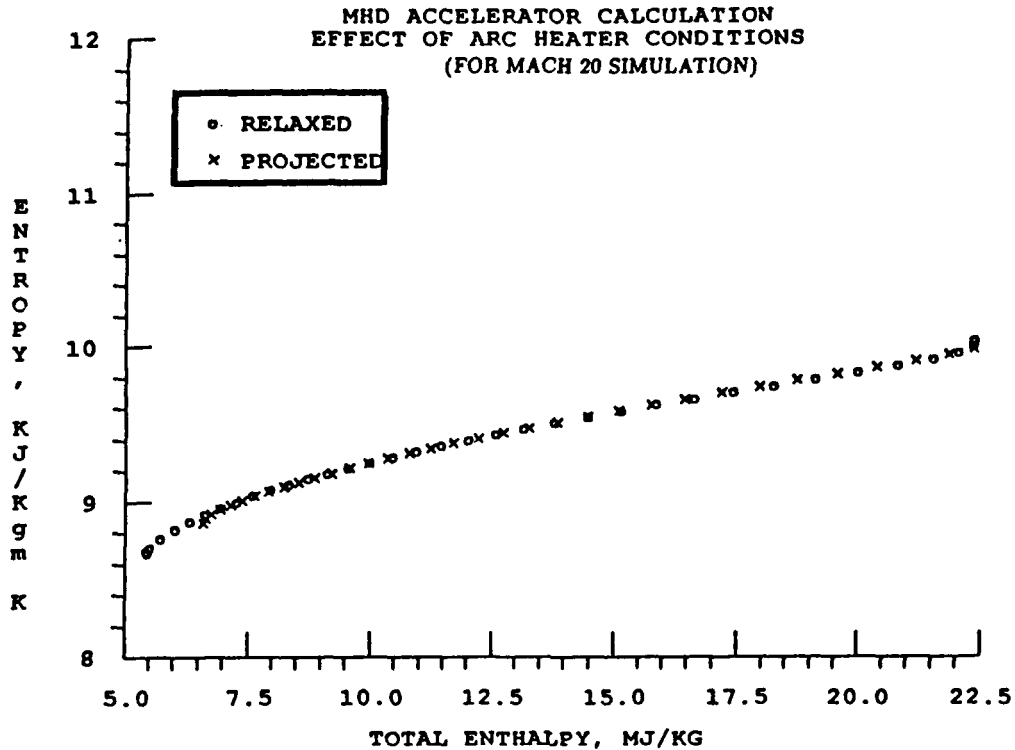
Figure 7. Comparison of relaxed to projected arc heater conditions.
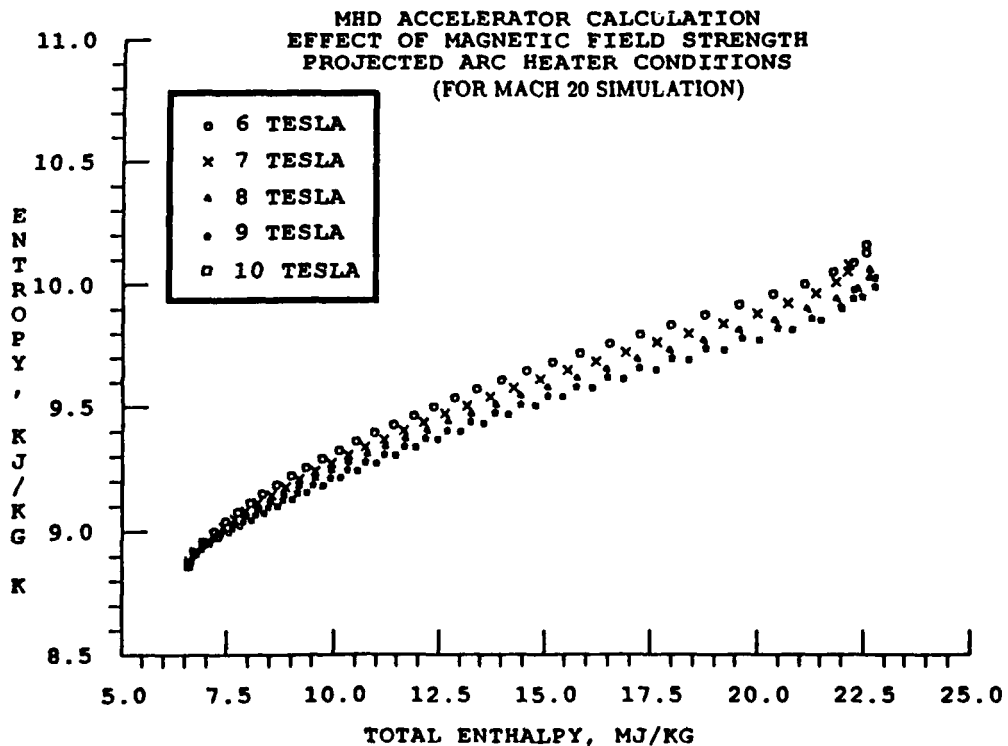
Figure 8. Magnetic field parametric study, entropy versus enthalpy.

conductivity is a function of pressure and temperature assuming chemical equilibrium. The conductivity of the equilibrium mixture can also defined as a function of pressure and entropy (Fig. 10). Since entropy has been identified as a primary performance variable for evaluating accelerator efficiency, the relationship between entropy and conductivity and pressure will be evaluated on the enthalpy versus entropy map. Figure 11 shows the lower left corner of the accelerator enthalpy versus entropy map containing the free-stream and combustor inlet simulation requirements. Lines of constant pressure and constant conductivity are presented as functions of enthalpy and entropy for a mixture of air and 2-percent potassium. The enthalpy is the static enthalpy when referring to the static pressure or conductivity and the total enthalpy when referring to the q = 1,000 flight trajectory curves or total pressure. To understand the implications of this curve, the baseline case has a total pressure of 200 atm and a total enthalpy of 6.67 MJ/kg. After an isentropic expansion to 20 atm the conductivity is over 50 mhos/m. This gas could be expanded to less than 10 atm and still have a conductivity greater than 20 mhos/m. The initial conditions required to have the acceleration follow the free-stream conditions would have total pressures exceeding 1,000 atm and total enthalpies over 6 MJ/kg with an expansion to 200 atm at the accelerator inlet and a starting conductivity of 10 mhos/m.

It is very important to recognize that the values of conductivity and pressure in Figs. 10 and 11 are totally independent of the hot gas generator design. If 10 mhos/m is considered the minimum conductivity for accelerator inlet conditions, then the starting entropy is a function of inlet pressure. At 10-atm inlet pressure the entropy is 8.6 KJ/kg °K, and at 100-atm inlet pressure the same conductivity of 10 mhos/m corresponds to an entrance entropy of 8.25 KJ/kg °K . Increasing the entrance conductivity at constant inlet pressure results in increased entrance entropy. It would require channel operating pressures near 500 atm to yield an entrance entropy less than 8 KJ/kg °K at conductivity levels of 10 mhos/m. The upper operating limit for channel pressure has not been established; however, current density and wall heat-transfer rate increase rapidly with increasing operating pressure. From these calculations it can be seen that regardless of the gas heating method, entropies below 8.5 MJ/kg °K will be very difficult to obtain, and those below 8.25 practically impossible, except at very high shock tunnel pressures above 1,000 atm.

The results of the analysis above are based on 2-percent potassium seed and for reduced levels of seeding the entropy/conductivity constraints are more restrictive. To evaluate the influence of seed concentration on accelerator performance the baseline accelerator simulation was run at seed mass fractions of 2.0-, 1.0-, 0.5-, 0.25-, and 0.1-percent potassium. The results are presented in Figs. 12, 13, and 14. Figure 12, total enthalpy versus entropy, shows an increase of 1 percent in entropy for a reduction of seed to 0.5 percent. This is a significant result and indicates that seeding levels below 1 percent are feasible. Figure 13 indicates that exit static temperature is increased about 100 °K for the same reduction to 0.5-percent seed.

33

MHD ACCELERATOR CALCULATION
EFFECT OF MAGNETIC FIELD STRENGTH
PROJECTED ARC HEATER CONDITIONS

S T A T I C   T E M P E R A T U R E ,   K

- 6 TESLA
- x 7 TESLA
- ▲ 8 TESLA
- • 9 TESLA
- □ 10 TESLA

TOTAL ENTHALPY, MJ/KG
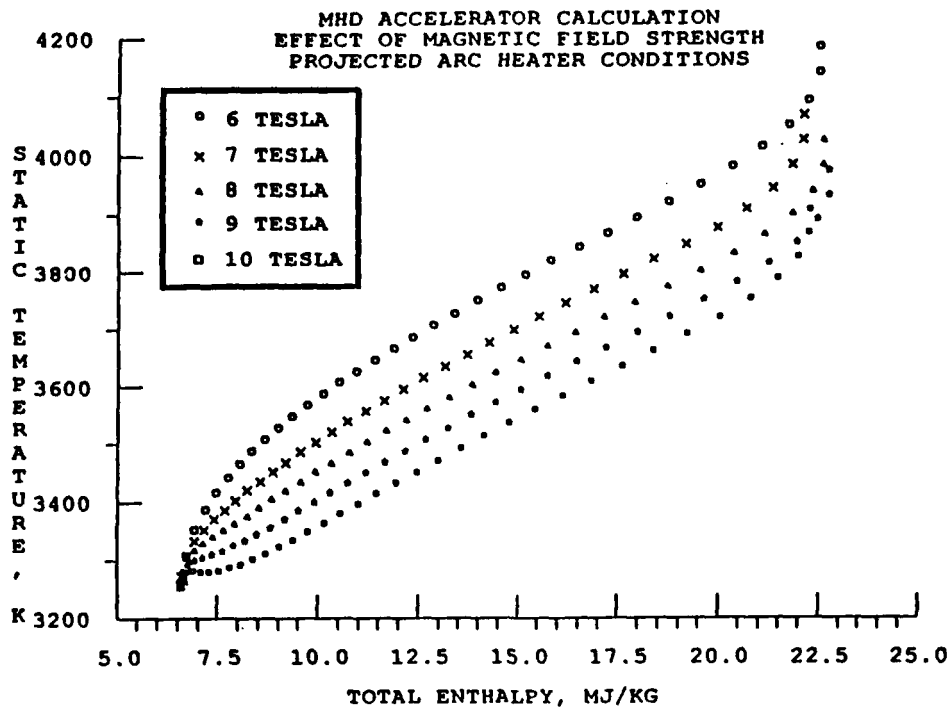
Figure 9. Magnetic field parametric study, static temperature versus enthalpy.

EFFECT OF PRESSURE ON CONDUCTIVITY

P R E S S U R E ,   A T M

- o SIGMA=10
- ▲ SIGMA=20
- ᴸ SIGMA=50

ENTROPY, KJ/KG K
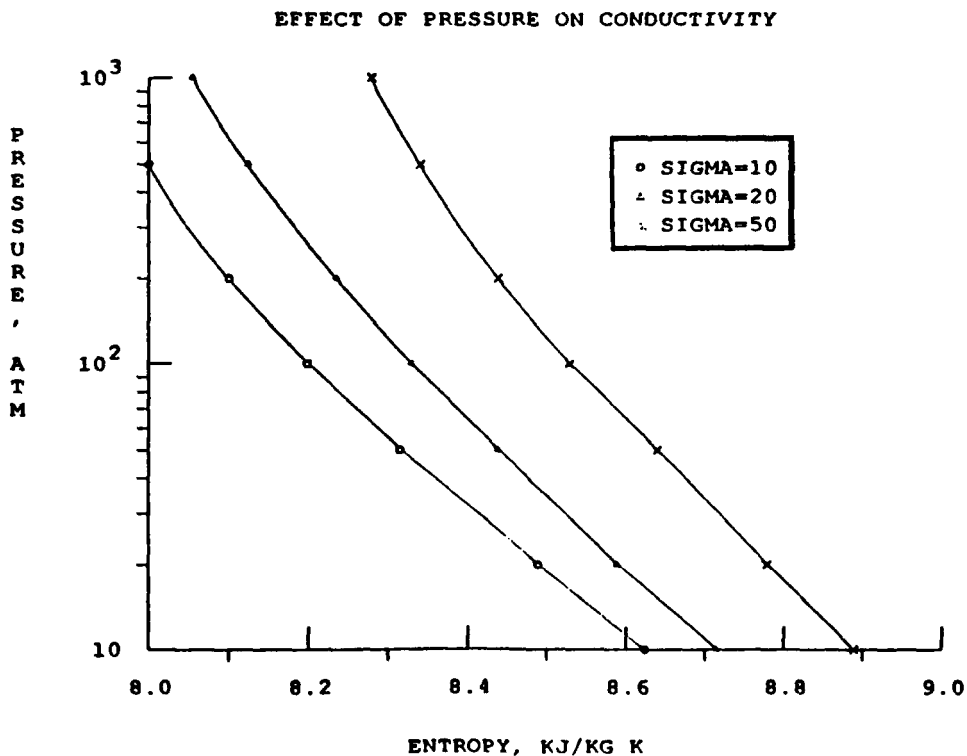
Figure 10. Effect of pressure on conductivity.
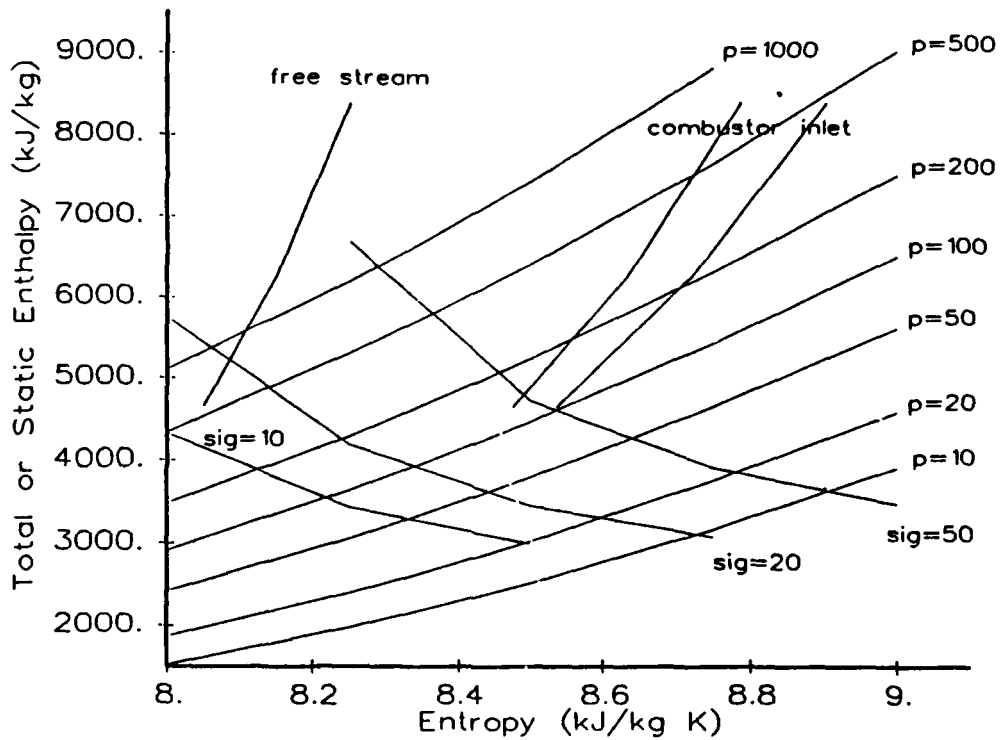
Figure 11. Conductivity, pressure, enthalpy, and entropy relationship.
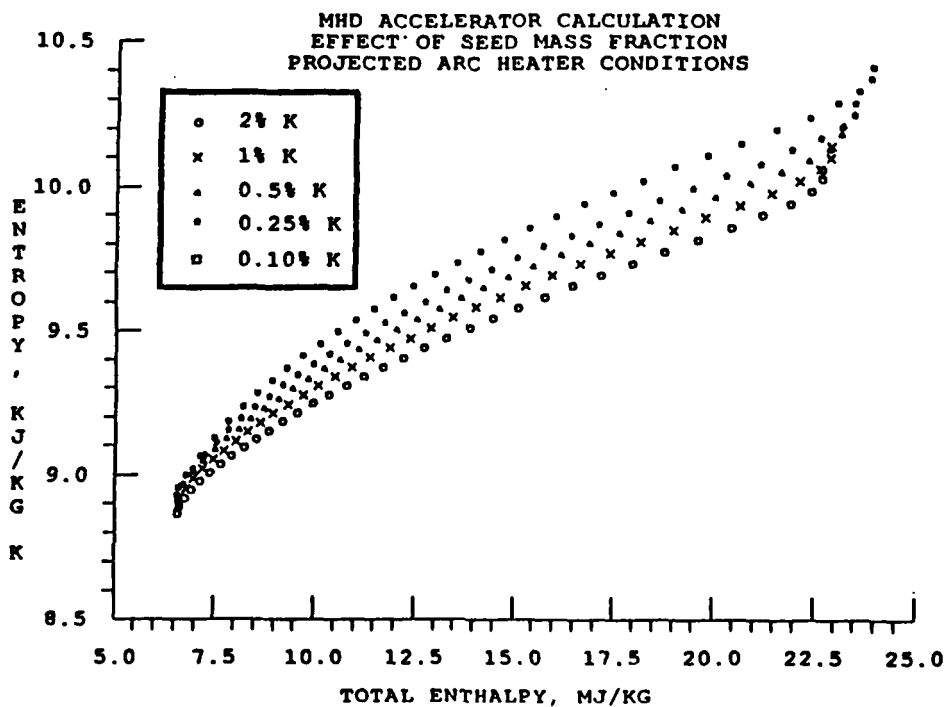
Figure 12. Base case with variation in seed fraction, entropy versus enthalpy.

Figure 14 helps explain the results of the seeding trade study and clearly shows the strong influence of seed density on conductivity. The results for the seeding levels below 0.5 percent should be evaluated with caution because of the possibility of electrode arcing at the lower conductivity levels. The results of the one-dimensional MHD model seeding trade studies are very encouraging because seed levels as low as 0.5 percent provide good accelerator performance. Additional analysis and experiments will be required to evaluate finite electrode effects in combination with reduced levels of conductivity.

5.2.4 Wall Friction Effects

During analysis of the baseline channel performance an energy distribution evaluation showed that the friction work or viscous losses were the dominant loss effect in the channel. Figure 15 presents the distribution of the useful work and loss effects for the baseline calculations. Figure 15 shows the power and work terms along the base case acceleration. The applied power is made up of the push work plus the Joulean dissipation. The friction and heat losses are shown for comparison of magnitudes with the other terms. Both Joulean heating and wall heat loss are smaller losses than the friction work. This result should not be surprising, considering the large length-to-average width ratio of the channel, 40.9. Thus the value of turbulent friction coefficient was reviewed to determine if the value was correct. A value of 0.006 (determined from input roughness) was used in the baseline calculations for friction coefficient, and this value is consistent with normal compressible turbulent boundary-layer theory for the defined wall roughness. A review of the published articles on turbulent boundary layers in MHD devices revealed that there was an influence of the magnetic field on the turbulence (Ref. 15). However there are no standard methods for estimating turbulent shear stress in the presence of strong magnetic fields, which would influence wall heat transfer.

A trade study was then conducted on the baseline channel to determine the influence of friction coefficient on accelerator performance. All simulation parameters were held constant including applied current, and the friction coefficient was varied from 0.75 to 1.25 of its nominal value calculated as outlined in Ref. 16 for roughness height $\cong$ 0.1 mm. The results were very significant and indicated that an incorrect value of friction coefficient would make large changes in channel performance. Table 3 presents the trade study results, and it must be pointed out that applied current was held constant resulting in a variation in total enthalpy. If the correct value of friction coefficient for the MHD channel was 75-percent of the baseline value, the performance and efficiency of the acceleration would be significantly improved. Only a major experimental investigation can determine the real value of turbulent shear stress in the influence of strong magnetic fields.
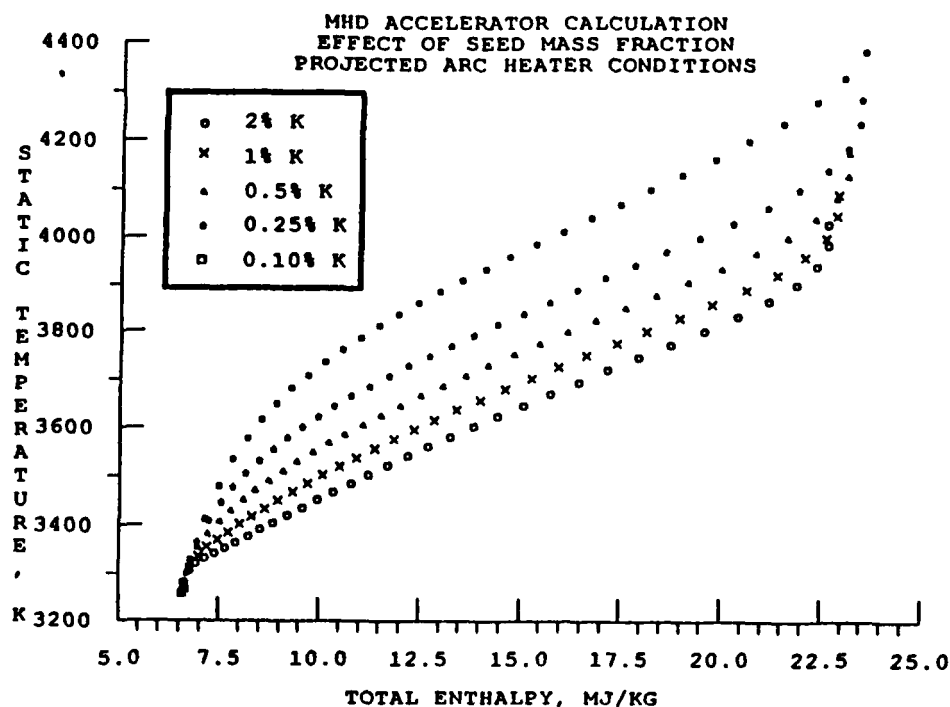
Figure 13. Base case with variation in seed fraction, static temperature versus enthalpy.
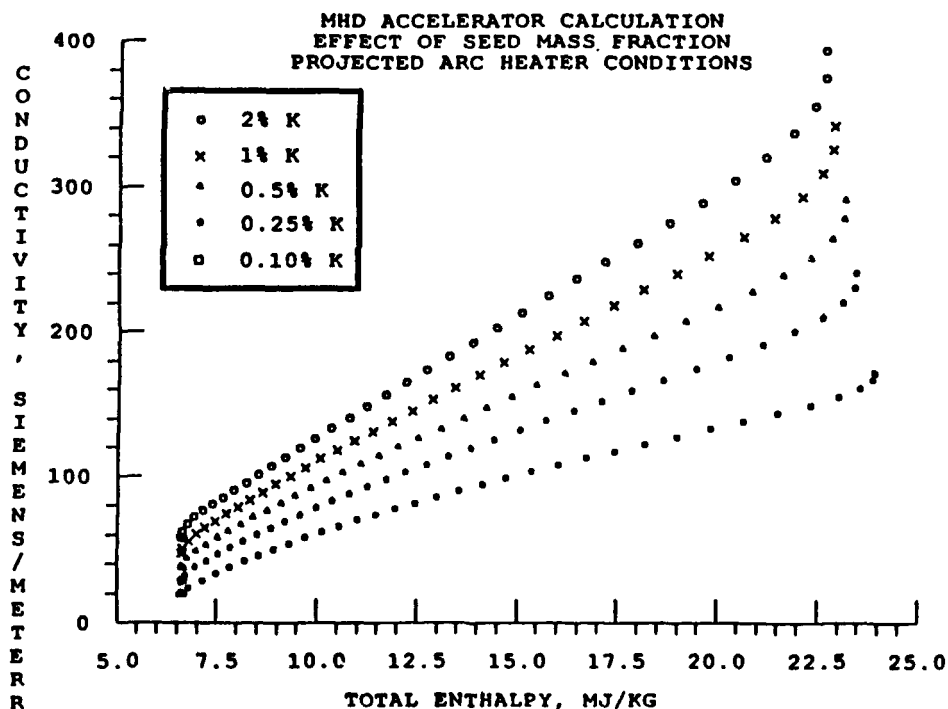
Figure 14. Base case with variation in seed fraction, conductivity versus enthalpy.

Table 3. Wall Friction Trade Study Results

Parameter	Baseline	0.75 Friction	1.25 Friction
Mass flow, kg/sec	22.10	22.10	22.10
P, atm	4.19	3.52	4.89
T, K	4025	3724.5	4304.1
U, m/sec	5648.5	6035.7	5294.3
h, MJ/kg	6.694	5.726	7.548
ϱ, kg/m^3	0.332	0.311	0.355
γ	1.189	1.177	1.206
σ, mhos/m	392.79	283.50	502.65
s, kJ/kg K	10.06	9.86	10.22
H, MJ/kg	22.65	23.94	21.56
P_t, atm	4068.8	11811.6	1687.3
Mach	4.585	5.196	4.078
J, max amps/cm^2	50	50	50
Q, max kw/cm^2	10.37	10.78	10.018

5.2.5 Inlet Pressure

The accelerator channel inlet pressure is one of the more interesting and complex design variables because of the numerous constraints on its value. In this trade study the baseline channel was modified to hold mass flow constant while the baseline arc heater flow was expanded to 10 atm. The resulting channel has an inlet area of 71 cm^2 and an exit area of 156 cm^2 which represents an increase of about 50 percent. The inlet static temperature drops to 2,915 °K , and conductivity is reduced to 33.25 mhos/m. For the baseline magnetic field of 8 Tesla and seed concentration of 2-percent potassium the maximum current density required to simulate the Mach 20 enthalpy was 33.5 amps/cm^2. Somewhat surprising was the overall performance of the lower pressure channel which was nearly identical to the baseline case with a small improvement in efficiency. Table 4 presents a summary of the inlet and exit comparisons for the 10- and 20-atm baseline cases.

38

Table 4. Inlet Pressure Trade Study Results

	Inlet Parameters		Exit Parameters	
P, atm	10.0	20.0	2.68	4.19
T, K	2915	3266	3771	4025
U, m/sec	2577	2306	5730	5648.5
h, MJ/kg	3.378	3.996	6.000	6.694
ϱ, Kg/m^3	1.207	2.141	0.247	0.332
γ	1.216	1.203	1.178	1.189
R, J/kg-K	288	289.8	311.4	317.1
σ, mhos/m	33.25	57.95	321.06	392.79
s, kJ/kg K	8.87	8.87	10.00	10.06
H, MJ/kg	6.67	6.67	22.42	22.65
P_t, atm	199.7	199.3	5263	4068.8
M	2.550	2.161	4.872	4.585
J, amps/cm^2	____	____	33.5	50.0
Q, kw/cm^2	____	____	7.657	10.37

The reduction of inlet pressure for this trade study has resulted in a very acceptable design with lower levels of current density and wall heat flux. This result should not be generalized without recognizing the influence of the arc heater performance on the lower pressure channel characteristics. The baseline arc heater provides sufficient enthalpy that conductivity remains high enough to provide efficient acceleration. Thus the best channel operating pressure will be determined by the required conductivity limits, the allowable current densities, and the allowable wall heat-transfer rates. Figure 16 illustrates the significant reduction in heat flux for the lower pressure channel. The corresponding lower current densities would allow the channel to be shorter if current density was held constant at 50 amps/cm^2. However, there is one problem with the lower pressure channel; the axial potential is higher, as shown in Fig. 17. The higher axial potential will require shorter electrodes or thicker insulators. The most significant conclusion from this study is recognition of the strong interaction between design parameters for the heater and the MHD accelerator channel.

5.2.6 Channel Length, Pressure, and Current Density

Based on the results of the trade studies in the preceding sections, one new design was selected and evaluated for the combined influence of length, pressure, and current density. The reduced inlet pressure design produced good performance at reduced current density and lower wall heating rates, thus the channel could be shortened from 3.6 m to reduce friction losses. The baseline Mach 20 simulation was run for the baseline arc heater conditions, 2-percent potassium seed, and 8-Tesla magnetic field at 10-atm inlet pressure. A channel length
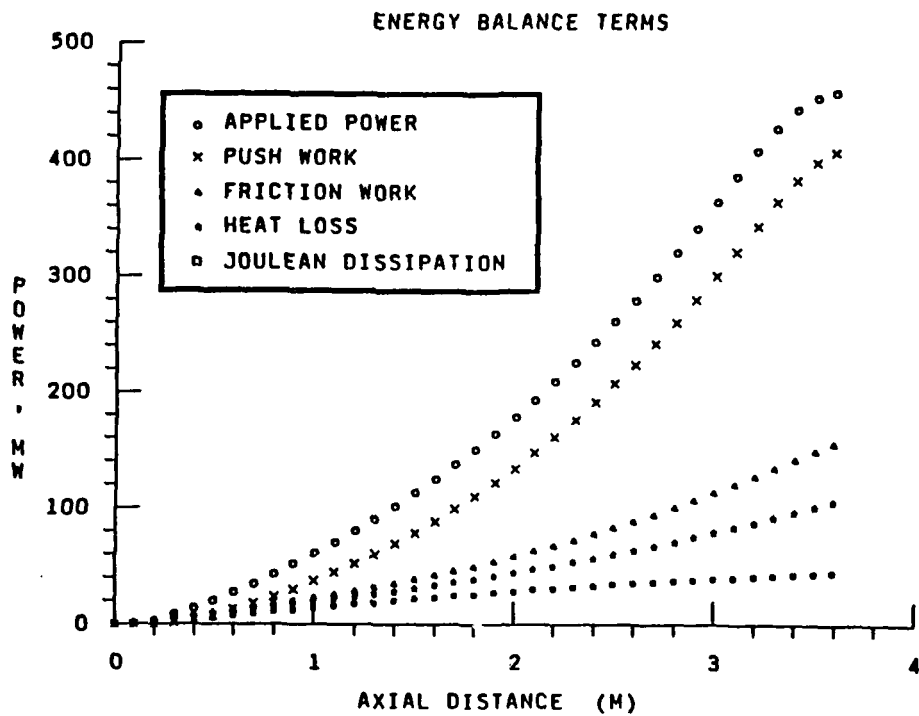
Figure 15. Base case energy balance terms.
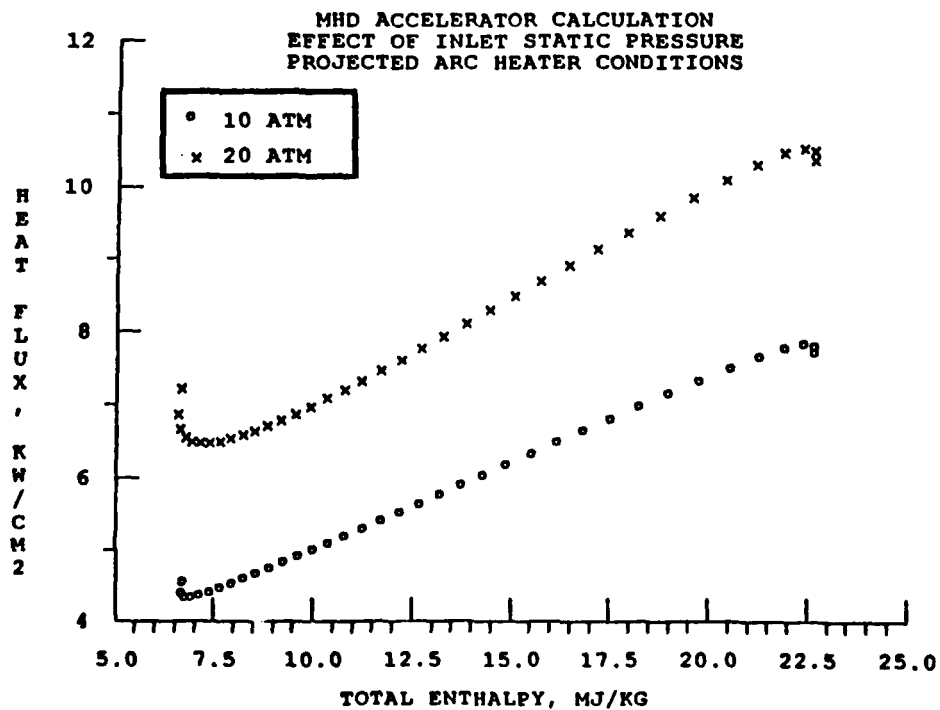
Figure 16. 10 Atm compared with base case, heat flux versus enthalpy.

of 2 m was selected, and maximum current density was varied to yield the required total enthalpy. The resulting channel was not optimized on any of the design parameters; however, it demonstrated excellent performance in a much shorter channel which would significantly reduce magnet size and cost. Performance of the short, 10-atm channel is compared with the performance of the baseline channel (20- and 10-atm inlet pressure) in Table 5. Channel inlet parameters are the same as Table 4 values.

Table 5. Channel Length, Pressure, and Current Density Trade Study Results - Exit Performance Parameters

	Baseline	10-atm Baseline	10-atm, 2 m
L_m	3.6	3.6	2.0
P_{atm}	4.19	2.68	3.92
T, °K	4025	3771	3874
U, m/sec	5648.5	5730	5680.7
h, MJ/kg	6.694	6.000	6.203
ϱ, kg/m^3	0.332	0.247	0.329
γ	1.189	1.178	1.182
R	317.1	311.4	312.3
σ, mhos/m	392.79	321.06	334.37
s, kJ/kg °K	10.06	10.00	9.96
H, MJ/kg	22.65	22.42	22.34
P_t, atm	4068.8	5263	5511.8
M	4.585	4.872	4.750
J, amps/cm^2	50.0	33.5	64.0
Q, kw/cm^2	10.37	7.657	10.08

The following preliminary conclusions result from the design trade study. Subject to the constraint that sufficient conductivity exists at the channel inlet, channel operating pressure, current density, and wall heating rate may be sub-optimized for a given channel length. Minimum channel length will be constrained by finite electrode effects and axial voltage in addition to maximum electrode current density and wall heating rate. Since the 2-m channel was evaluated only at the Mach 20 design point, the Mach number simulation range for the shorter channel was not calculated but should be smaller than the baseline channel. These results are very encouraging because the channel performance is somewhat insensitive to specific design values, which allows design flexibility subject only to constraints on conductivity, electrode current density, and wall heating rate.
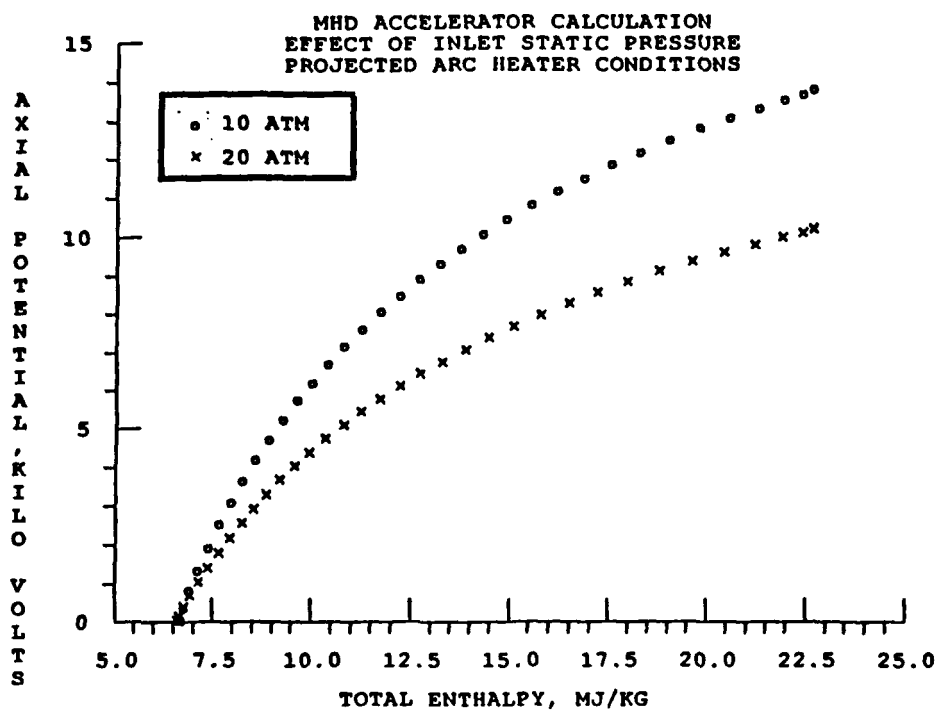
Figure 17. 10 Atm compared with base case, axial potential versus enthalpy.
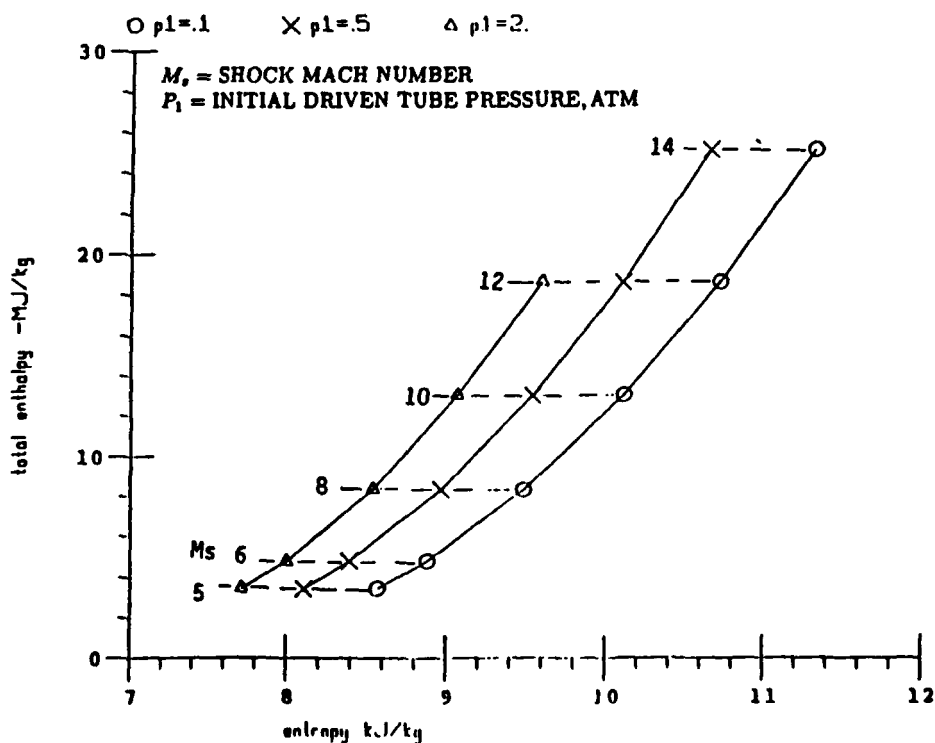
Figure 18. Shock tube total enthalpy and entropy map.

5.3 SHOCK-DRIVEN ACCELERATOR PERFORMANCE

An alternate application of an MHD accelerator to a reflected shock-driven hypersonic flow tunnel is investigated in this section. Hypersonic impulse flow facilities driven by two-stage reflected shock tubes have provided "clean air" flow simulation. Addition of a free piston to the driver section of a shock tube provides much higher stagnation conditions at the driven tube burst diaphragm, which produces higher stagnation conditions in the reflected shock region for the hypersonic expansion. The tunnel J facility operated at AEDC during the 1966-1970 period, and demonstrated MHD augmentation of a reflected shock driven tunnel. Current free-piston shock tunnel research by Stalker (Ref. 17) has produced a high pressure and temperature driver suitable for an MHD-augmented hypersonic facility.

A brief trade study was conducted to determine the shock tube parameters necessary to allow efficient MHD augmentation for the Mach 20, q = 1,000 flow simulation. Performance maps for stagnation conditions in the reflected shock region were obtained from a one-dimensional, equilibrium shock code. Pressure and shock Mach number in the driven tube are the primary variables for determining the shock tunnel stagnation conditions. Figure 18 presents the total enthalpy versus entropy map for driven tube pressure of 0.1 atm to 2.0 atm and shock Mach numbers of 5, 6, 8, 10, 12, and 14. Note that shock Mach numbers above 12 provide a near free-stream total enthalpy for Mach = 20 simulation without augmentation. Figure 19 contains the total pressure versus total temperature map for the same shock tunnel conditions as Fig. 18. It appears that shock Mach number around 8.0 will provide sufficient temperature for seeded flow conductivity without excessive dissociation. Three shock tunnel cases were selected for input stagnation conditions to the baseline MHD accelerator code. The 3.5-m channel,with 2-percent potassium seed and an 8-Tesla field was run for the Mach 20 simulation.

The shock tube driven pressure of 2.0 atm at shock Mach of 8.0 produced very high stagnation pressures as can be seen in Fig. 19, and the expansion to 20 atm at the accelerator inlet resulted in low temperature and conductivity. Note that limitations on accelerator electrode current density and wall heating rates will limit channel entrance pressure to approximately 20 atm or lower.Thus this first case did not yield good accelerator performance because too much expansion was required.The second and third cases used shock tube-driven pressure of 0.5 atm and shock Mach of 8.0. One was expanded to 20 atm and run in the baseline accelerator channel. The other was expanded to 10 atm at the accelerator entrance and run in the baseline (10 atm) channel. Both of these simulations produced good results, with the 10-atm case being the more efficient. Table 6 contains the results of the reflected shock driven, MHD accelerator runs.

43

Table 6. Shock Tube-Driven MHD Accelerator Performance

	Inlet	Conditions	(20 atm)	Exit Cond. (Baseline)	(10 atm)
P, atm	20.0	10.0	4.36	(4.19)	2.22
T, °K	3444	3097	4043.6	(4025)	3629.6
U, m/sec	2676	2928.7	5546.1	(5648.5)	5788.7
h, MJ/kg	4.377	3.722	6.743	(6.694)	5.609
ϱ, kg/m^3	2.016	1.131	0.345	(0.332)	0.201
γ	1.196	1.204	1.190	(1.189)	1.173
R	291.8	289.4	317.3	(317.1)	308.2
σ, mhos/m	85.95	55.57	396.57	(392.79)	284.76
s, kJ/kg °K	8.99	8.99	10.06	(10.06)	9.97
H, MJ/kg	7.96	7.98	22.12	(22.65)	22.36
P_t, atm	330.9	333	3528.1	(4068.8)	6060.1
M	2.441	2.820	4.488	(4.585)	5.054
J, amps/cm^2	——	——	48	(50)	27
Q, kw/cm^2	——	——	10.321	(10.37)	6.242

The Table 6 results clearly show that the performance of the shock-driven MHD-augmented facility (although short duration) can be as good as the arc-heated facility. Since a shock-driven facility would be significantly lower cost to develop and operate, it would be a good choice for a research facility to investigate the critical technologies associated with MHD accelerator development, which do not require steady-state thermal effects.

5.4 ELECTRODE SEGMENTATION

All the previously discussed accelerator calculations were based upon relations that assume infinitely fine electrode segmentation. Since that is clearly not possible, the performance as a function of electrode and insulator width (length in the direction of flow) needs to be considered.

In the Faraday accelerator, a separate power supply is required for each pair of electrodes so the cost and complexity of the power supply tends to increase with increasing numbers of electrodes. If there were no segmentation, as in a continuous electrode Faraday accelerator, axial currents would flow in the plasma due to generated Hall potential and circulate back through the electrode which would be at a constant potential along its length. This results in power loss (also entropy gain) due to the Ohmic power dissipation and also distorts the flow due to the $\overline{J} \times \overline{B}$ body force in a direction perpendicular to the flow.

shock tube total pressure and temperature

O p1=.1   X p1=.5   △ p1=2.

M_s = SHOCK MACH NUMBER
P_1 = INITIAL DRIVEN TUBE PRESSURE, ATM
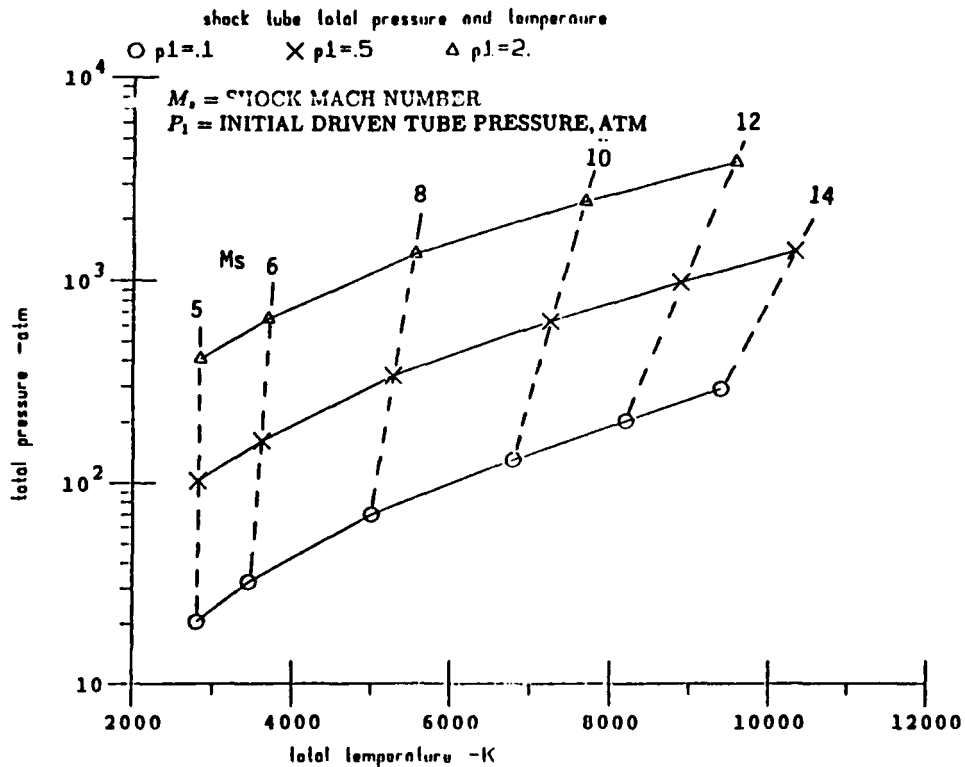
Figure 19. Shock tube total pressure and temperature map.

EFFECT OF FINITE SEGMENTATION

|<——— 2.83cm ———>|

| ELECTRODE | I N S U L A T O R | ELECTRODE |
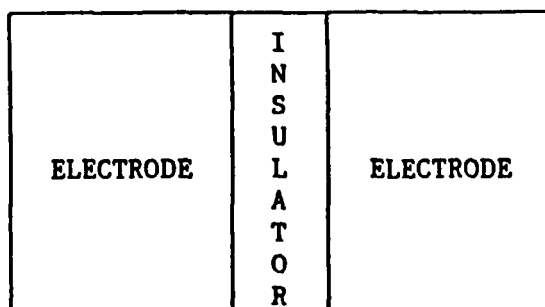
s = 2.83cm

c = .3175cm

h = 9.06cm (MID-CHANNEL)

w/r = 1.06 (MID-CHANNEL)

$\frac{1''}{8}$ = .3175cm

Figure 20. Electrode segmentation geometry.

45

The criteria for selection of segmentation are:

1. Reduction of circulating currents in the axial direction to negligible effects.

2. Sufficiently low axial voltage across each insulator that electrical breakdown will not occur.

There is no precise theory that permits determination of the segmentation (axial length of an electrode insulator pair) or insulator width, even for an MHD generator. A tentative choice has been made of 80 volts/gap for insulators 1/8-in. thick. This needs experimental verification.

For the base case accelerator, the total axial voltage is calculated by the 1D Code as 10,182 volts over a length of 3.6 m. Thus, the number of electrodes is estimated as:

$$\text{\# Electrodes} = \frac{\text{Potential}}{\text{Potential/Electrode}} = \frac{10,182 \text{ Volts}}{80\text{v/Electrode}} = 127 \text{ Electrodes}$$

$$\text{Electrode Pitch} = s = \frac{360\text{cm}}{127 \text{ Electrodes}} = 2.83 \text{ cm/Electrode}$$

The geometry is shown in Fig. 20, along with other properties of the accelerator channel.

This geometry affects current paths in the accelerator and thus the apparent electrical conductivity and Hall parameter. These effects are given approximately by Refs. 11 and 19.

$$\frac{\sigma \text{ apparent}}{\sigma \text{ real}} = \frac{w\tau \text{ (apparent)}}{w\tau \text{ (real)}} \approx \frac{1}{1 + s/h(w\tau - 0.44)}$$

For the base case accelerator, using values at mid-channel,

$$\frac{\sigma \text{ apparent}}{\sigma \text{ real}} = \frac{w\tau \text{ (apparent)}}{w\tau \text{ (real)}} = 0.838$$

The base case recalculated for these reduced parameters results in only slightly degraded performance as shown in Table 7.

Table 7. Base Case With Reduced Parameters

	T_{Out}	HT MJ/kg	P_S (Atm)	Power, MW	S, J/kg K
Base Case	4029	22.65	4.19	458.1	10.07
Finite					
Segmentation Case	4084	22.81	4.27	462.8	10.10

5.5 FINITE RATE EXPANSIONS FROM ACCELERATOR EXIT

One-dimensional finite rate expansions were calculated using the computer code, described in Section 4.4, for selected cases to provide a prediction of the gas properties at simulated combustor inlet and free-stream conditions. A 15-deg half-angle nozzle was chosen for these calculations. The exact choice of a nozzle contour would not be expected to have a large effect on the results, and this nozzle is considered typical of what might be used. The flow is assumed to be uniform at the accelerator exit and one-dimensional and at local thermodynamic (but not chemical) equilibrium during the expansion. The gas is assumed to be thermally perfect with the thermodynamic properties obtained from the curve fit data provided withthe NASA one-dimensional equilibrium code (ODE) (Ref. 6).

5.5.1 Test Cases

The gas properties for a one-dimensional equilibrium expansion were calculated for the baseline case to provide a basis for comparison.These calculations were made with the ODE using the same composition and entropy with a series of pressures to obtain the static properties. The velocity at each of these points was obtained from the difference between the total enthalpy predicted by the accelerator code and the static enthalpy from the ODE.

The following cases were selected for nozzle expansion calculations.

1. The baseline case

2. Acceleration to Mach 15 conditions

3. Acceleration to Mach 25 conditions

4. Reduced arc heater output

5. 0.25-percent potassium

6. 0.25-percent potassium with reduced arc heater output

7. 125 percent of the standard wall drag coefficient

8. 75 percent of the standard wall drag coefficient

9. 10-atm inlet pressure

10. 10-atm inlet pressure with short accelerator

11. Baseline equilibrium expansion

The following set of chemical reactions was used for all of the nozzle expansion calculations. The forward rate of each reaction is calculated from a rate constant expressed in Arrehenius form where E is the activation energy, R the universal gas constant, and T the temperature.

$$Kf = Ae^{-E/RT}/T^n$$

	reaction					A	n	E
O	+ O	+ M	= O2	+ M		0.3991E+19	1.0	0.0
N	+ N	+ M	= N2	+ M		0.1996E+19	1.0	0.0
N	+ O	+ M	= NO	+ M		0.5987E+17	0.5	0.0
O	+ N2		= NO	+ N		0.1807E+15	0.0	76000.0
N	+ O2		= NO	+ O		0.6626E+10	0.0	6300.0
K+	+ E	+ M	= K	+ M		0.1451E+25	1.0	0.0
K	+ O	+ M	= KO	+ M		0.3628E+18	1.0	0.0
O2	+ E	+ M	= O2-	+ M		0.3628E+18	0.0	0.0
O2-	+ O		= O2	+ O-		0.9999E+14	0.5	0.0
O	+ E	+ M	= O-	+ M		0.1201E+21	0.0	0.0
O-	+ O		= O2	+ E		0.3000E+05	-1.0	0.0
NO	+ O2		= NO2	+ O		0.1100E+13	0.0	54000.0
O2	+ N2O		= NO2	+ NO		0.1000E+14	0.0	70000.0
KO	+ E	+ M	= KO-	+ M		0.3991E+20	0.0	0.0

5.5.2 Initial Conditions for Expansions

The initial conditions for the cases selected for expansion were obtained from a calculation with the ODE using a gas with the composition of air with potassium (K) and the final pressure, entropy, and velocity from the MHD accelerator code. The initial temperature and pressure for case 1 and 4 through 10 are shown along with a constant entropy (s = 10 kJ/kg) line in Fig. 21. The nozzle area ratio is shown as a function of pressure for the baseline case in Fig. 22. Thermodynamic properties and species concentrations at the inlet to the expansion nozzle are listed for cases 1 through 10 in Table 8.

5.5.3 Results for the Selected Channel Operating Conditions

The approximate combustor inlet and free-stream thermodynamic properties and species concentrations are listed in Table 9. The approximations occur because the pressure selected was that closest to the actual pressure which occurred in the printout from the expansion calculation.
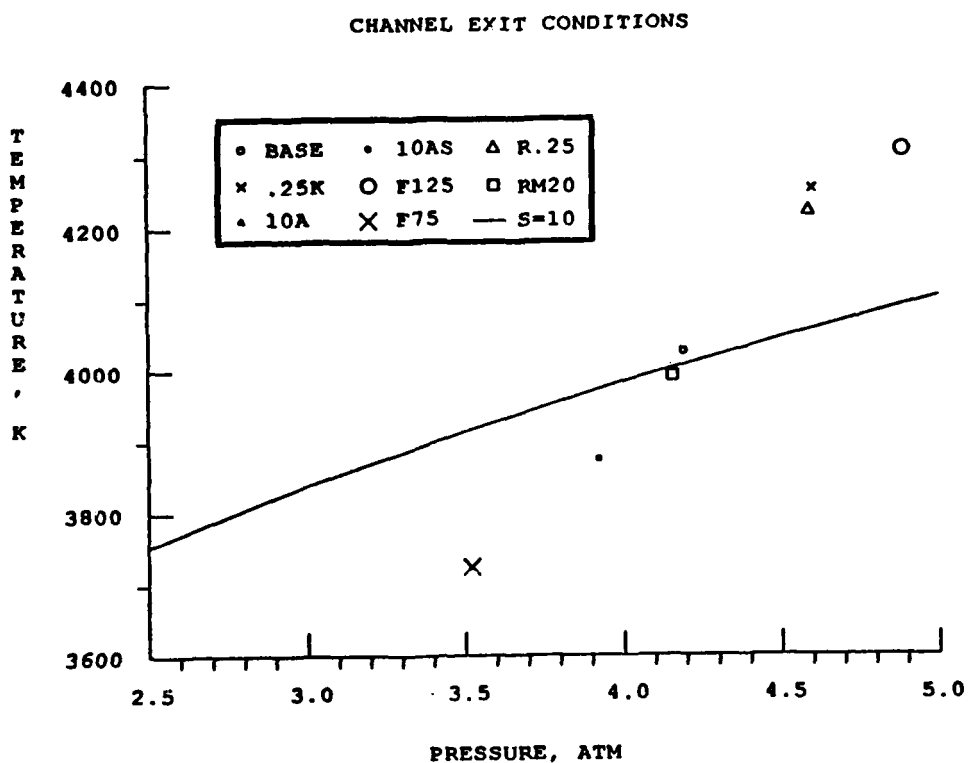
CHANNEL EXIT CONDITIONS

Figure 21. Summary channel exit conditions, temperature and pressure.
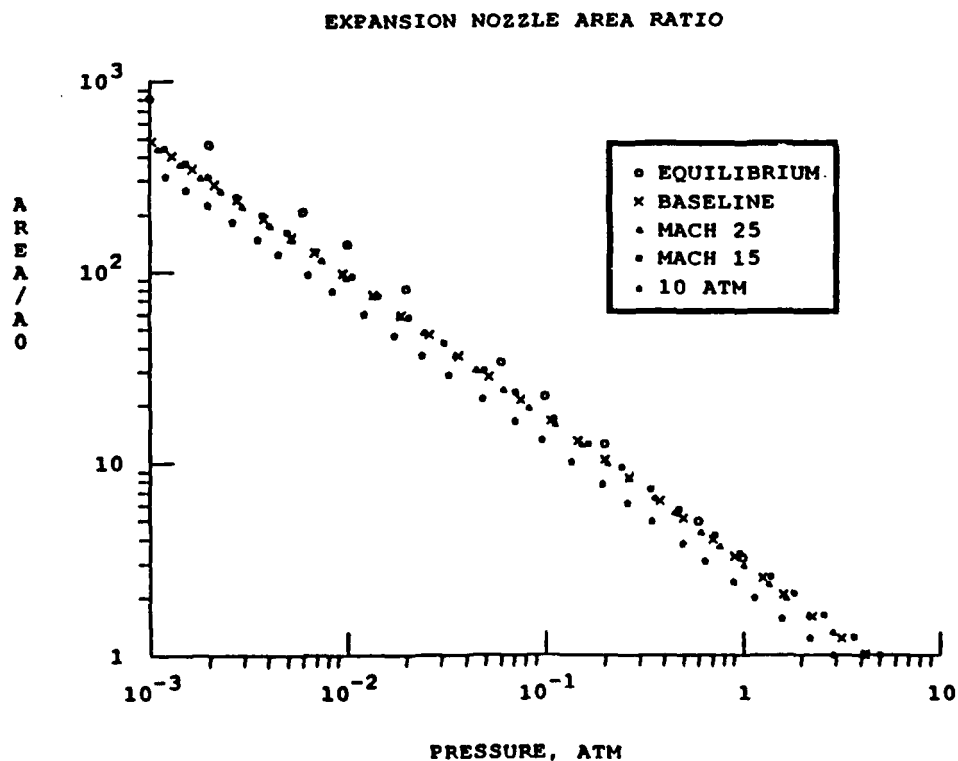
EXPANSION NOZZLE AREA RATIO

Figure 22. Expansion nozzle area ratio.

Table 8. Thermodynamic and Transport Properties, Nozzle Inlet

	base	m15	m25	rm20	.25h	r.25h	f125	f75	10s	10ss
ax dia -m	0.000E+00	0.000E+00	0.000E+00	0.000E+00	0.000E+00	0.000E+00	0.000E+00	0.000E+00	0.000E+00	0.000E+00
vel -m/s	5.649E+03	3.732E+03	7.168E+03	5.621E+03	5.564E+03	5.520E+03	5.295E+03	6.036E+03	5.730E+03	5.601E+03
pres -atm	4.100E+00	3.010E+00	4.060E+00	4.150E+00	4.590E+00	4.500E+00	4.000E+00	3.519E+00	2.059E+00	3.919E+00
temp -K	4.025E+03	3.406E+03	4.609E+03	3.990E+03	4.251E+03	4.219E+03	4.304E+03	3.724E+03	3.771E+03	3.074E+03
area/a0	1.000E+00	1.000E+00	1.000E+00	1.000E+00	1.000E+00	1.000E+00	1.000E+00	1.000E+00	1.000E+00	1.000E+00
mach	4.365E+00	3.262E+00	4.950E+00	4.373E+00	4.127E+00	4.113E+00	3.998E+00	4.939E+00	4.625E+00	4.517E+00
ht -kJ/kg	2.261E+04	1.146E+04	3.437E+04	2.233E+04	2.204E+04	2.250E+04	2.151E+04	3.309E+04	2.237E+04	2.229E+04
eq mhos/m	3.946E+02	1.504E+02	7.009E+02	3.000E+02	2.361E+02	2.397E+02	3.055E+02	3.047E+02	3.333E+02	3.359E+02
s kJ/kgK	1.002E+01	9.309E+00	1.050E+01	9.900E+00	1.021E+01	1.019E+01	1.017E+01	9.010E+00	9.954E+00	9.931E+00
rho kg/m3	3.339E-01	5.063E-01	2.627E-01	3.156E-01	3.304E-01	3.139E-01	3.557E-01	3.233E-01	4.777E-01	3.295E-01
mu N s/m2	1.013E-04	1.140E-05	1.116E-04	1.010E-04	1.051E-04	1.046E-04	1.059E-04	9.669E-05	9.741E-05	9.911E-05
k J/m sec	1.773E-01	1.331E-01	2.500E-01	1.739E-01	1.999E-01	1.965E-01	2.052E-01	1.501E-01	1.561E-01	1.631E-01
Pr no	6.907E-01	6.897E-01	7.055E-01	6.903E-01	9.945E-01	9.399E-01	6.950E-01	6.000E-01	6.070E-01	6.091E-01
Re no	1.050E+07	2.062E+07	1.607E+07	1.069E+07	1.792E+07	1.001E+07	1.770E+07	1.950E+07	1.457E+07	1.099E+07

Mole Fractions

	base	m15	m25	rm20	.25h	r.25h	f125	f75	10s	10ss
ar	0.567E-03	9.177E-03	0.005E-03	0.599E-03	0.504E-03	0.530E-03	0.363E-03	0.025E-03	0.723E-03	0.699E-03
e	1.113E-02	1.207E-02	0.056E-03	1.125E-02	0.793E-04	9.076E-04	1.015E-02	1.207E-02	1.179E-02	1.163E-02
h+	1.035E-02	4.017E-04	0.494E-03	1.736E-02	7.208E-04	7.031E-04	2.619E-03	1.150E-03	1.306E-03	1.456E-03
ho	4.990E-04	1.069E-03	1.549E-04	5.211E-04	3.309E-05	3.541E-05	3.720E-04	4.467E-04	5.203E-04	5.014E-04
ho-	0.000E+00	0.000E+00	0.000E+00	0.000E+00	0.000E+00	0.000E+00	0.000E+00	0.000E+00	0.000E+00	0.000E+00
o2	6.443E-01	7.153E-01	6.329E-01	6.667E-01	6.601E-01	6.619E-01	6.493E-01	6.057E-01	6.701E-01	6.746E-01
n	7.676E-04	5.244E-05	5.940E-03	6.796E-04	1.580E-03	1.427E-03	1.000E-03	2.637E-04	3.537E-04	4.546E-04
no	6.140E-02	5.806E-02	4.272E-02	6.107E-02	5.000E-02	5.960E-02	5.735E-02	6.191E-02	9.979E-02	6.250E-02
no2	1.947E-05	4.176E-05	5.144E-06	2.043E-05	1.499E-05	1.575E-05	1.400E-05	5.438E-05	0.286E-05	2.296E-05
n2o	6.223E-06	6.524E-06	0.000E+00	6.246E-06	6.317E-06	6.391E-06	6.322E-06	5.772E-06	0.000E+00	6.116E-06
o	1.002E-01	6.370E-02	2.793E-01	1.010E-01	2.350E-01	2.306E-01	2.305E-01	1.357E-01	1.544E-01	1.615E-01
o2	6.144E-02	1.379E-01	1.485E-02	6.311E-02	4.203E-02	4.550E-02	3.095E-02	9.300E-02	0.150E-02	1.700E-02
e	1.737E-03	4.415E-04	1.642E-03	1.642E-03	6.936E-04	6.603E-04	2.494E-03	1.048E-03	3.199E-03	1.373E-03
o-	9.179E-05	3.090E-05	1.246E-04	0.024E-05	3.363E-05	3.192E-05	1.200E-04	5.932E-05	6.106E-05	7.561E-05
o2-	5.265E-06	6.054E-06	0.000E+00	5.412E-06	0.000E+00	0.000E+00	0.000E+00	5.617E-06	0.000E+00	5.640E-06

Table 9a. Thermodynamic and Transport Properties, Combustor Inlet

	base	m15	m25	rm20	.25h	r.25h	f125	f75	10s	10ss
ax dia -m	2.270E-01	2.430E-01	2.397E-01	2.300E-01	2.462E-01	2.495E-01	2.630E-01	1.977E-01	1.921E-01	2.155E-01
vel -m/s	6.004E+03	4.164E+03	7.515E+03	5.975E+03	5.972E+03	5.930E+03	5.745E+03	6.312E+03	5.999E+03	6.006E+03
pres -atm	5.945E-01	5.003E-01	5.601E-01	5.030E-01	5.020E-01	5.693E-01	5.573E-01	5.935E-01	5.909E-01	5.945E-01
temp -K	3.017E+03	2.200E+03	3.320E+03	2.779E+03	2.941E+03	2.906E+03	2.940E+03	2.615E+03	2.765E+03	2.713E+03
area/a0	2.212E-01	2.054E-01	2.193E-01	2.026E-01	2.026E-01	1.996E-01	1.875E-01	2.540E-01	2.594E-01	2.363E-01
mach	5.619E+00	4.554E+00	6.341E+00	5.639E+00	5.411E+00	5.414E+00	5.214E+00	6.199E+00	5.690E+00	5.763E+00
ht -kJ/kg	2.261E+04	1.146E+04	3.437E+04	2.233E+04	2.204E+04	2.250E+04	2.151E+04	3.309E+04	2.237E+04	2.229E+04
eq mhos/m	6.566E+01	3.144E+00	2.210E+02	7.076E+01	4.044E+01	5.930E+01	1.310E+02	1.142E+01	7.466E+01	6.401E+01
s kJ/kgK	1.003E+01	9.397E+00	1.050E+01	9.999E+00	1.023E+01	1.020E+01	1.010E+01	9.037E+00	9.964E+00	9.920E+00
rho kg/m3	6.947E-03	5.296E-02	5.476E-02	6.925E-02	6.300E-02	6.342E-02	6.148E-02	7.610E-02	7.007E-02	7.209E-02
mu N s/m2	0.077E-05	6.095E-05	0.782E-05	0.001E-05	0.293E-05	0.332E-05	0.391E-05	7.693E-05	7.974E-05	7.076E-05
k J/m sec	1.134E-01	1.163E-02	1.032E-01	1.114E-01	1.212E-01	1.193E-01	1.216E-01	1.020E-01	1.097E-01	1.072E-01
Pr no	6.745E-01	6.030E-01	6.691E-01	6.747E-01	7.300E-01	6.732E-01	6.727E-01	6.765E-01	6.751E-01	6.756E-01
Re no	5.160E+06	5.614E+06	4.606E+06	5.172E+06	4.600E+06	4.560E+06	4.360E+06	6.244E+06	5.320E+06	5.557E+06

Mole Fractions

	base	m15	m25	rm20	.25h	r.25h	f125	f75	10s	10ss
ar	0.790E-03	9.202E-03	0.310E-03	0.816E-03	0.774E-03	0.799E-03	0.661E-03	0.954E-03	0.050E-03	0.001E-03
e	1.290E-02	1.334E-02	1.190E-02	1.301E-02	1.514E-03	1.527E-03	1.376E-02	1.322E-02	1.310E-02	1.311E-02
h+	2.474E-04	2.140E-05	0.620E-04	2.196E-04	1.347E-04	1.300E-04	9.032E-04	1.220E-04	2.104E-04	1.731E-04
ho	5.901E-04	1.222E-03	2.164E-04	6.139E-04	4.506E-05	4.763E-05	4.661E-04	7.200E-04	5.943E-04	6.729E-04
ho-	4.019E-07	1.094E-06	1.206E-07	4.210E-07	1.020E-06	1.099E-06	2.900E-07	5.470E-07	4.104E-07	4.795E-07
o2	6.024E-01	7.236E-01	6.552E-01	6.042E-01	6.026E-01	6.042E-01	6.742E-01	6.954E-01	6.002E-01	6.092E-01
n	1.072E-05	7.992E-06	1.603E-06	5.560E-06	3.369E-05	1.944E-05	2.385E-05	2.122E-06	7.931E-06	5.520E-06
no	6.226E-02	5.953E-02	7.030E-02	6.270E-02	5.914E-02	6.010E-02	5.765E-02	6.250E-02	6.032E-02	6.330E-02
no2	3.320E-06	2.611E-06	1.009E-06	3.254E-06	3.154E-06	3.126E-06	2.994E-06	3.153E-06	3.390E-06	3.302E-06
n2o	6.770E-06	6.590E-06	1.092E-06	6.309E-06	6.095E-06	6.570E-06	6.520E-06	5.009E-06	5.593E-06	6.333E-06
o	1.450E-01	4.260E-02	2.449E-01	1.397E-01	1.722E-01	1.671E-01	1.719E-01	1.107E-01	1.324E-01	1.261E-01
o2	0.740E-02	1.504E-01	3.910E-02	9.046E-02	7.534E-02	7.793E-02	7.362E-02	1.000E-01	9.607E-02	0.034E-02
e	2.260E-04	1.421E-03	0.201E-04	2.000E-04	1.242E-04	1.300E-04	1.526E-04	1.065E-04	1.871E-04	1.547E-04
o-	1.949E-05	3.591E-06	3.770E-05	1.026E-05	6.667E-06	8.251E-06	2.356E-05	1.341E-05	1.717E-05	1.602E-05
o2-	5.730E-07	1.044E-07	5.075E-07	5.445E-07	2.316E-07	2.140E-07	5.093E-07	4.570E-07	5.603E-07	5.164E-07

Table 9b. Thermodynamic and Transport Properties, Free Stream

	base	m15	m25	rm20	.25h	r.25h	f125	f75	10s	10ss
ax dia -m	3.505E+00	3.537E+00	3.401E+00	3.526E+00	3.432E+00	3.609E+00	3.726E+00	3.321E+00	3.416E+00	3.404E+00
vel -m/s	6.444E+03	4.622E+03	7.937E+03	6.410E+03	6.441E+03	6.394E+03	6.227E+03	6.946E+03	6.437E+03	6.250E+03
pres -atm	1.648E-03	1.650E-03	1.692E-03	1.600E-03	1.650E-03	1.602E-03	1.626E-03	1.574E-03	1.670E-03	1.660E-03
temp -K	4.433E+02	4.993E+02	7.266E+02	6.332E+02	6.992E+02	6.770E+02	6.790E+02	5.975E+02	3.495E+02	6.204E+02
area/a0	2.097E-03	2.035E-03	3.000E-03	2.064E-03	2.713E-03	2.763E-03	2.744E-03	3.203E-03	3.967E-03	2.067E-03
mach	1.320E+01	1.026E+01	1.300E+01	1.333E+01	1.104E+01	1.198E+01	1.147E+01	1.347E+01	1.277E+01	1.353E+01
ht -kJ/kg	2.281E+04	1.146E+04	3.437E+04	2.333E+04	2.204E+04	2.250E+04	2.151E+04	3.309E+04	2.237E+04	2.229E+04
eq mhos/m	6.544E-05	1.441E-06	2.921E-06	6.275E-07	2.130E-05	6.600E-05	4.718E-05	3.320E-05	5.901E-05	3.542E-05
s kJ/kgK	1.005E+01	9.409E+00	1.053E+01	1.002E+01	1.025E+01	1.032E+01	1.020E+01	9.047E+00	9.902E+00	9.939E+00
rho kg/m3	0.470E-04	1.156E-03	7.307E-04	4.429E-04	7.931E-04	0.017E-04	7.017E-04	6.016E-04	7.559E-04	8.937E-04
mu N s/m2	3.095E-05	3.610E-05	3.341E-05	3.063E-05	3.206E-05	3.202E-05	3.205E-05	9.154E-05	3.069E-05	3.023E-05
k J/m sec	3.915E-02	2.907E-02	4.695E-02	3.802E-02	4.109E-02	4.165E-02	4.194E-02	1.507E-02	3.546E-02	3.777E-02
Pr no	6.736E-01	6.030E-01	6.630E-01	6.742E-01	6.711E-01	6.716E-01	6.700E-01	7.670E-01	6.745E-01	6.754E-01
Re no	1.765E+05	3.041E+05	1.766E+05	1.764E+05	1.593E+05	1.614E+05	1.519E+05	2.071E+05	1.034E+05	1.900E+05

Mole Fractions

	base	m15	m25	rm20	.25h	r.25h	f125	f75	10s	10ss
ar	0.030E-03	9.395E-03	0.377E-03	0.060E-03	0.031E-03	0.057E-03	0.710E-03	0.905E-03	0.091E-03	0.921E-03
e	1.322E-02	1.333E-02	1.204E-02	1.323E-02	1.420E-03	1.631E-03	1.315E-02	1.333E-02	1.330E-02	1.327E-02
h+	3.107E-05	9.950E-06	7.460E-05	0.010E-05	1.191E-05	1.191E-05	1.300E-05	3.145E-05	3.730E-05	3.730E-05
ho	6.709E-04	1.261E-03	2.404E-04	6.539E-04	5.025E-05	5.375E-05	5.069E-04	7.642E-04	6.337E-04	7.126E-04
ho-	2.323E-06	3.172E-06	9.907E-07	4.200E-06	1.197E-07	1.252E-07	1.000E-06	2.763E-06	2.104E-06	2.540E-06
o2	6.061E-01	7.346E-01	6.607E-01	6.077E-01	6.071E-01	6.004E-01	7.707E-01	6.900E-01	6.915E-01	6.923E-01
n	3.346E-12	1.350E-12	3.115E-12	2.304E-12	2.490E-13	3.459E-12	1.054E-13	3.002E-13	2.061E-12	2.061E-12
no	6.259E-02	5.961E-02	3.045E-02	6.309E-02	5.950E-02	6.045E-02	5.001E-02	6.200E-02	6.660E-02	6.366E-02
no2	1.977E-06	1.376E-07	4.605E-09	2.144E-06	1.160E-06	1.359E-06	1.037E-06	4.446E-06	3.696E-06	2.916E-06
n2o	6.404E-06	6.599E-06	1.707E-06	6.420E-06	6.536E-06	6.609E-06	6.563E-06	5.029E-06	6.604E-06	6.266E-06
o	1.355E-01	3.994E-02	3.325E-01	1.107E-01	1.607E-01	1.562E-01	1.605E-01	1.043E-01	1.211E-01	1.181E-01
o2	9.307E-02	1.520E-01	4.670E-02	9.573E-02	0.314E-02	0.441E-02	0.032E-02	1.117E-01	0.108E-01	0.300E-01
e	2.510E-10	3.165E-10	1.961E-09	3.637E-10	2.012E-10	3.590E-10	4.502E-10	2.020E-10	4.246E-10	2.200E-10
o-	2.057E-05	3.099E-06	7.016E-05	2.732E-05	2.023E-05	3.319E-05	3.096E-05	1.996E-05	1.403E-05	2.297E-05
o2-	6.023E-12	4.145E-13	1.790E-11	5.336E-12	5.917E-12	5.076E-12	7.009E-12	4.309E-12	5.005E-12	4.924E-12

5.5.3.1 Area Ratio

Different nozzle area ratios are required to get the desired simulations (Fig. 22) depending on the channel operating conditions. The finite rate chemical effects (cases 1 and 11) reduce the area required to achieve a given simulation, particularly for the expansions to free-stream conditions. The channel with a 10-atm inlet pressure (case 9) has a lower exit pressure and requires a smaller area ratio than the cases at 20 atm pressure for any given simulation. For combustor inlet testing it might be possible to simulate different flight Mach numbers (cases 1, 2, and 3) with the same nozzle since the combustor pressure does not change a great deal with flight Mach number. For free-stream simulation, different nozzles would be required. These results are based on not having a boundary layer so that the actual nozzles would have somewhat larger area ratios.

5.5.3.2 Mach Number Simulation

The effect of varying the channel operating parameters to simulate a range of Mach numbers on the expansion nozzle Mach number, temperature, and velocity is shown in Figs. 23, 24, and 25 as a function of nozzle pressure for cases 1, 2, and 3. The combustor inlet and free-stream conditions from Ref. 4 are indicated on the plots by the notation q = 1,000. The predicted velocities agree quite well (Fig. 25) with the velocities for the q = 1,000 flight case for both the combustor inlet and free-stream conditions for Mach 15 to Mach 25 flight conditions. The combustor inlet temperature (Fig. 24) is about 200 K low for the Mach 25 case and the same amount high for the Mach 15 case. The temperature after expansion to the free-stream pressure is high for all Mach numbers. The Mach number (Fig. 23) differences depend primarily on temperature since the velocities agree. Mach number is well matched at the combustor inlet conditions and low for the free-stream conditions.

5.5.3.3 Initial Accelerator Conductivity

Reducing the initial channel conductivity is expected to reduce the channel performance. Cases 4, 5, and 6 give examples where this will occur by reducing the potassium concentration and/or temperature at the accelerator inlet. The result of this change on the gas properties during the nozzle expansion is shown in Figs. 26, 27, and 28 for Mach number, temperature, and velocity as a function of pressure. These parameters for the baseline and the baseline equilibrium expansion are also shown for comparison. The results of the expansions differ little from the baseline case as would be expected since the accelerator exit properties show only a marginal decrease in performance as the initial conductivity is reduced.

15 DEG HALF ANGLE K/AIR
VARIABLE ACCELERATION
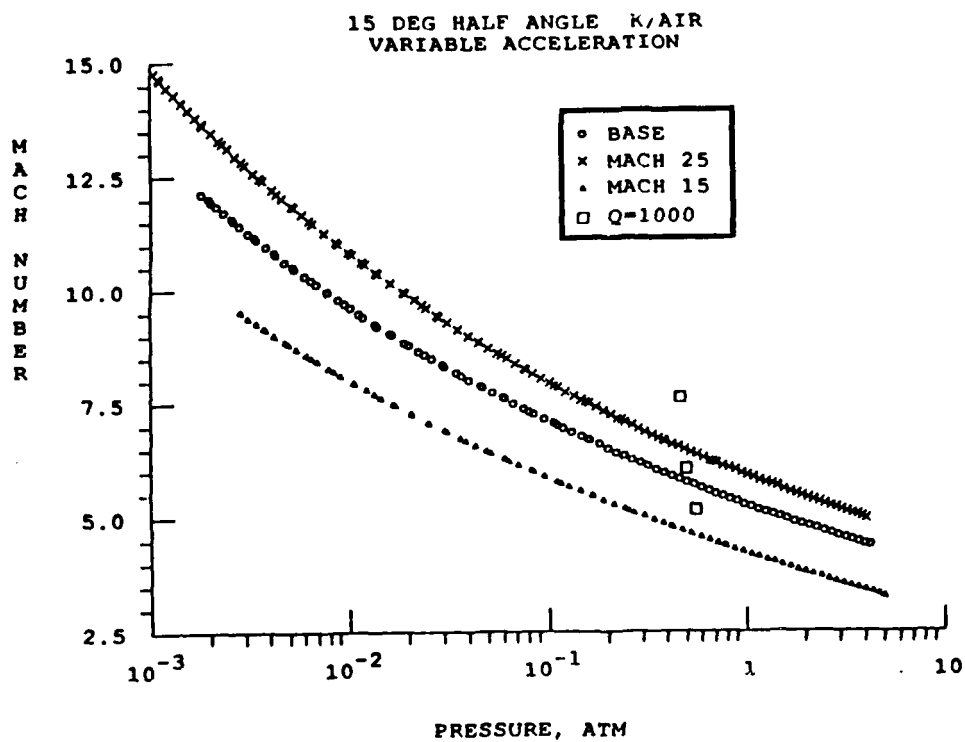
Figure 23. Finite rate expansion, mach number versus pressure.

15 DEG HALF ANGLE K/AIR
VARIABLE ACCELERATION
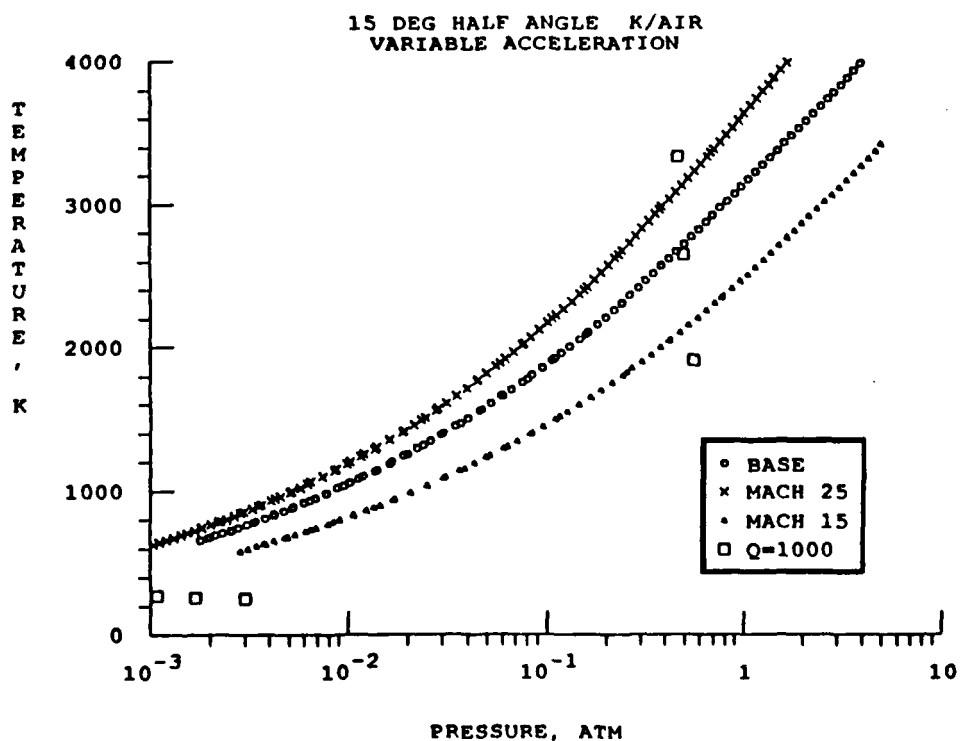
Figure 24. Finite rate expansion, temperature versus pressure.

15 DEG HALF ANGLE K/AIR
VARIABLE ACCELERATION

o BASE
x MACH 25
▲ MACH 15
□ Q=1000
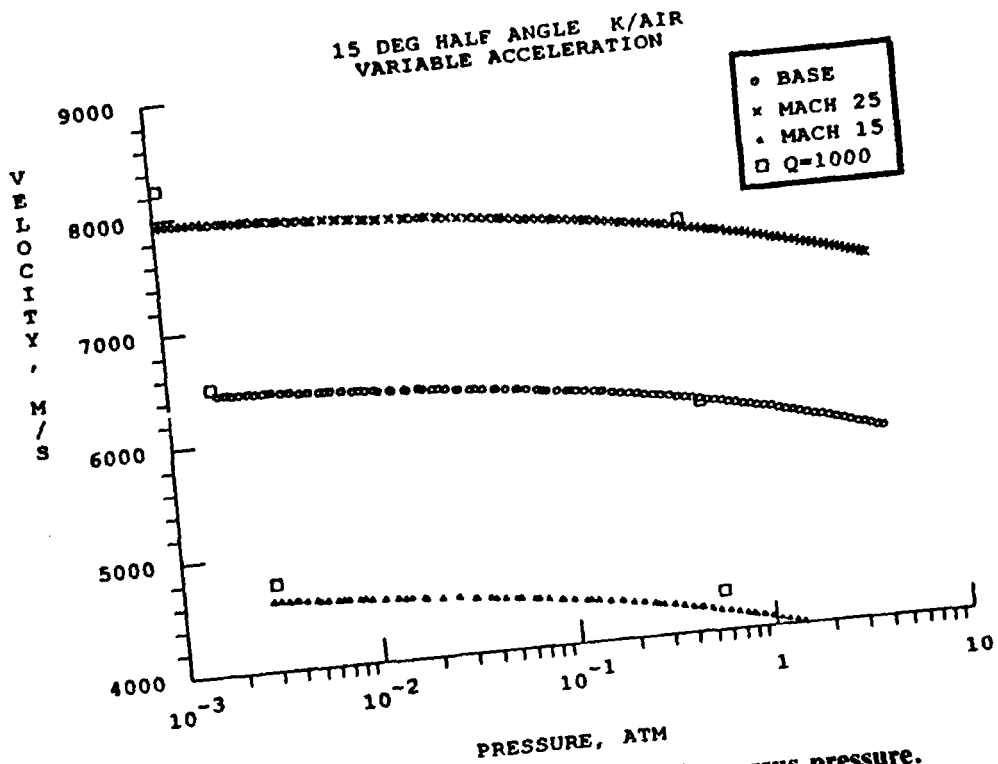
Figure 25. Finite rate expansion, velocity versus pressure.

15 DEG HALF ANGLE K/AIR
REDUCED ARC HEATER AND K

o BASE
x RED AC
▲ .25%K
• RED .25%K
• BASE EQ
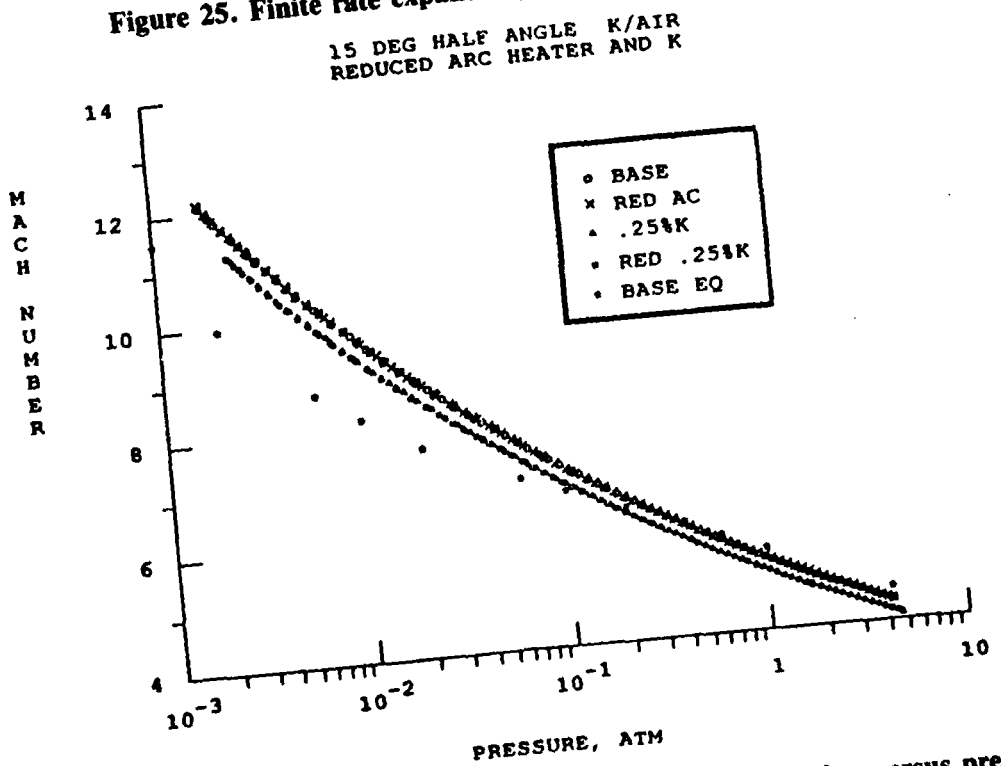
Figure 26. Heater and seed trade study expansions, Mach number versus pressure.

53
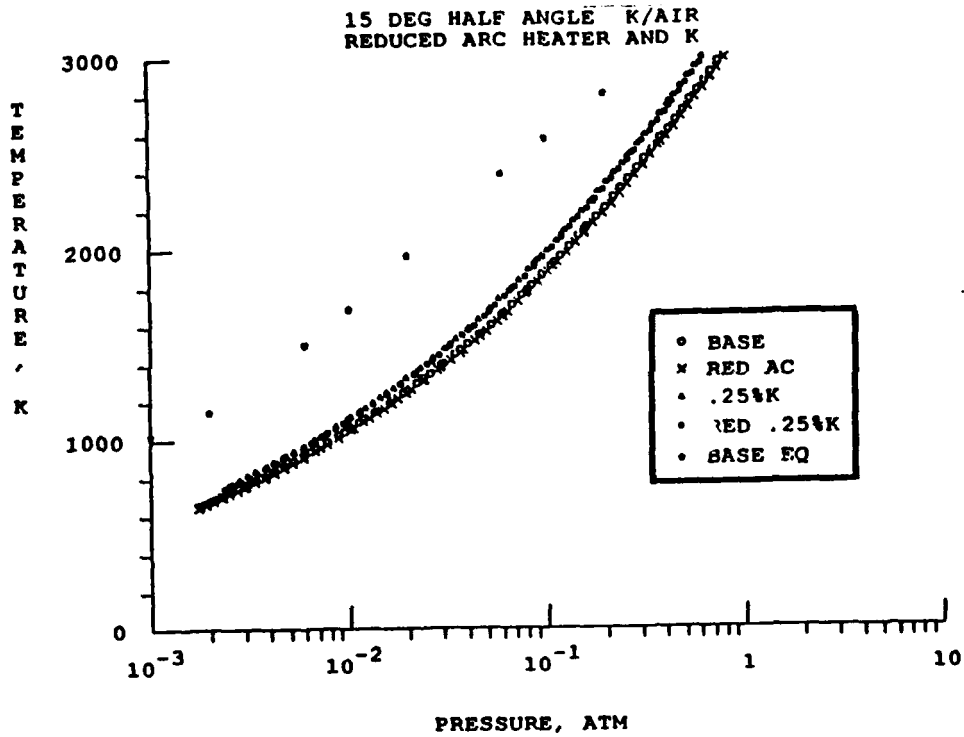
Figure 27. Heater and seed trade study expansions, temperature versus pressure.

Figure 28. Heater and seed trade study expansions, velocity versus pressure.

Figure 29. Friction trade study expansions, Mach number versus pressure.

Figure 30. Friction trade study expansions, temperature versus pressure.

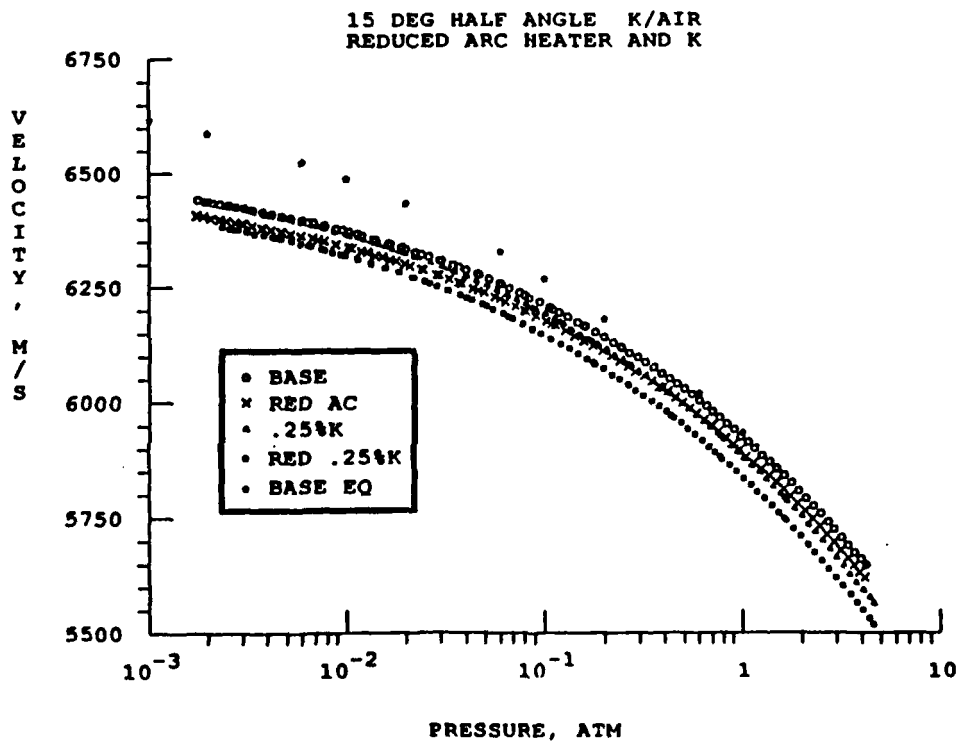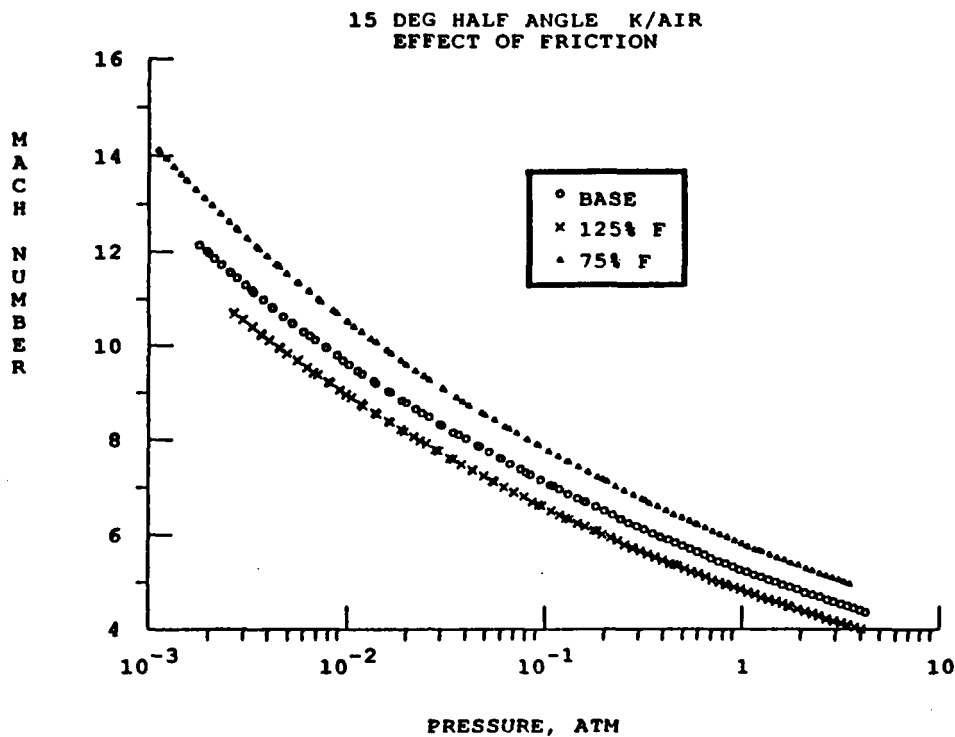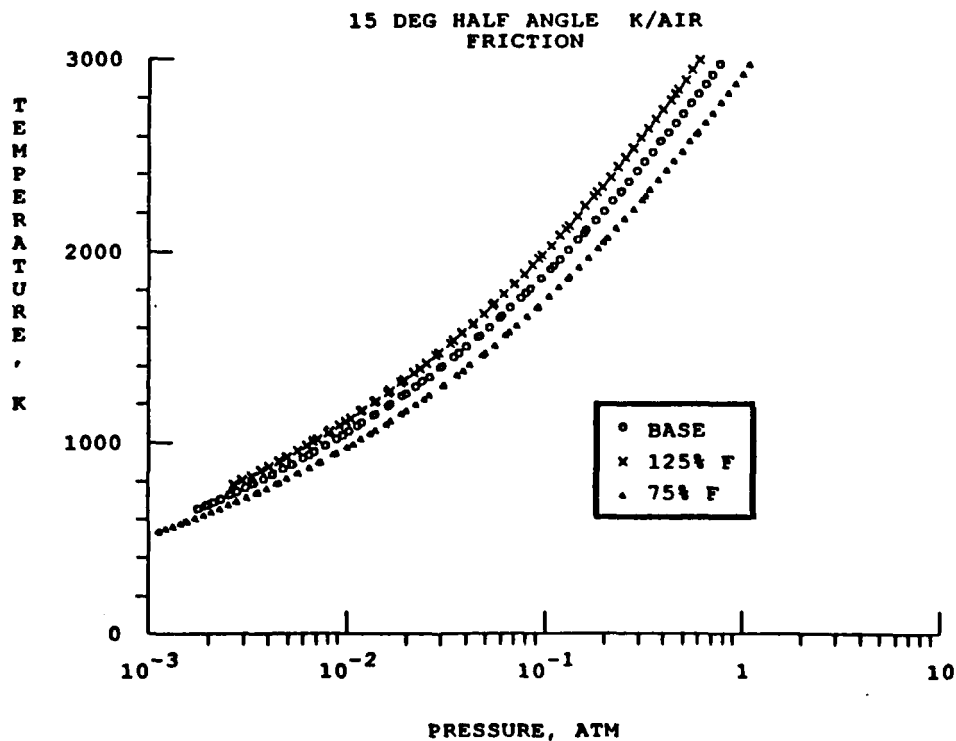55
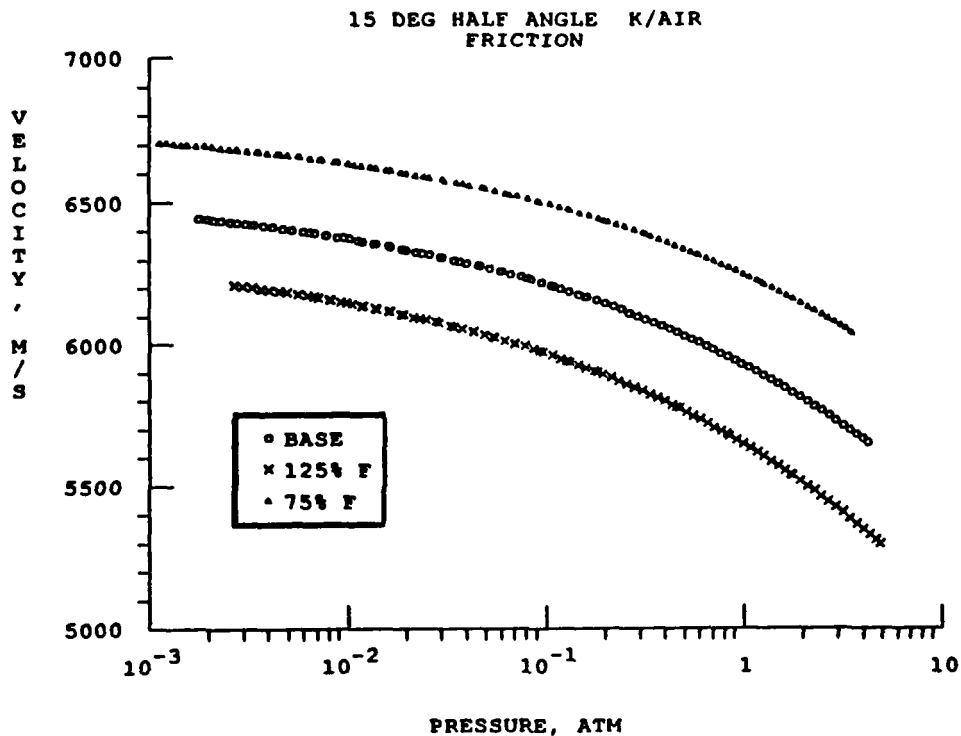
Figure 31. Friction trade study expansions, velocity versus pressure.
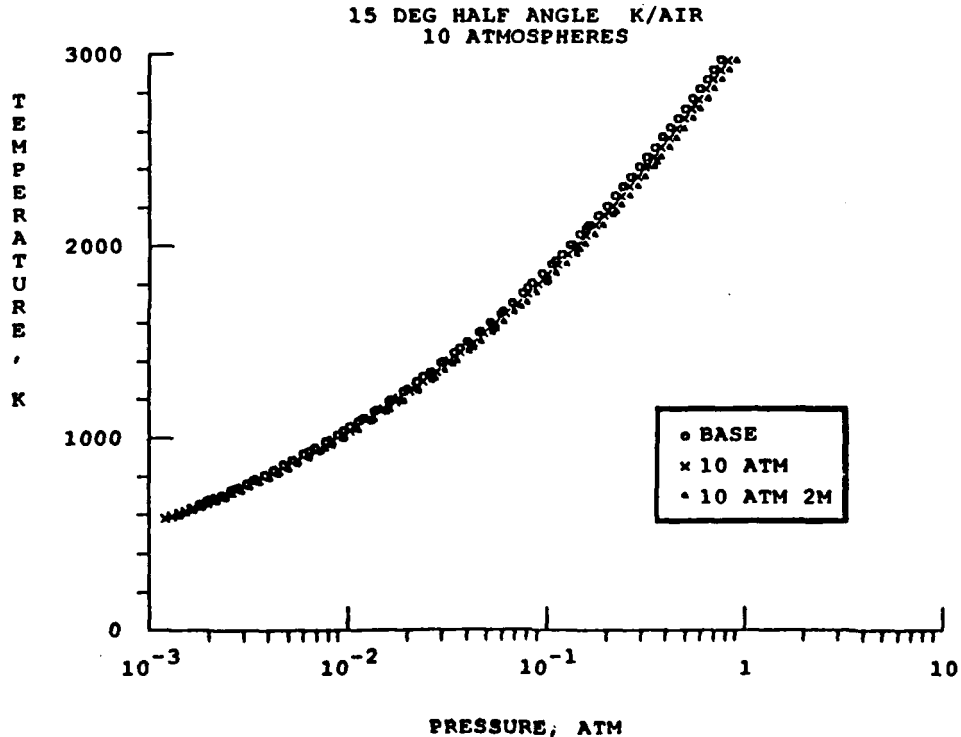
Figure 32. Channel pressure trade study expansions, temperature versus pressure.

5.5.3.4 Accelerator Wall Friction

The assumed value of wall roughness and friction (cases 1, 7, and 8) has a large effect on the accelerator channel performance and shows a correspondingly large effect on the predicted Mach number, temperature, and velocity during the nozzle expansion (Figs. 29, 30, and 31) when compared with the baseline case. With the exception of the free-stream temperature and Mach number simulation the performance with either increased or reduced friction gives a poorer simulation of these properties. This result would be expected to change if the accelerator channel power were adjusted to account for the change in friction.

5.5.3.5 Accelerator Pressure

The effect of lower accelerator pressure and reduced accelerator length (cases 9 and 10) on temperature and velocity during the nozzle expansion are shown in Figs. 32 and 33 as a function of nozzle pressure. There are only marginal differences from the baseline in the properties obtained from the expansion of these cases.

5.5.4 Implications for Combustor Testing

Species concentrations during an expansion with finite rate chemistry are compared with those during an equilibrium expansion at corresponding pressures. The ionic species are nearly in equilibrium at a pressure typical of a combustor inlet and are essentially gone when free-stream pressure is reached (Fig. 34). The oxygen bearing species (O2, O, and NO) freeze their composition rapidly (Fig. 35). There is almost no change in the NO, and roughly half the O recombines. Because of the high combustor inlet temperature proposed for flight at Mach numbers greater than 15, the O and NO concentrations do not seem to have much effect on the kinetics of the reaction between the 'air' and H2. A one-dimensional, fully mixed ignition and combustion calculation was made to compare the reaction progress for a stoichiometric mixture of H2 with equilibrium air and with the simulated air from the baseline case at the same pressure and entropy. The effect of the potassium on combustion of H2 was also investigated by using equilibrium air with 2-percent K as the oxidizer. In addition to the reactions used in the nozzle expansion, nine reactions for the hydrogen-bearing species are considered for the combustion of hydrogen with air. These are:

Reaction					A	n	E
H	+ O2		= OH	+ O	0.2199E + 15	0.0	16800.0
O	+ H2		= OH	+ H	0.1699E + 14	0.0	9460.0
OH	+ H2		= H2O	+ H	0.2199E + 14	0.0	5200.0
OH	+ OH		= H2O	+ O	0.6005E + 13	0.0	780.0
H	+ OH	+ M	= H2O	+ M	0.7003E + 20	1.0	0.0
O	+ H	+ M	= OH	+ M	0.3991E + 19	1.0	0.0
H	+ H	+ M	= H2	+ M	0.2003E + 20	1.0	0.0
K	+ H2O		= + KOH	+ H	0.6023E + 14	0.0	-10000.0
H	+ NO		= OH	+ N	0.3460E + 13	-0.5x7	-47800.0

15 DEG HALF ANGLE K/AIR
10 ATMOSPHERES
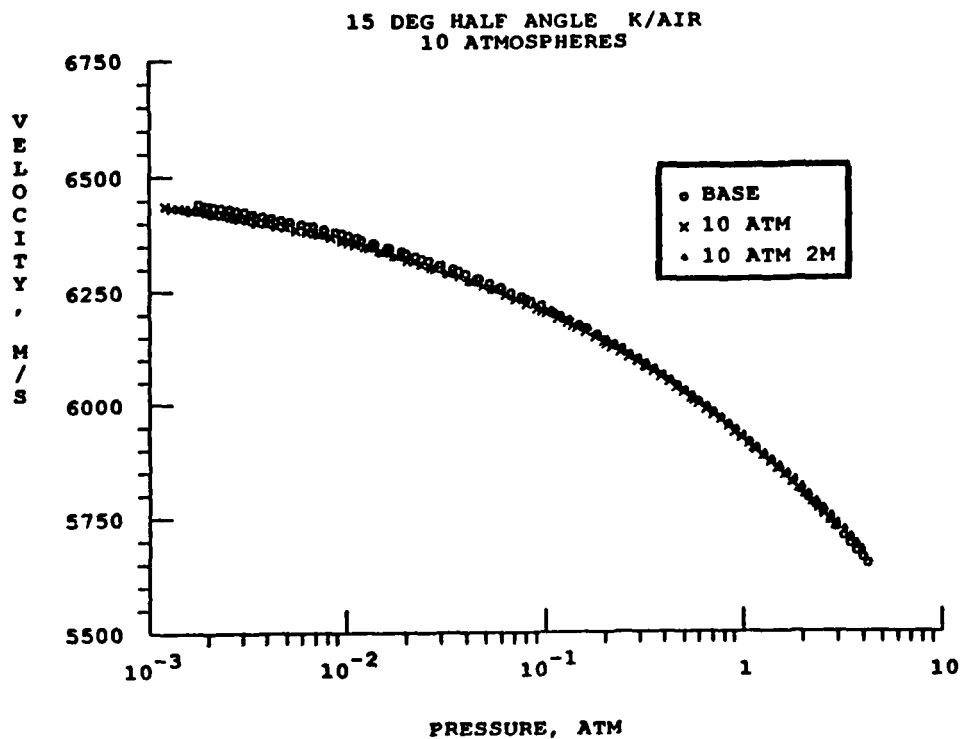
Figure 33. Channel pressure trade study expansions, velocity versus pressure.

15 DEG HALF ANGLE K/AIR
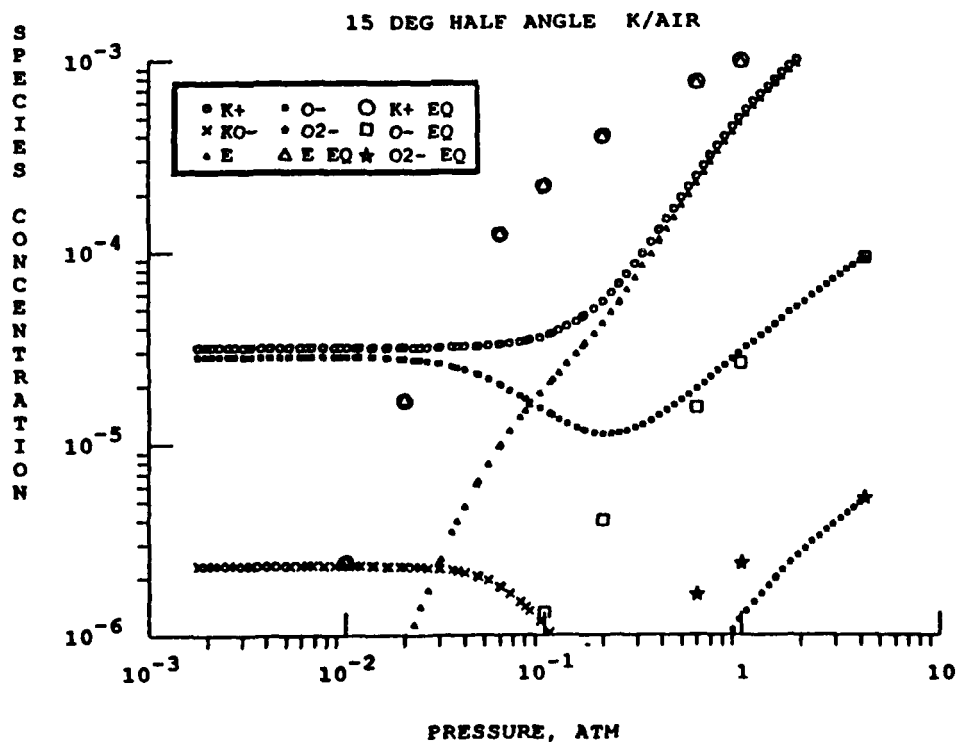
Figure 34. Species (neg.) concentration finite rate expansion.
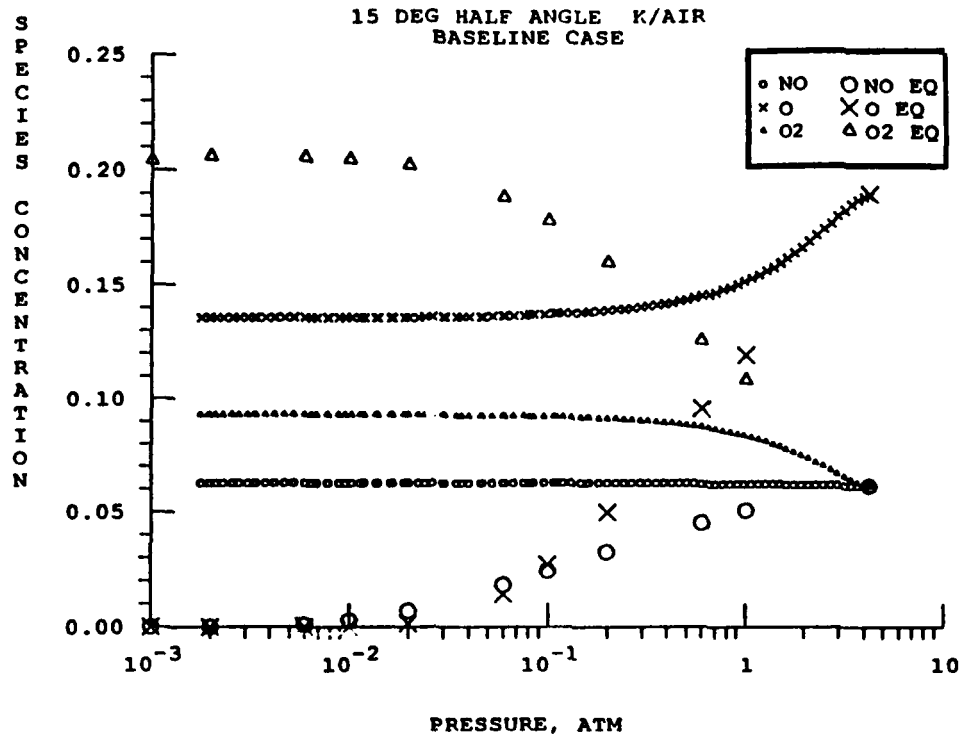
Figure 35. Species (oxygen) concentration finite rate expansion.
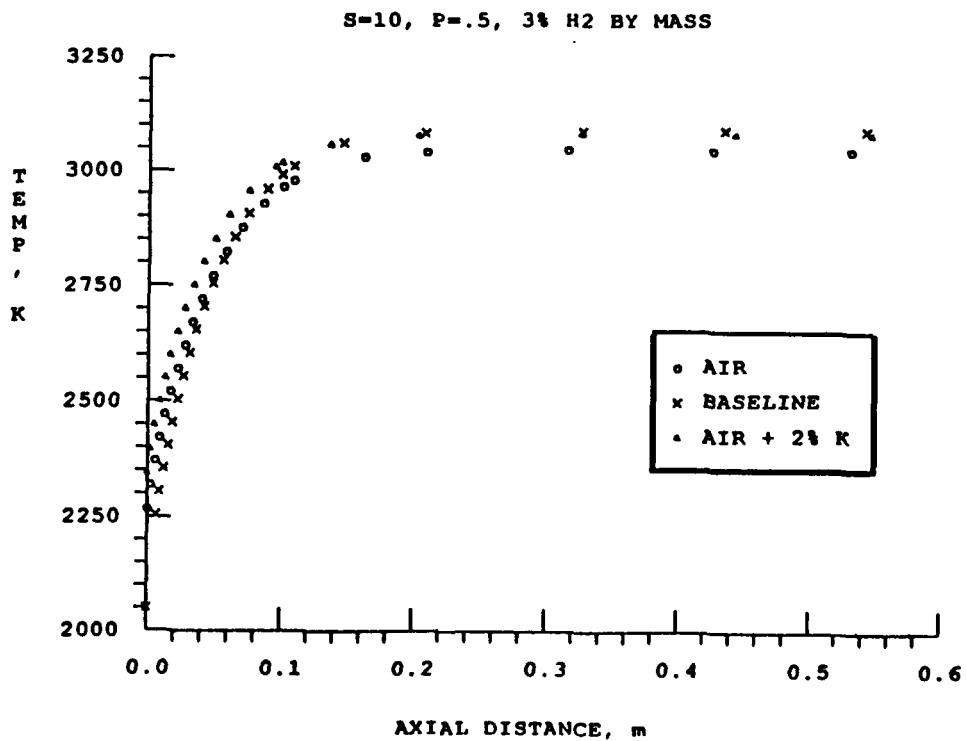
Figure 36. Constant pressure combustion with H₂ and air.

where the forward rate is $Kf = Ae^{-E/RT}/T^n$. The results (Fig. 36) indicate that the reactions are very fast (< 100 μsec to equilibrium for all cases). There is about a 30 K difference in temperature at equilibrium between the cases with and without the 2-percent potassium. This appears to be a difference in the enthalpy caused by the potassium when the entropy is fixed as it was for this example.

5.5.5 Implications for Aerodynamic and Thermal Testing

The implications of using this gas for aerodynamic or thermal testing need to be studied, considering the large amount of energy tied up in the disassociated oxygen. As shown above, true temperature simulation of free-stream conditions was not achieved in any of test cases and may not even be practical considering the difficulty in starting the MHD acceleration process at entropies below 8.25 kJ/kg. The high temperatures will result in low Mach numbers for the simulation. Some additional parameters of interest in various types of testing were calculated to show the type of simulation which might be expected. The Prandtl number for the baseline case was evaluated during the nozzle expansion as a function of temperature (Fig. 37) and found to be only marginally different from air. Reynolds number (Fig. 38) agrees well at the combustor inlet, but is about a factor of 5 low for the free-stream conditions. This occurs since density (Fig. 39) is low and with high T's, viscosity is high. However, the similarity parameters $M^2/\sqrt{(Re)}$ and $M/\sqrt{(Re)}$ (Figs. 40 and 41) agree fairly well for all the cases.

5.6 NONEQUILIBRIUM ACCELERATOR CALCULATIONS

The one-dimensional accelerator model used for these studies contains anassumption of chemical equilibrium. A calculation of the baseline accelerator performance was made with the finite rate chemistry code including the MHD terms in the momentum and energy equations (Section 4.4). The $J \times B$ force and the J^2/σ heating term were obtained from the equilibrium calculation. The chemical rate equations were the same as those used in the nozzle expansion calculations. The electrical conductivity profile (Fig. 42) along the channel is nearly identical in both codes. Since the MHD terms for a specified B-field and current depend only on conductivity, it appears that at least at these operating conditions there is no loss in computational accuracy by neglecting the chemical nonequilibria in the accelerator calculations. The exit conditions for the two calculations show only marginal differences in their chemical and thermodynamic properties, as presented in Table 10.
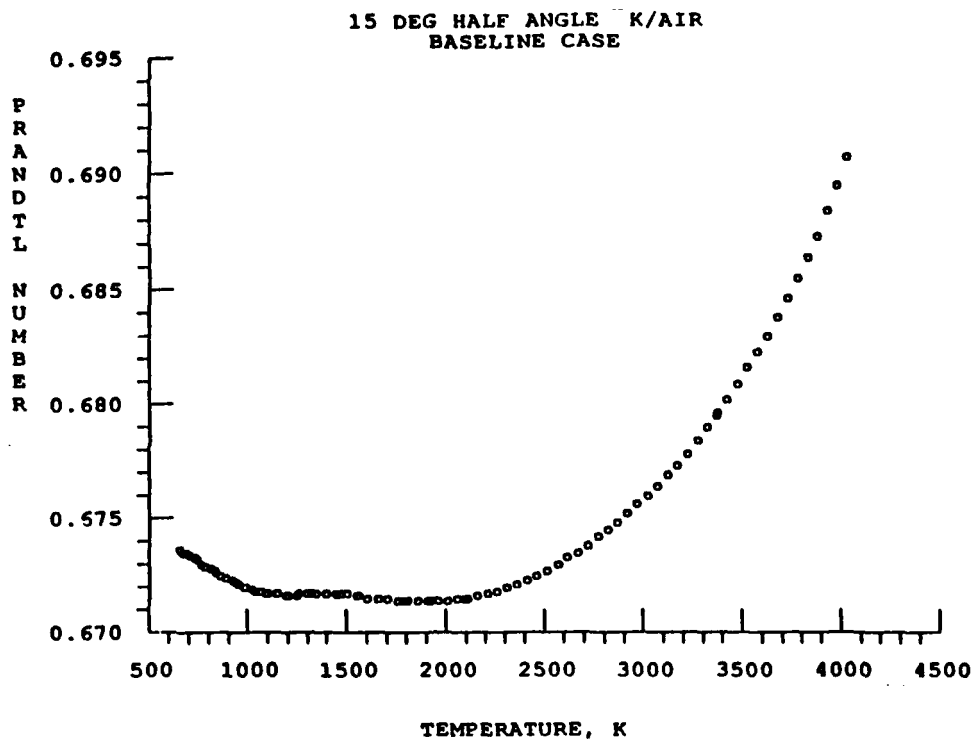
Figure 37. Base case finite rate expansion, Prandtl number.
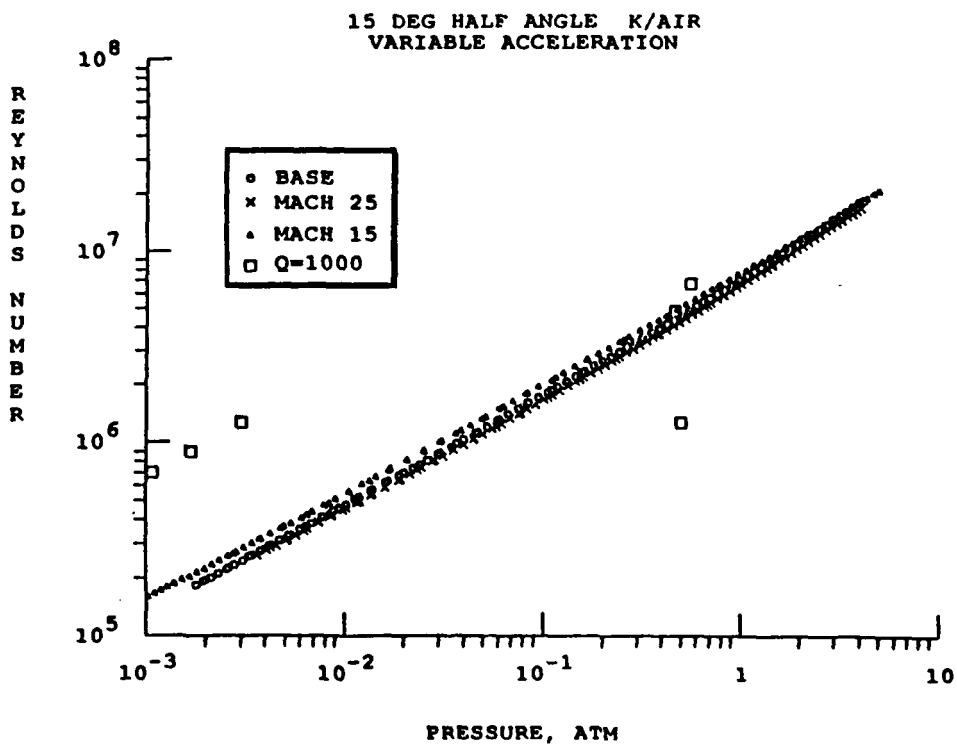
Figure 38. Base case, finite rate expansions, Reynolds number.
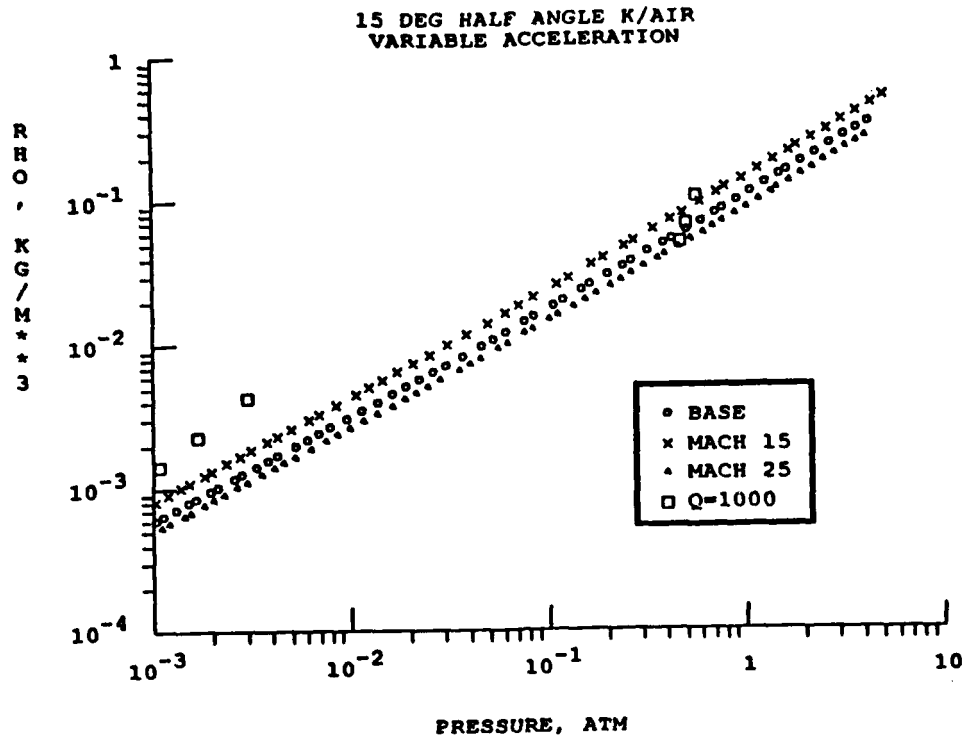
Figure 39. Base case, finite rate expansions, density.
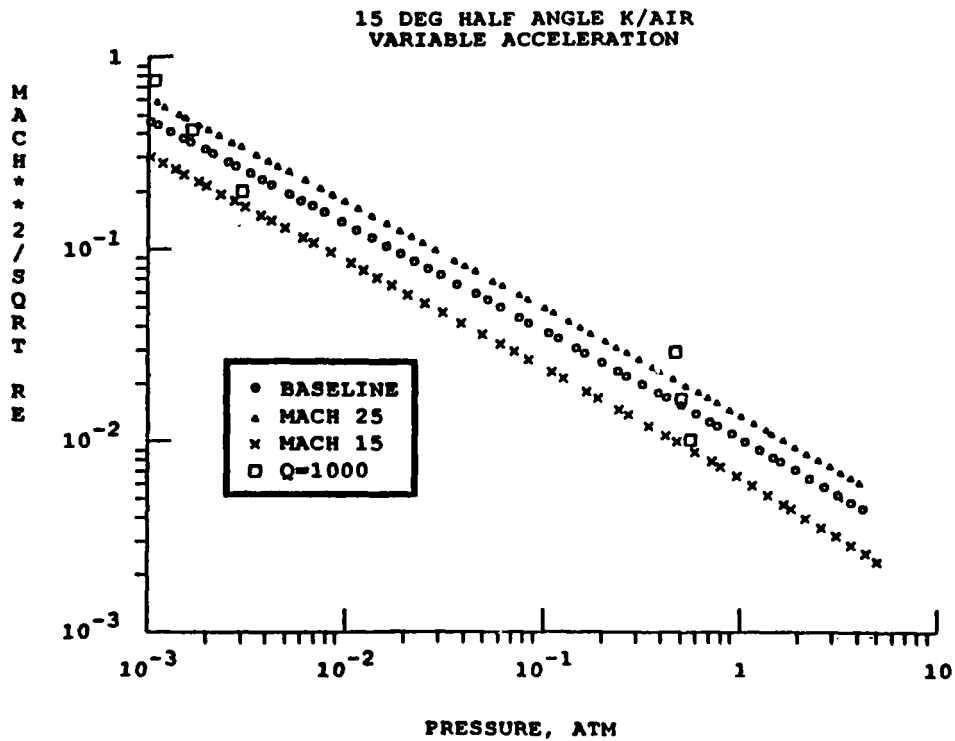
Figure 40. Base case, finite rate expansions, $M^2/\sqrt{Re}$.

15 DEG HALF ANGLE K/AIR
VARIABLE ACCELERATION
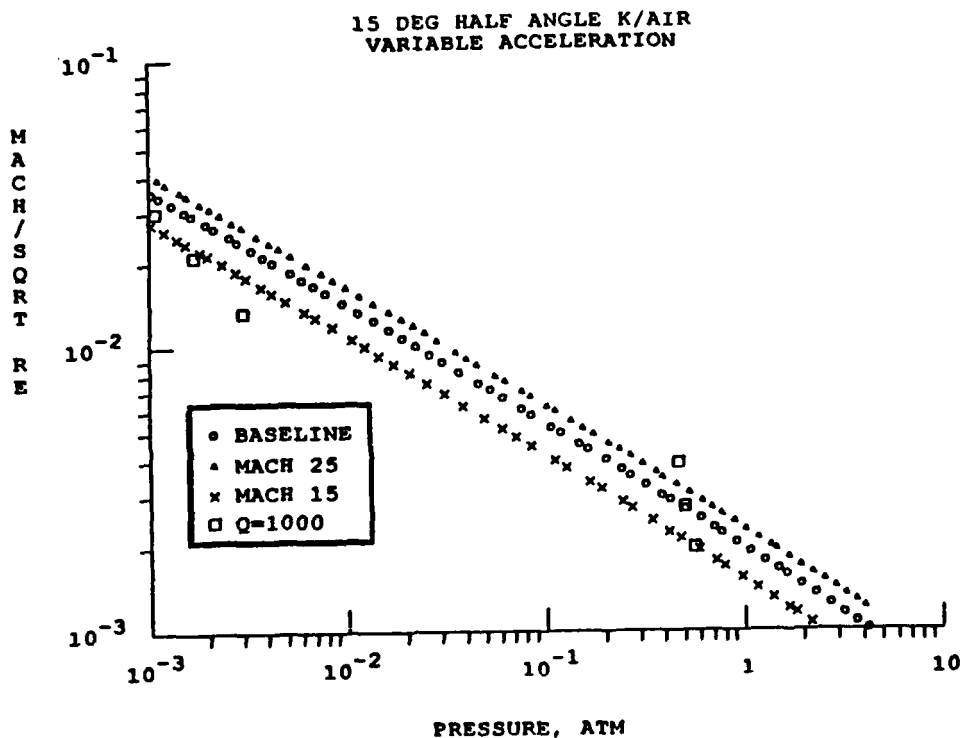
Figure 41. Base cases, finite rate expansions, $M/\sqrt{Re}$.

K/AIR BASELINE CASE
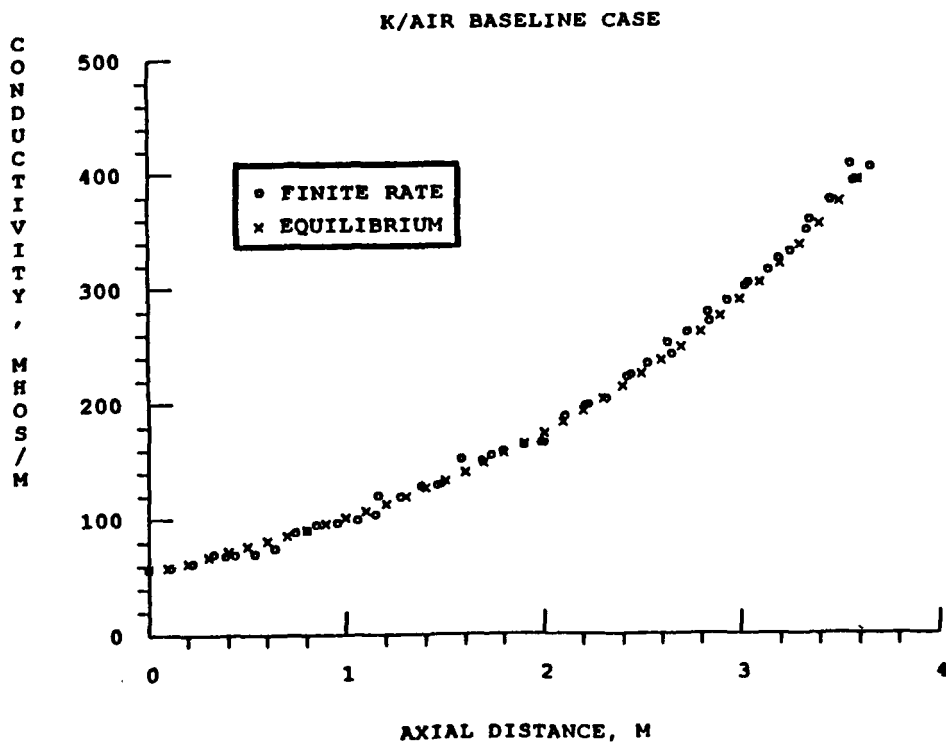
Figure 42. Baseline accelerator, finite rate and equilibrium.

Table 10. Accelerator Calculations - Exit Conditions

	Finite Rate	Equilibrium
P, atm	4.295E+00	4.190E+00
T, °K	4.082E+03	4.030E+03
s, kJ/(kg)	1.005E+01	1.002E+01
Ht, kJ/kg	2.249E+04	2.265E+04
V, m/sec	5.601E+03	5.652E+03
σ, mhos/m	4.044E+02	3.928E+02
mole fractions		
e	1.803E-03	1.752E-03
VO	5.533E-02	6.130E-02
O	1.973E-01	1.892E-01
O2	5.894E-02	6.086E-02

6.0 CRITICAL TECHNOLOGY ISSUES

This investigation has reconfirmed the potential capability of the MHD accelerator for hypersonic flow simulation which was recognized and first demonstrated in the 1960's. During the 25 years since the first experimental demonstrations of MHD-augmented flow facilities, there have been virtually no major research efforts directed at developing this unique technology for application to a large-scale facility. The renewed interest in hypersonic flight vehicle development has opened a window of opportunity to start a program to develop and exploit the MHD accelerator. There are a number of critical technology areas which must be addressed and resolved to assure the successful development of an MHD-augmented hypersonic simulation facility. A critical technology is defined as one that significantly influences the simulation capability or reduces development risk or cost. In the following sections each of the major components in the facility will be evaluated to determine critical technology issues.

6.1 HOT GAS GENERATOR

There are three candidate gas generators for providing the high-pressure, high-enthalpy flow to the accelerator channel. The two continuous flow heaters which offer the potential performance required are the electric arc and carbon combustor. The reflected shock tunnel has been demonstrated successfully as a driver for a short duration MHD-augmented flow facility. All three candidate gas generators will require a research and development program to obtain the levels of performance required for a full-scale facility; however, the current state of technology is adequate to use these heaters in a small-scale research facility.

The performance requirements for the gas generators can be summarized in terms of mass flow rate, run duration, total pressure, total enthalpy, and flow stability. Each of the candidate gas generators will have different critical technologies which will be addressed in the following sections. The one common technical issue is flow uniformity. Thermodynamic properties and species distribution must be as spatially and temporally uniform as possible to provide the accelerator with a uniform conductivity distribution. The gas generator and seeding system must be integrated to provide uniform seeding at the low seed concentrations required.

6.1.1 Electric Arc Heater

The requirement to limit the entropy gain in the flow during the heating and acceleration process to obtain the correct velocity and temperature simulation places a severe constraint on the heater. Obtaining high stagnation enthalpy at minimum entropy requires the heater to operate at very high pressures. Current arc heaters operate at 100 atm and 100 MW, with advanced arc heaters pushing for operation at 200 atm and up to 400 MW. Initial studies indicated that the best MHD accelerator performance would be obtained at maximum arc heater enthalpy and pressure; however, this is only true if the accelerator channel can be operated at corresponding high pressures (50 atm). When limits on electrode current density and wall heat-transfer rates in the accelerator are considered, the operating pressure in the accelerator may be limited to about 20 atm. Accelerator operating pressure limits will require experimental validation as theoretical prediction of wall heating rates in the presence of high electrode current has not been validated. Thus the requirement to operate the arc heater above 150 atm may be relaxed. The relatively large mass flow requirements (20 kg/sec minimum) for a full-scale facility (one propulsion unit) may be obtained from a single heater; however, larger flow rates may require multiple heaters connected to a single accelerator channel.

Arc heater technology issues include electrode erosion, arc stability, and maximum throat heat-transfer rate in addition to the increased performance requirements described above. Flow contamination from electrode and insulator erosion must be minimized along with NO and O production which is higher in arc heaters than combustion or shock heaters. The requirement to operate the arc heater at pressures of 150 to 200 atm is considered a critical technology issue when combined with the large size of the heater (mass flow and power). The trade studies indicated that the overall performance of an arc heater and MHD accelerator combination was relatively insensitive to the power split between the two components. Subject to the conductivity, pressure, and velocity requirements at the inlet of the accelerator, reduced arc heater performance was made up in the accelerator at the same efficiency. The arc heater operating requirements have been relaxed by this study; however, the large high-pressure heater is still a critical technology component.

6.1.2 Combustion Heaters

In this study the combustion heater was not considered in the trade studies for two reasons. First, the AEDC emphasis was directed toward MHD augmentation of a planned arc heater facility upgrade, and second the facility primary usage was identified as propulsion testing in which products of combustion were undesirable. A carbon-fueled oxygen-enhanced combustor will provide sufficient total enthalpy to drive an augmentor channel. Experience from the coal-fired MHD power generation has demonstrated required conductivity. Maximum operating pressure of the combustor will limit the simulation quality (entropy gain). Development of a high-pressure carbon combustor would be a critical technology task because of the problems of fuel injection, combustion stability, and combustor wall cooling. One advantage of a combustion heater would be in seed injection, which could be mixed into the fuel to provide uniform seeding. Although the combustion heater produces non-air species, it may be a very acceptable hot gas source for an MHD accelerator research facility. A combustion heater does not require a large power supply to operate, thus reducing facility cost compared to an electric heater.

6.1.3 Reflected Shock Tunnel

The technology is well developed for the reflected shock tunnel utilizing both free shock and free piston drivers. An analytic design study should be able to size and design a reflected shock driver for an augmentor channel. The only critical parameter would be run time due to nozzle/accelerator starting. The shock-driven facility has the advantage of "cleaner" air simulation due to the reduction of contaminants in the driver. A low-cost research facility could be developed around the shock-driven MHD augmented tunnel where transient power supplies could be used to power both the magnet and the channel. Thus the reflected shock heater is considered state of the art with no critical technology issues.

6.2 SEEDING SYSTEM

The MHD accelerator requires seeding with an easily ionized element or compound to obtain sufficient conductivity at the desired accelerator operating pressures and temperatures. Both elemental cesium and potassium were considered as seed materials. Because of lower cost and molecular weight considerations, potassium was selected as the seed material for the trade study calculations in this investigation. The technology issues for the seeding system would be identical regardless of the seed choice. Since seeding a combustor or a shock tunnel is considered a simple task, only the seeding system for the arc heater is addressed. The basic concept is to vaporize the elemental seed in an oven and mix with the high-temperature working gas as a vapor. This approach is best from a performance viewpoint; however, there is very little experience with this technique. Potassium requires a very high temperature to vaporize

at the operating pressures of the arc heater. Thus injection of elemental potassium into an arc heater stagnation region is considered a critical technology task.

The common mode of seeding is with a compound such as potassium carbonate ($K_2 CO_3$). When potassium carbonate encounters high temperatures it dissociates into elemental potassium, oxygen, and carbon dioxide. Potassium hydroxide (KOH) can be used, but the hydroxide radical has an affinity for electrons, producing a reduction in electrical conductivity. Similarly potassium chloride (KCl) suffers from the same disadvantage as potassium hydroxide, since the chlorine atom has a strong affinity for electrons. Thus seeding with compounds would be acceptable when the resulting additional species were acceptable in the flow. When the minimum seed contamination is required, elemental seeding must be used. The accelerator seeding trade studies indicated that concentrations of seed as low as 0.5 percent may be acceptable for some operating conditions. The uniformity of the seed distribution will be very important to accelerator operation.

The critical technology issues for seeding include elemental potassium vapor injection into the arc heater stagnation region, uniform seed distribution and seeding rate at the low seed concentrations, and influence of the seed material on the accelerator electrodes.

6.3 TRANSITION NOZZLES

The two transition nozzles in the MHD-augmented flow facility are very important to the performance and flow quality of the system. The first transition nozzle, which accelerates the heater flow to supersonic speed and transitions the flow cross section from round to rectangular, has the following design requirements: near-uniform flow properties with thin turbulent boundary layers and minimum flow energy loss. The second nozzle expands the accelerator exit flow to the required test conditions. Again flow quality and energy loss considerations are the primary requirements. The design of these transition nozzles should be within the current state of the art; however, the very high total enthalpies, pressure, nonequilibrium species distribution, and flow cross-section transition are beyond most 3-D gasdynamic code capabilities. In addition to flow uniformity and correct species distribution, the wall heat-transfer rates must be accurately predicted.

The primary critical technology issue for the nozzles is the development and validation of a 3-D aerothermodynamics code with complete gas chemistry and viscous/thermal boundary-layer effects. The finite rate gas chemistry will be important for the second nozzle, which establishes the test section conditions. A secondary technology issue is the application of advanced materials to the nozzle design. High-temperature radiation-cooled nozzles would have significantly less energy loss than the heat sink or actively cooled structures. The high-temperature materials issue extends to the accelerator channel as well and should be considered a generic technology area.

6.4 MHD CHANNEL

The accelerator channel surrounded by the primary magnet is the critical component in the MHD-augmented tunnel. Reference 5 by Whitehead contains a good description of the various MHD channel electrode design options. For this investigation the segmented Faraday accelerator was selected because the operating pressures and temperatures produce low Hall parameters. The channel performance requirements include efficient kinetic energy addition with minimum entropy increase, minimum insulator ablation, and minimum electrode erosion. Since this channel produces the flow field for a hypersonic wind tunnel, the uniformity of the exit flow properties is very important. Because of the length-to-diameter ratio of the channel, 20 to 40, the exit flow will contain significant boundary-layer flow effects. Thus the flow uniformity requirement is constrained by viscous boundary-layer profiles which develop in the accelerator. In this investigation the accelerator design trade studies were based on a one-dimensional MHD model which neglects all three-dimensional effects in the flow field. The first critical technology task is the development and application of a 3-D, viscous, MHD-coupled CFD code to the accelerator performance analysis to evaluate the significance of the three-dimensional effects. Each of the critical technology issues for the channel is presented and discussed in the following sections. The channel structural and electrical design are not listed as a critical technologies because the necessary design and analysis tools are available to address this difficult task.

6.4.1 3-D, Viscous, MHD Code Analysis and Modeling

The justification has already been presented for the importance of determining and understanding the three-dimensional electrical and fluid flow properties in the accelerator channel. Accurate heat-transfer rate prediction requires complete description of the viscous dissipation and electrical dissipation in the three-dimensional flow field. It must be recognized that this technology task is complicated by real gas effects which require an equilibrium gas chemistry code in the math model, and by turbulent viscous flow coupling with the magnetic field. Since experimental research facilities are very expensive it makes good sense to update analytic capabilities and complete the three-dimensional design analysis before designing a prototype facility. Some questions can not be answered by analysis alone; for example, the electrode current density limits can only be determined experimentally.

6.4.2 Electrode and Channel Current Density Limits

The relatively high-pressure channel designs resulting from the trade studies in this investigation produced very high electrode current densities (50 to 70 amps/cm²) when compared to MHD power generator technology. High electrode current densities are associated with electrode erosion and flow contamination. Small-scale research facility experiments will

be required to determine realistic current density limits for this application. In addition to the electrode limits there is a channel current density/voltage/conductivity combination which will produce channel arcing. Thus experiments are needed to determine lower limits on conductivity for specified current densities or cross channel voltage before diffuse current flow breaks down. Channel operating pressures will be limited by electrode current density and associated wall heat-transfer rates, and minimum conductivity will most likely be limited by channel arcing.

6.4.3 Finite Electrode 3-D Effects

The Faraday channel design should be the most electrically efficient design because axial current flow is expected to be small. This is only true for infinitely fine electrode segmentation due to induced axial currents in finite electrodes. The number of electrodes will be a significant factor in the cost of a Faraday channel design because each electrode pair requires a separate power supply. Detailed modeling of the electrodes is required to evaluate the localized three-dimensional effects on the electrodes. Sizing of electrodes and insulators will be determined by this analysis, which should aid in determining the minimum insulator thickness between electrodes.

6.4.4 Improved Wall Friction and Heat-Transfer Modeling

This critical technology area could be considered a subset of Section 6.4.1; however, the wall boundary layers in the MHD accelerator are sufficiently different from classic supersonic viscous flows. The very high total enthalpies, combined with a conducting fluid in a strong magnetic field, produce wall transport effects which are not well modeled by current CFD techniques. Basic fluid physics experiments will be required to develop turbulent viscosity models for MHD boundary layers. Laboratory MHD channel experiments may be required to validate wall heat-transfer rates in the presence of large electrical energy dissipation in the electrode sublayers. Accurate viscous and heat-transfer modeling are critical technology areas when the development costs of large-scale facilities depend on accurate estimates of these effects. Research on current density influence and magnetic field strength influence on wall transport properties must be done in small-scale facilities to minimize the technical risks in developing high-performance prototype facilities.

6.4.5 MHD Accelerator Channel Flow Quality

Flow quality (uniformity) is a very important characteristic of flow simulation facilities, and the MHD-augmented hypersonic facility must have good flow quality to be useful. Early experiments in small channels produced very nonuniform velocity profiles which may have resulted from the viscous effects in the small accelerators. It is very important that the 3-D

codes from Section 6.4.1 be used with all available experimental data to evaluate the potential flow quality of prototype and full-scale facilities. Flow quality is the bottom line critical technology issue which must be resolved before development of a large-scale MHD-augmented facility.

6.5 MAGNET

Magnetic field strength influences primarily the efficiency of the acceleration process. Lower magnetic field results in longer channel lengths, higher current densities, and larger entropy gain. Thus performance will require the maximum field strength technically available at an affordable cost. The magnet is a critical component of the facility, but there are no critical technologies limiting the availability of an acceptable magnet. The design choices range from 6-Tesla water-cooled magnets to 10-Tesla super-conducting, cryogenically cooled magnets. The two technical issues which must be considered critical in magnet design are cooling and structural integrity. Facility run time will strongly influence cooling design, and size and magnetic field strength will determine structural loads. Since each large magnet for MHD application has been a unique design, the magnet cannot be considered an off-the-shelf item. Design of a new high-technology magnet based on previously demonstrated technology must be considered high risk due to lack of industrial base and recent construction experience.

There is one approach to reducing the technical risk and cost of the magnet. A short duration facility may use a pulsed magnet driven by a stored power supply. The cooling requirements for a pulsed magnet are significantly reduced; however, the structural loading requirements remain critical. The trade study results of this investigation confirmed the influence of magnetic field strength on performance of the MHD accelerator. The 6-Tesla magnetic field is adequate for a propulsion facility; however, a hypersonic aerodynamic facility needs the maximum field available to improve free-stream simulation parameters. Thus the primary magnet will be a major cost item for the MHD accelerator, and cost and risk both increase rapidly with field strength and bore size. A detailed cost versus performance study will be required to select magnetic field strength for each accelerator design.

6.6 POWER SUPPLY AND CONTROLS

It is important to recognize that the channel power supply and associated controls are a significant design task and a major cost item. For direct-connect testing of a single hypersonic engine module at 50 lbm/sec the direct current power supply must operate at 1,000 to 5,000 v at currents to 5,000 amps each in multiple power supplies requiring a total power output of approximately 2,000 MW. The considerable effort being expended by the SDI program to develop high-density, high-power supplies and associated switches and controls should

assure an adequate technology base. Again the impulse facility, which can be powered by stored electrical energy supplies, will be much lower in cost. The gas generator power supply should also be considered when evaluating the total electrical load requirements for the MHD-augmented facility, as available electrical power may limit facility size. Voltage regulation and current switching are considered the critical technology issues for the channel power supply, and large facility design studies should address their design in detail.

7.0 CONCLUSIONS AND RECOMMENDATIONS

The critical technology issues identified during this investigation have already been presented in Section 6.0 and will not be repeated here. The results of this investigation support the potential for improved hypersonic flow simulation provided by MHD acceleration. The significant technical conclusions from the MHD accelerator design trade studies are presented in Section 7.1. Conclusions on flow simulation quality from the finite rate nozzle expansions are presented in Section 7.2. Brief recommendations and a summary of the technology road map and research plan conclude the investigation.

7.1 CHANNEL DESIGN TRADE STUDY CONCLUSIONS

The following conclusions are not ordered by importance, but presented in the same order as the Section 5.0 Design Studies and Analyses.

- A single-channel geometry and primary magnet may provide a large Mach number simulation capability (15-25) by varying only the applied electrode power and exit nozzle area ratio.

- Hot gas generator performance requirements result from accelerator inlet constraints on Mach number, static pressure, and conductivity. Study results concluded that acceptable arc-heater performance was in the range of 150 atm with total enthalpy of 5.5 to 6.0 MJ/kg.

- Magnetic field strength is important for acceleration efficiency and improves aerodynamic simulation capability at free-stream conditions. Direct-connect propulsion simulation requirements may be satisfied by a 6-Tesla field.

- Required seed density is determined by inlet conductivity limits and gas generator performance. Seed density of 0.5- to 1.0-percent potassium was found to be adequate for most accelerator calculations made during this study. Reduced hot gas generator performance would require increased seed density.

- Wall viscous losses are the dominant loss mechanism in the MHD accelerator, and accurate analysis of viscous effects requires three-dimensional flow modeling and MHD wall boundary-layer research.

- For an MHD accelerator of fixed mass flow and performance, inlet pressure controls channel cross-sectional area, electrode current density, and wall heating rates. The maximum operating pressure will be determined by either maximum current density or maximum wall heating rate.

- Given a fixed electrode current density, a reduction in operating pressure results in an increase in cross section area and a reduction in channel length.

- A reflected shock tunnel operating as a gas generator provides good MHD accelerator inlet conditions for a few milliseconds duration.

- Finite electrode effects did not significantly influence MHD accelerator performance; however, a large number of electrode pairs would be required for the baseline accelerator.

7.2 FLOW EXPANSION AND SIMULATION CONCLUSIONS

The following conclusions summarize the results of the finite rate expansions from the accelerator design trade studies. All expansions presented in Section 5.5 were calculated for an assumed 15-deg half-angle nozzle. Contoured nozzles of the same area ratios would yield slightly different finite rate effects;, however, the following conclusions would be valid. In Section 5.5 the data were presented as a function of static pressure instead of area or nozzle length. This method allows the simulation parameters to be evaluated over the complete simulation range from combustor inlet to free-stream pressures.

- Velocity was well simulated because total enthalpy was correctly simulated and the kinetic energy term dominates.

- Static temperature was properly simulated at combustor inlet pressures, but ranged 300 to 400°K too hot at free-stream conditions. Finite rate effects were significant in reducing temperature as equilibrium calculations increased temperature about 500°K over finite rate calculations.

- Mach number simulation was influenced by the higher static temperatures which produced 10-percent low values at the combustor inlet and 50- to 60-percent low values at free-stream pressures. In hypersonic flow, exact Mach number simulation is not required as long as the simulated Mach number is "high."

- Density followed the inverse of temperature with good simulation at combustor inlet conditions and low values at free stream.

- Reynold number simulation was again good at the combustor inlet but was only 20 percent of the desired free-stream value.

- The hypersonic similarity parameter Mach number squared divided by the square root of Reynolds number was very well duplicated over the expansion. Mach number divided by the square root of Reynolds number was well simulated at combustor inlet conditions and was higher than free-stream values by 50 percent.

- The finite rate expansion, species distributions show significant differences from the equilibrium distributions which indicates that frozen flow conditions are reached early in the expansion.

7.3 RECOMMENDATIONS

The MHD-augmented hypersonic simulation facility offers capabilities beyond all current facilities and is technically feasible. A recommended technology road map and research plan is presented in Appendix B. The following summary recommendations have been extracted from the plan:

- Three-dimensional MHD accelerator modeling is a very important task for evaluation and understanding of three-dimensional coupled fluid mechanics and electromagnetic effects.

- Sub-scale laboratory experiments are required to improve understanding of electrode current density limits, diffuse current flow limits, and viscous losses and wall heat transfer.

- The MHD accelerator channel structural design is sufficiently complex and unique to warrant a separate design study to include the use of new high-temperature materials.

- The channel electrode power supplies, control, and regulation can benefit from recent advances in power supply technology.

- Most Important! An experimental MHD accelerator facility should be developed to address the critical technology issues and support the technology development necessary to build a full-scale hypersonic simulation facility.

REFERENCES

1. *Magnetohydrodynamics Power Generation and Theory: a Bibliography.* U.S. Energy Research and Development Administration, Office of Public Affairs/Technical Information Center, TID-3356, November 1975.

2. "Assessment of MHD Application to Hypersonic Propulsion Testing Facilities." AEDC White Paper, April 1987.

3. Ring, L.E. "General Consideration of MHD Acceleration for Aerodynamic Testing." Paper presented at the AGARD Specialists' Meeting "Arc Heaters and MHD Accelerators for Aerodynamic Purposes." September 21-23, 1964, Rhode-Saint-Genese, Belgium.

4. Waltrup, P.J., Billig, F.S., and Stockbridge, R.D. "Engine Sizing and Integration Requirements for Hypersonic Airbreathing Missile Applications." AGARD Propulsion and Energetics Panel, 58th Symposium, Ramjets and Ramrockets for Military Applications, London, England, October 26-30, 1987.

5. Whitehead, G.L. "Analytical Studies of High-Pressure MHD Accelerators." AEDC-TR-81-18, September 1981.

6. Gordon, S., and McBride, B.J. "Computer Program for Calculation of Complex Chemical Equilibrium Compositions, Rocket Performance, Incident and Reflected Shocks, and Chapman-Jouguet Detonation." NASA SP-273, 1971.

7. Frost, L.S. "Conductivity of Seeded Atmospheric Pressure Plasma." *Journal of Applied Physics,* Vol. 32, No. 10, October 1961.

8. *Proceedings of the Chemical Equilibrium and Transport Properties Workshop.* U.S. Department of Energy, Germantown, MD, September 1979.

9. Svehla, R.A. and McBride, B.J. "Fortran IV Computer Program for Calculation of Thermodynamic and Transport Properties of Complex Chemical Systems." NASA Technical Note TN-7056, NASA Lewis Research Center, January 1973.

10. Mikatarian, R.R., Kau, C.J., and Pergament, H.S. "A Fast Computer Program for Nonequilibrium Rocket Plume Predictions." AeroChem TP-282, August 1972.

11. Rosa, R.J. *Magnetohydrodynamic Energy Conversion.* McGraw-Hill Book Company, New York, 1968.

12. Carter, A.F., et al. "Research on a Linear Direct-Current Plasma Accelerator." *AIAA Journal,* Vol. 3, No. 6, 1965.

13. Tempelmeyer, K.E., Rittenhouse, L.E., and Wilson, D.R. "Experiments on a Faraday-Type MHD Accelerator with Series-Connected Electrodes." *AIAA Journal,* Vol. 3, November 1965, p. 2160.

14. Mitchell, Jim. "Assessment of MHD Application of Hypersonic Propulsion Testing Facilities." Executive Summary, Technical Report, AEDC, April 1987.

15. Sukoriansky, S., and Branover, H. " Turbulence Peculiarities Caused by Interference of Magnetic Fields with the Energy Transfer Phenomena." *Turbulence in Magnetic Fields,* AIAA Progress in Astronautics and Aeronautics, Vol. 112, pp. 87-99, 1988.

16. Sood, H.S. and Jonsson, V.K. "Some Correlations for Resistances to Heat and Momentum Transfer in the Viscons Sublayer at Rough Walls." *Journal of Heat Transfer,* November 1969, pp. 488-494.

17. Stalker, R.J. "Hypervelocity Aerodynamics in Australia." *British Interplanetary Society Journal,* Vol. 41, December 1988, pp. 611-618.

18. Witalis, E.A. " Analysis of Linear MHD Power Generators." *Journal of Nuclear Energy,* Part C., pp. 455-473, Vol. 7, 1965.

APPENDIX A

MHD ACCELERATOR BIBLIOGRAPHY OF REFERENCES
NOT CITED IN REPORT

1. Spitzer, L., Jr., and Härm, R. "Transport Phenomena in a Completely Ionized Gas." Physical Review, Vol. 89, No. 5, March 1953, pp. 977-981.

2. Friel, P.J. "Electron Density and Electrical Conductivity of High Temperature Aid Seeded with Alkali and Alkaline Earth Metals." General Electric Document No. R595D459, December 1959.

3. Hogan, W.T., Mather, N.W., and Sutton, G.W, Eds. "Experiments with a Transient DC Crossed-Field Accelerator at High Power Levels." Engineering Aspects of Magnetohydrodynamics, Proceedings of the Third Symposium, Rochester University, 28-29, March 1962, MIT Cambridge.

4. Byron, S., Bortz, P.I., and Russell, G.R. "Electron-Ion Reaction Rate Theory. Determination of the Properties of Non-Equilibrium Plasmas in MHD Generators and Accelerators and in Shock Tubes (Theoretical Analysis)." Philco-Ford Corp., Newport Beach, CA, Aeronutronic Division, 1963, p. 33.

5. Hess, R.V., et al. "Study of Instabilities and Transition to Turbulence in a Linear Hall Accelerator." NASA, Langley Station, VA, Langley Research Center, 5th Symposium of the Engineering Aspects of Magnetohydrodynamics, Cambridge, MA, April 1964.

6. Dicks, J.B. "Design and Operation of Open Cycle Hall Current Neutralized MHD Accelerators and Generators with Diagonal Conducting Strip Walls." *Proceedings of the Fifth Symposium of the Engineering Aspects of Magnetohydrodynamics.* University of Tennessee Space Institute, Arnold AFB, TN, 5th Symposium on the Engineering Aspects of Magnetohydrodynamics, Cambridge, MA, 2 April 1964.

7. "Recent Results in Theoretical and Experimental Hypersonics and Theoretical Magnetohydrodynamics." Report No.: ARL-65-18, Cincinnati University, OH, August 1964, p. 59.

8. Head, R.M., Valensi, J., and Charvet, Y. "Fundamental Studies on Plasmas in a Magnetohydrodynamic (MHD) Shock Tube, Arc Heaters and MHD Accelerators for Aerodynamic Purposes." Part I, AGARD Fluid Dynamics Institute Specialists Meeting, Rhode-Saint-Genese, Belgium, 21 September 1964.

9. Dicks, John B. "Improvements in Design of MHD Accelerator Channels for Aerodynamic Purposes." University of Tennessee Space Institute and ARO, Inc., AGARD Specialists' Meeting on Arc Heaters and MHD Accelerators for Aerodynamic Purposes. Rhodes-Saint-Genese, Belgium, September 21-23, 1964.

10. Ring, L.E. "Optimization of MHD Crossed-Field Accelerators and Generators." Arnold Engineering Development Center, Arnold Air Force Station, TN, January 1965, p. 54.

11. "Recent Results in Theoretical and Experimental Hypersonics and Theoretical Magnetohydrodynamics, Final Summary Report for 1 July 1961 - 30 June 1964." AD-615933, Cincinnati University, OH, January 1965, p. 69.

12. Powers, W.L., ARO Inc., Dicks, J.B., and Snyder, W.T., UTSI. "A Generalized Graphical Presentation of MHD Generator and Accelerator Performance Characteristics." Sixth Symposium on Engineering Aspects of Magnetohydrodynamics, Research Report for AF 40(600)-1000, April 1965, pp. 115-117.

13. Grabowsky, W.R., et al. "MHD Wind Tunnel Program," Semiannual Technical Report, 1 January - 30 June 1964. TDR-469-5240-10-2, AD-462151, Aerospace Corp., El Segundo, CA, April 1965, p. 53.

14. Tempelmeyer, K.E., Rittenhouse, L.E., and Wilson, D.R., ARO Inc. "Experiments on a Faraday-Type MHD Accelerator with Series-Connected Electrodes." *AIAA Journal*, Vol. 3, No. 11, September 1965, pp. 2160-2162.

15. Norman, W. "One-Dimensional Magnetohydrodynamic Equations for a Non-Ideal Gas with Application to Single Ionized Argon." AEDC-TR-65-185 (AD470771), September 1965.

16. Harris, C.J., et al. "High Density Shock Tunnel Augmented by a Faraday MHD Accelerator." Technical Information Series. General Electric Co., Philadelphia, PA, Missile and Space Division, December 1965, p. 51.

17. Carter, A.F., et al., "Operating Characteristics, Velocity, and Pitot Distribution, and Material Evaluation Test in the Langley One-Inch-Square Plasma Accelerator." AIAA Plasmadynamics Conference, Monterey, CA, March 2-4, 1966.

18. Tempelmeyer, K.E. "End Effects in a Steady-State Magnetohydrodynamic J X B Accelerator." *AIAA Journal*, Vol. 4, April 1966, p. 723.

19. Dicks, J.B., et al. "An Experimental and Theoretical Comparison of the Performance of Diagonal Wall Generators, Faraday Generators and Hall Current Generators." AF 33(615)-2691, Electricity from MHD, Vol. III, Salzburg, pp. 677-686, July 4-8, 1966.

20. Harris, C.J., Marston, C.H., and Warren, W.R. "MHD Generator and Accelerator Experiments in Seeded and Unseeded Air Flows." Technical Information Series, General Electric Co., Philadelphia, PA, Missile and Space Division, September 1966, p. 29.

21. Demetriades, S.T., and Argyropoulos, G.S. "Ohm's Law in Multicomponent Nonisothermal Plasmas with Temperature and Pressure Gradients." *The Physics of Fluids*, Vol. 9, November 1966, pp. 2136-2149.

22. Powers, W.L., Dicks, J.B., and Snyder, W.T. "A Graphical Presentation of Magnetogasdynamic Accelerator and Generator Performance Characteristics." AF 33 (615)-2691, *AIAA Journal*, Vol. 5, No. 12, December 1967, pp. 2232-2236.

23. Leonard, R.L. and Rose, P.H. "Feasibility of a High-Performance Aerodynamic Test Facility." *AIAA Journal*, Vol. 6, No. 3, March 1968, pp. 448-457.

24. Wu, Y.C.L., et al., "MHD Generator in Two-Terminal Operation." *AIAA Journal*, Vol. 6, No. 9, September 1968, pp. 1651-1657.

25. Denzel, D.L., et al., "Experimental Study of Diagonal Conducting Wall Generators Using Solid Propellants." *Proceedings of the IEEE*, Vol. 56, No. 9, September 1968, pp. 1574-1578.

26. Grabowsky, W.R., Darron, D.A., and Mirels, H. "Performance of a 500-K Joule MHD Wind Tunnel." *AIAA Journal*, Vol. 7, No. 10, October 1969, pp. 1846-1852.

27. Teno, J., Brogan, T.R., and Petty, S.W. "Research Studies and the Development of MHD Generators and Accelerators." AEDC-TR-70-14, January 1970, p. 287.

28. Dicks, J.B., et al., "Fluctuations in Series Connected Open Cycle MHD Generators." *Proceedings of the Fifth International Conference on MHD Electrical Power Generation.*, Munich, W. Germany, April 19-23, 1971.

29. Muehlhauser, J.W. and Dicks, J.B. "Arc Spots and Voltage Losses in a Hall Generator." *Proceedings of the 14th Symposium on Engineering Aspects of MHD*, UTSI, April 8-10, 1974.

30. Volkov, Yu. M., Keilin, V.E., and Klimenko, E. Yu. "Superconducting Magnets for an Experimental MHD Generator Foundations of Superconducting Magnetic System Design. Superconducting Systems for Accelerators." Vol. 2, Conference on Technical Applications of Superconductivity, Alushta, USSR, September 1975.

31. Williams, John. "A 7T Superconducting Magnet for MHD Studies at Stanford University." Final Design Report, Francis Bitter National Magnet Lab, November 1977.

32. Williams, John E.C. "Superconducting MHD Magnet Development Program." Annual Progress Report No. 1, Francis Bitter National Magnet Lab, December 1977.

33. Alferov, F.I., et al., "Investigation of an Aerodynamic Device with Magnetogasdynamic Acceleration of the Gas Flow." *Teplofizika Vysokikh Temperature*, Vol. 17, No. 1, January - February 1979, pp. 163-172.

34. "Final Design of a Superconducting MHD Magnet." ANL-MHD-79-6, Argonne National Laboratory, pp. 1-11, March 6, 1979.

35. Marston, P.G., et al., "Superconducting MHD Magnets: Technology Development, Procurement and Path to Commercial Scale." 18th Symposium Engineering Aspects of MHD, June 1979.

36. Zar, J.L. "A Modular Design for a Superconducting Magnet for the ETF and Larger MHD Generators." 18th Symposium Engineering Aspects of MHD, June 1979.

37. Wang, S.T., et al., at Argonne National Lab, Young, W., Stoy, S., and Vanderarend, P.C. "A Superconducting Dipole Magnet for the CFFF MHD Facility at The University of Tennessee Space Institute." 18th Symposium Engineering Aspects of MHD, June 1979.

38. Unkel, W. "Approximate Three-Dimensional Solution for Finitely Segmented Frame Type MHD Channels." 18th Symposium Engineering Aspects of MHD, June 1979.

39. Alferov, V.I., et al., "Investigation of the Electrodynamic Characteristics of MHD Accelerators." *High Temp.* (USSR) (Engl. Transl.) (United States) Vol. 17:2, September 1979, pp. 334-340.

40. Maus, J.R., et al. "Hypersonic Mach Number and Real Gas Effects on Space Shuttle Orbiter Aerodynamics." *Journal of Spacecraft and Rockets*, Vol. 21, No. 2, March-April 1984.

41. Hasel, Lowell E. "Ground Test Facilities for Aerodynamic Testing." NASA Langley Research Center, SCN 84-17-RLY, November 15, 1984.

42. Potter, J.L. "Transitional Hypervelocity Aerodynamic Simulation and Scaling in Light of Recent Flight Data." AIAA 20th Thermophysics Conference, Williamsburg, VA, June 19-21, 1985.

43. Verga, R. "Experiments to Develop Scaling Parameters for the Ultra-High Power Density MHD Generator." Executive Summary, Research Report, Power Technology Office, Strategic Defense Initiative Office, The University of Tennessee-Calspan Center for Aerospace Research, January 1986.

44. Tipton, R.E. "2D Lagrange MHD Code." Lawrence Livermore National Lab, CA, 4th International Conference on Megagauss Magnetic-Field Generation and Related Topics, Santa Fe, NM, 14 July 1986.

45. Dicks, John B. "The Use of MHD in Hypersonic Wind Tunnels." 22nd Intersociety Energy Conversion Engineering Conference, Philadelphia, PA, pp. 1429-1443, August 10-14, 1987.

46. Schmidt, H.J. "Pulsed MHD Generators." 22nd Intersociety Energy Conversion Engineering Conference, Philadelphia, PA, pp. 1473-1478, August 10-14, 1987.

47. Rosa, R., Farrar, L., and Trudnowski, E. "Electric Arc Behavior in a Boundary Layer," *AIAA Journal of Propulsion,* Vol. 4, No. 5, September-October, 1988.

48. Liu, B.L., et al., "Three Dimensional Analysis of the IEE Mark II MHD Generator." *Proceedings of the 9th International Conference on MHD Electrical Power Generation.* Vol. II; pp. 313-322, Japan, November 1986.

49. Lineberry, J., et al. *"Analysis of IEE Mark II MHD Generator Experiments,"* 26th AIAA Aerospace Sciences Meeting; Paper No. AIAA-88-0274, Reno, NV, January 1988.

50. Wu, Y.C.L. and Rajogopal, G. "Three Dimensional Current Distribution in Diagonal Conducting Wall Channels." 16th Symposium on the Engineering Aspects of MHD, Philadelphia, PA, May 1977.

APPENDIX B

TECHNOLOGY ROAD MAP AND RESEARCH PLAN

The approach to any environmental simulation facility technology plan depends upon the primary objectives of the resulting technology application. Thus this plan is based on the assumption that the USAF (AEDC or others) has an objective of developing a large MHD-augmented hypersonic facility as soon as technically feasible. The technology road map , as outlined in Fig. B-1, has a short 3-year technology development period before start of facility design for a prototype facility. The experimental prototype facility would have two primary functions: first, the continued development of accelerator technology, and second, the testing of hypersonic flight components as an operational facility. Each of the technical tasks in the following research plan will be presented in a statement of work format in the order they appear on the technology road map.

B.1 THREE-DIMENSIONAL MHD ACCELERATOR MODELING

Section 4.5 contains a strong justification for the 3-D modeling tasks, and Section 6.4 recognizes the accelerator modeling as a critical technology task. A mathematical model shall be developed for the MHD accelerator channel including transition nozzles. This model shall be theoretically based, satisfy the governing physical relations and conservation equations, and utilize empirical relations and validated empirical models only when essential. The resulting model or series of models will have the following capabilities.

B.1.1 Combined 3-D, Viscous, MHD Flow Effects

The primary CFD model will be a coupled compressible, viscous, MHD code with equilibrium gas chemistry. The finite electrode effects may be input from a separate code along with insulator and electrode wall sublayer effects. The model must be three-dimensional as symmetry is not expected in the resulting flow field.

B.1.2 Finite Electrode 3-D Electromagnetic Effects

Section 5.4 presented the discussion of the finite electrode effects for the Faraday channel, and Section 6.4.3 recognized the technical importance of electrode segmentation effects. A detailed 3-D model for evaluating finite electrode-coupled electromagnetic and fluid dynamic flow fields is required to address the design and analysis of the electrode/insulator pairs. Sublayer electrical conductivity and arcing should be evaluated for inclusion in this model.

TECHNOLOGY ROAD MAP AND RESEARCH PLAN

3-D MHD ACCELERATOR
MODELING AND ANALYSIS

START DATE

PHYSICS EXPERIMENTS
LABORATORY SCALE
MHD FACILITY

SIX MONTHS

TWELVE MONTHS

CHANNEL STRUCTURAL
DESIGN/ANALYSIS

TWENTY-FOUR MONTHS

POWER SUPPLY
CONTROL. REGULATION
DESIGN/ANALYSIS

THIRTY-SIX MONTHS

EXPERIMENTAL MHD
ACCELERATOR FACILITY
DESIGN AND FABRICATION

FORTY-EIGHT MONTHS

MHD ACCELERATOR RESEARCH PROGRAM
TECHNOLOGY REFINEMENT
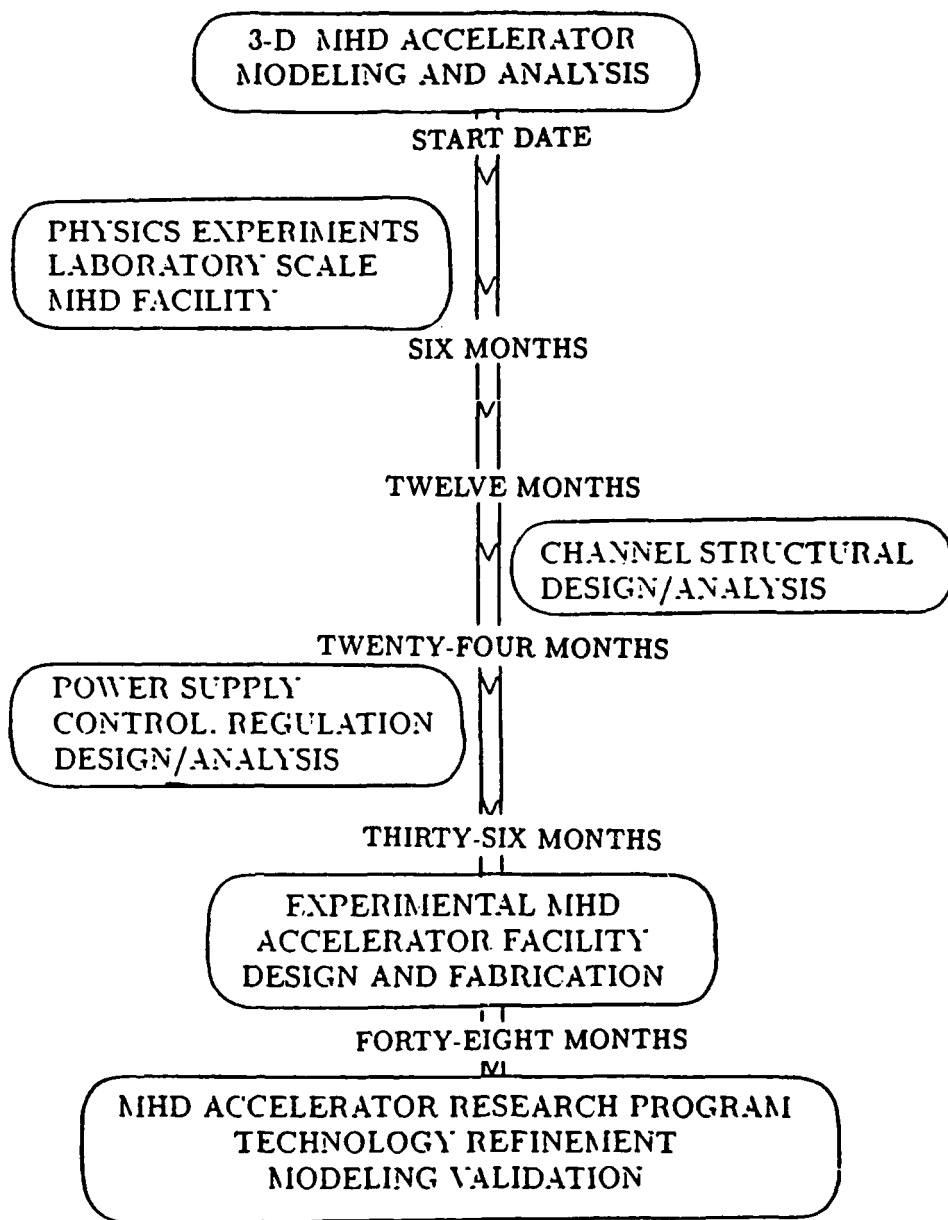MODELING VALIDATION

Figure B-1. Technology road map and research plan.

B.1.3 Insulator and Electrode Wall Turbulence

High Mach number turbulent boundary layers have been characterized for flows over simple shapes; however, the turbulent MHD boundary layer is not well defined or modeled. In this task the influence of strong magnetic fields on turbulence in a conducting fluid shall be analyzed, previous work reviewed, and improved models recommended.

B.1.4 Real Gas and Finite Rate Chemistry

It is not economical to include finite rate gas chemistry in the models described above; however, the capability must exist to evaluate finite rate effects when required. A finite rate gas chemistry model shall be selected and modified if necessary to support the MHD accelerator and nozzle flow codes described above. Validation of the finite rate results should be one of the tasks to be conducted in the laboratory-scale MHD facility.

B.2 PHYSICS EXPERIMENTS, LABORATORY FACILITY

The second program of the technology road map supports the modeling effort through laboratory-scale MHD accelerator experiments. These experiments will address the critical technology issues which require additional experimental data to formulate or validate models. The size of the laboratory facility will be constrained by available funds; however, it must be recognized that this is a significant research effort. Diagnostic instrumentation and power supplies are major cost items along with the gas generator and magnet. A majority of the research issues could be addressed in an impulse facility which would be much less expensive than a continuous flow facility. The following tasks represent typical research topics for the facility, but should not be considered all-inclusive. Appendix C contains a description of a proposed UTSI research facility and a plan for its utilization.

B.2.1 Electrode Current Density Limits

The facility must be capable of simulating the operational conditions of an MHD accelerator design of interest. For example, the operating pressure and conductivity are very important when investigating electrode current density limits. Measurements of electrode erosion and flow contamination shall be obtained for correlation with current density. Finite electrode experiments shall be conducted to support the work in tasks B.1.2 and B.1.3.

B.2.2 Gas Conductivity and Diffuse Current Flow Limits

The limits of diffuse current flow must be determined experimentally since they will establish the acceptable starting conditions for the accelerator. It has been well determined

that current arcing occurs in the sublayer near the electrodes due to low gas conductivity in the cool boundary layer. At specific conditions of bulk conductivity and electrode potential the accelerator can arc across the channel. This breakdown of diffuse current flow represents a limit to acceptable operation which must be established experimentally.

B.2.3 Viscous Losses and Heat Transfer

The turbulent viscous losses represent the largest loss effect in the accelerator based on current estimates for wall friction factors. The actual wall shear stress must be measured on both insulator and electrode walls through velocity profile surveys and heat-transfer correlations. Experimental determination of wall heat-transfer rates is important for establishing design requirements. Correlation of wall transport properties with tunnel operating conditions is a critical task for the research facility.

B.3 CHANNEL STRUCTURAL DESIGN AND ANALYSIS

The third program element on the technology road map addresses the design and analysis of the accelerator channel structure. Although the channel structural design was not considered a critical technology issue, it is a significant engineering challenge requiring detailed analysis. The following tasks should be completed before the experimental facility design is started to assure the structural analysis tools are available.

B.3.1 Electrical Loads and Pressure Loads

Theoretical electrical loads on the electrodes and conducting cables in the presence of the strong magnetic field must be calculated and added to the pressure loads. Because of the segmented design of the channel, all joints must be sealed to prevent hot gas leaks; thus, additional loads will be imposed by the restraining structure. In addition to the electromagnetic-induced loads in the accelerator channel, the magnet will induce high loads on the magnet containment structure. A highly integrated design may have redundant load paths requiring extensive stress analysis.

B.3.2 Thermal Loads and Cooling Requirements

The steady-state operational time will be limited in most designs by cooling limits. The accurate prediction of channel and nozzle thermal loads is just as important as prediction of the structural loads. Short duration facilities will be designed for heat sink operation where transient thermal analysis is required. Longer duration facilities will require active cooling of electrodes and possibly insulator walls. The structural complexity of an actively cooled structure greatly complicates the loading analysis. The thermal modeling codes from this

section will be combined with the electrical and pressure loading from Section B.3.1 to obtain a complete steady-state loads analysis.

B.3.3 Transient Loading and Thermal Shock

The starting and shut-down transients will produce large pressure loadings and high thermal shock. The segmented channel design provides many opportunities for thermal stress concentrations and thermal shock. The candidate channel design will be analyzed for transient mechanical, electrical, and thermal loads.

B.3.4 High-Temperature Electrodes and Coatings

The majority of MHD channels tested have used copper electrodes because of the high electrical and thermal conductivity of copper. Copper has a relatively low melting temperature and can be liquefied and vaporized at high current densities. Alternate electrode materials will be investigated in this task with the goal of retaining good electrical properties while improving erosion resistance. Thin coatings of high-temperature conductors over a copper base will be evaluated for application to accelerator electrodes.

B.3.5 Advanced Ceramic Insulators

Ablating insulators have been used in most accelerator experiments. Both flow quality and wall smoothness are reduced with insulator ablation. Recent advances in ceramic technology should be evaluated for application to the accelerator design. Ceramic nozzles with radiation cooling should be evaluated for improved efficiency in the transition nozzles.

B.4 POWER SUPPLY CONTROL AND REGULATION DESIGN

Two years into the technology road map, a project should be initiated to conduct design and analysis studies on the power supply system. The critical component of the power supply system is the regulation and control design. Switching and regulation of high currents is a difficult technical task, and the design solutions could be costly. The following two tasks are proposed to reduce the cost and technical risk in the accelerator power supply.

B.4.1 Survey Advanced Power Supply Technology

High density power supplies for short high-power application have advanced significantly under the SDI program, and the power supply options for the MHD accelerator have increased correspondingly. A complete relook at available power supplies for the accelerator is required with emphasis on reliability and cost. Capacitor banks, homopolar generators, and compulsators should be evaluated along with solid-state converters.

B.4.2 Design Study of Control and Regulation Systems

For each of the power supplies evaluated in Section 7.4.1, a control system concept should be developed. The total cost of the power supply must include the control system. The regulation, switching, and control design should be completed to the detail necessary to estimate the relative costs of the systems. The control system must contain safety and fault logic to protect critical components in the event of most likely failures.

B.5 EXPERIMENTAL FACILITIES FOR RESEARCH AND TECHNOLOGY DEVELOPMENT

All of the above technology road map programs are focused to support the design and development of an experimental MHD accelerator facility. This facility design could start as early as year three in the plan and would be a prototype size facility. One or more facilities could be developed around the three gas generator concepts: arc heater, combustion heater, and reflected shock driver. The purpose of the facility would be two-fold with the primary purpose being technology development and modeling validation for future facility programs. The secondary function would be development testing of hypersonic vehicle components. The following section will present a description of a typical MHD accelerator facility.

B.5.1 Description of a Typical MHD Accelerator for Hypersonic Flow Simulation

Artist concepts of the operational Hypersonic Flow Simulation Facility utilizing an MHD accelerator are shown in Figs. B-2 for free stream simulation and B-3 for direct-connect combustion testing.

In both cases an arc heater supplies heated air at 200 atm and 4,640 K. For the base case considered, the mass flow rate is 22.1 kg/sec. Thus, the arc heater must transfer 145 MW to the air.

The seed injection system is intended to model the initial NASA Langley seed injection system. The potassium seed reservoir is placed under pressure and the injection pipe heated to a high enough temperature ($>1,033$ K) to vaporize the seed prior to injection into the stilling chamber. However, it is likely that a much more workable system would result if the potassium is injected in the arc heater itself. This was the conclusion from the NASA Langley experiments. It was also found that injection rates corresponding to 2 mole percent cesium resulted in greatly reduced arc heater voltage and thus energy input to the air. When the seed flow rate was reduced to 0.3 mole percent, however, the arc heater operation was "satisfactory" (actual voltages and currents not given).

The present concept utilizes a square accelerator so the round-to-square transition is made in the stilling chamber.

The stilling chamber is followed by a contoured converging-diverging nozzle to a Mach number of 2.16, where the flow enters the accelerator. The nozzle needs to be designed for minimum length to minimize heat and friction losses, but contoured to assure desired flow quality.

The accelerator is currently envisioned as a square duct, but circular and other rectangular shapes may be desirable after additional research. The construction is similar to a segmented Faraday MHD generator. The electrode walls consist of 127 sets of electrode and insulator, 2.5 cm of electrode segmented by 0.3-cm insulators. Current MHD generator technology would suggest highly-cooled copper electrodes with Boron Nitride insulators. Other materials need to be investigated for the accelerator application, particularly with regard to accommodating the high heat fluxes, at least an order of magnitude higher and a comparable generator. The insulating walls are made of refractory with as many cooled pegs as feasible provided to cool the walls. The entire device is inside the warm bore of a superconducting magnet that produces an 8-Tesla magnetic field, uniform except tapered in the end regions. The warm bore is sized to house the accelerator channel, electrical leads, and cooling fluid piping. For the base case, the required diameter is estimated at 35 cm. (Note that the warm bore volume of the required magnet is less that 14 percent the size of the 6-Tesla magnet previously built by Argonne National Laboratories for UTSI under the DOE MHD Program.)

Although not shown in Figs. B-2 and B-3, the accelerator must have a separately isolated power supply for each of the 127 anode-cathode pairs. The total power required is 463 MW distributed as indicated in Section B.3.1.

The accelerated air is expanded by a second nozzle to free-stream test pressure as shown in Fig. B-2, or to the static pressure at the Cowl Lip Plane for direct-connect testing as shown schematically in Fig. B-3.
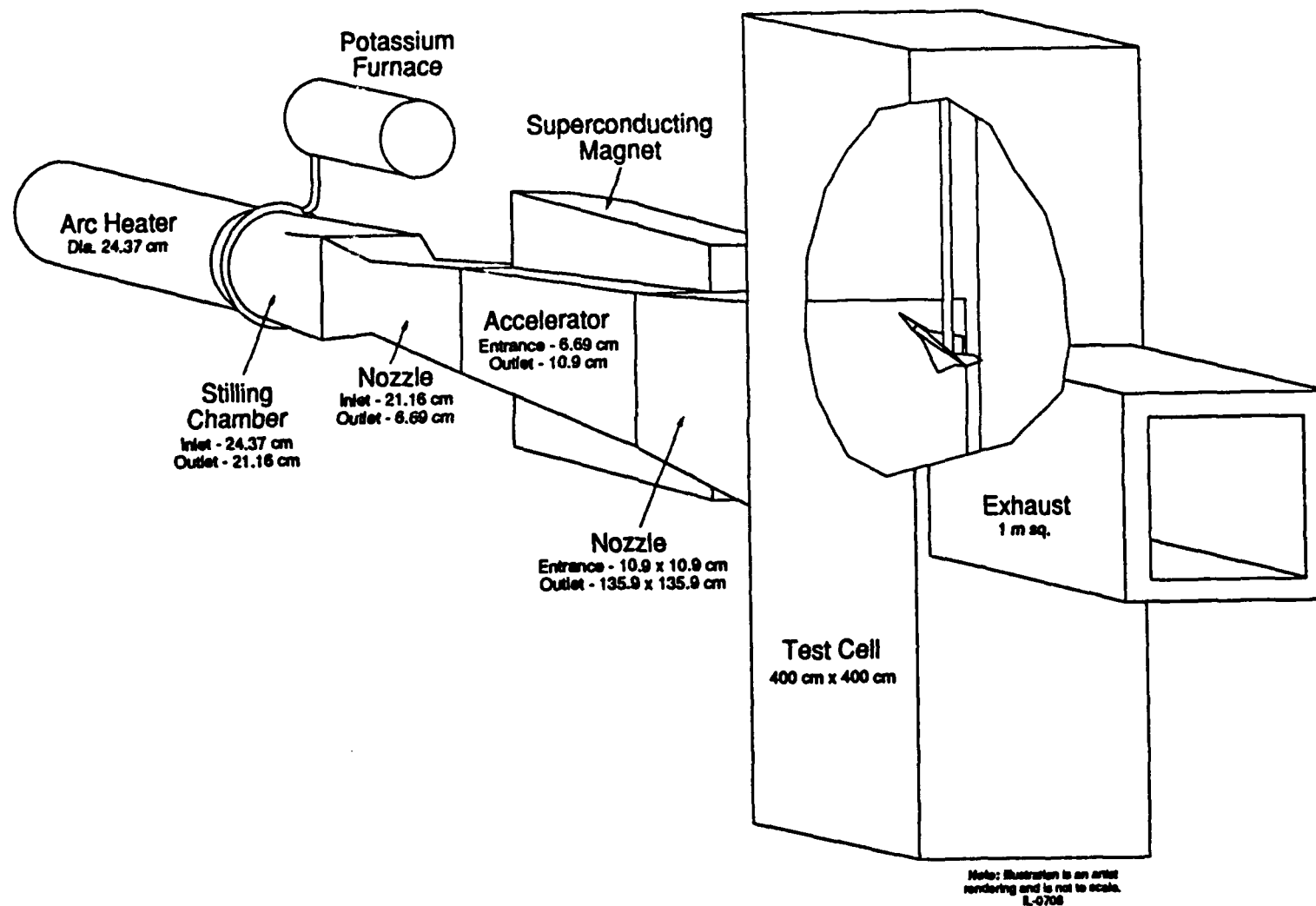
Figure B-2 Hypersonic flow simulation facility, free stream.

Potassium
Furnace

Superconducting
Magnet

Arc Heater
Dia. 24.37 cm

Stilling
Chamber
Inlet - 24.37 cm
Outlet - 21.16 cm

Nozzle
Inlet - 21.16 cm
Outlet - 6.69 cm

Accelerator
Entrance - 6.69 cm
Outlet - 10.9 cm

Nozzle
Entrance - 10.9 x 10.9 cm
Outlet - 135.9 x 135.9 cm

Exhaust
1 m sq.

Test Cell
400 cm x 400 cm

Note: Illustration is an artist
rendering and is not to scale.
IL-0708

Potassium Furnace

Arc Heater
Dia. 24.37 cm

Superconducting Magnet

Stilling Chamber
Inlet - 24.37 cm
Outlet - 21.16 cm

Nozzle
Inlet - 21.16 cm
Outlet - 6.69 cm

Accelerator
Entrance - 6.69 cm
Outlet - 10.9 cm

Scramjet Combustor Module

27.2 x 6.6 cm

Diffuser
27.2 x 6.6 cm
(Constant Area)

Exhaust System

Nozzle
Entrance - 10.9 x 10.9 cm
Outlet - 27.2 x 6.6 cm

Note: Illustration is an artist rendering and is not to scale.
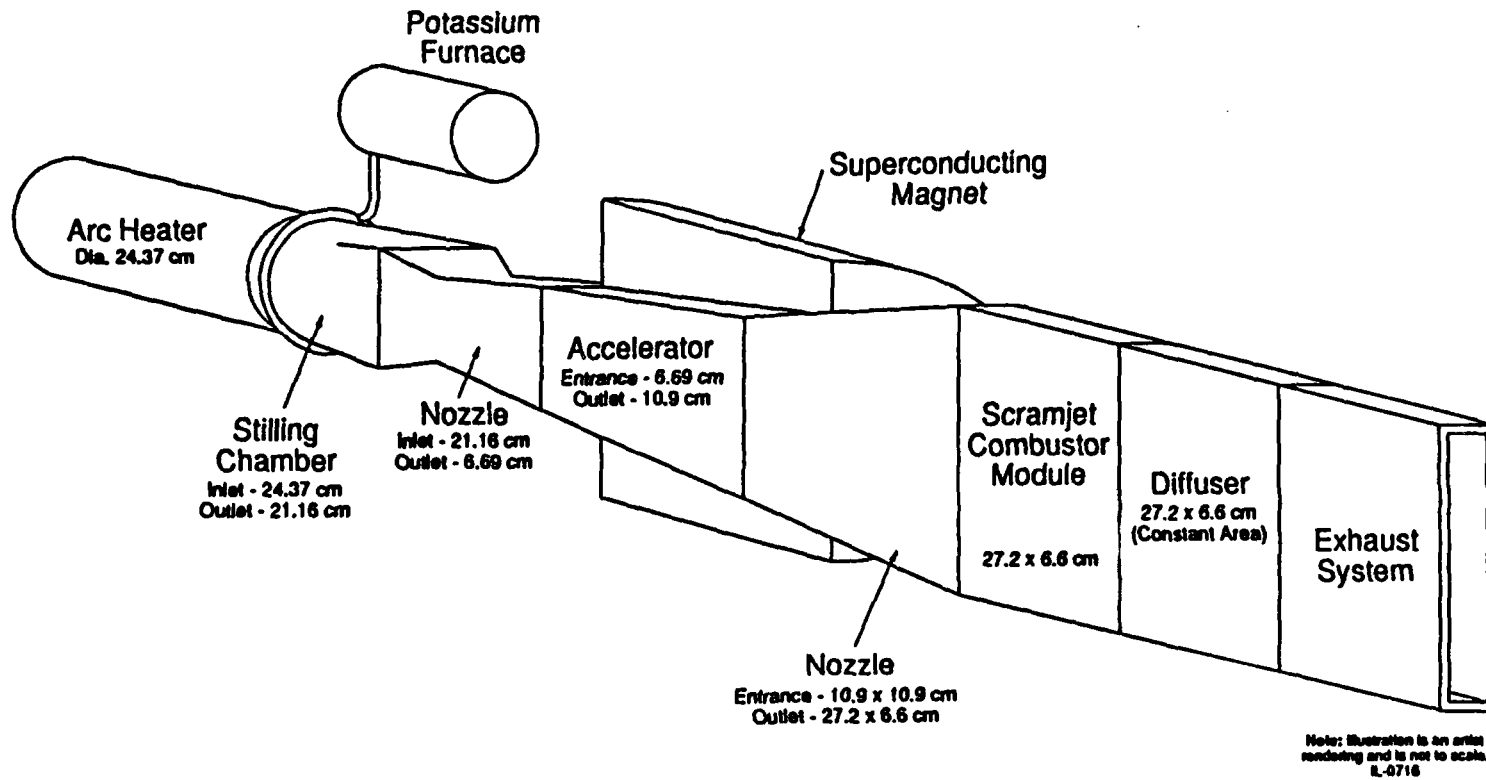IL-0716

Figure B-3. Hypersonic flow simulation facility, direct connect.

APPENDIX C

STEADY-STATE MHD ACCELERATOR RESEARCH FACILITY

C.1 RESEARCH FACILITY

It is proposed to establish a small-scale accelerator experimental facility in the UTSI laboratory area. The scale of the facility would be compatible with the small 6-Tesla magnet which was procured by AEDC for accelerator research in 1976 and donated to UTSI several years later. The major components of the experimental facility would be magnet, power supply for magnet and accelerator, hot gas generator and flow train, and instrumentation and controls. These major sub-systems are discussed below:

C.1.1 Magnet

The existing 6-Tesla magnet provides a warm bore 10 cm wide, 10 cm high (top can be open for electrical leads and cooling water pipes) and 20 cm long (field above 6 Tesla) or 31.5 cm long (field above 5.5 Tesla). It is designed to be pre-cooled with liquid nitrogen. After pre-cooling, a power supply of 10,000 amps at 300 v will provide magnetic fields in the warm bore in excess of 6 Tesla for 5 sec.

C.1.2 Power Supply

The most economical method of powering the above magnet and the accelerator with DC power is by providing some method of energy storage over a relatively long time for use in a short time. An array of 12-v automobile storage batteries seems to be the most economical approach, at least for the magnet power supply which must remain active for 10-15 sec. Based upon manufacturer's specifications for a 24GMF5 battery, 37 parallel strings of 33 batteries in series will provide the desired 300-v, 10,000-amp power supply. An additional 2,660 batteries will be required to power the proposed accelerator at a current density, 50 amps/cm². Additional capacity is needed to experiment with higher current density so additional batteries are needed, up to a total of 4,000 for both the magnet and the accelerator.

A separate building will be required for the batteries because of safety considerations. Shelves will be fabricated so they can be arranged efficiently. Copper bus bars will be installed for the magnet power. Individual accelerator electrode current requirements can be transported by moderate size wire. Power supplies are available that can be used to recharge the batteries as needed between runs.

C.1.3 Hot Gas Generator and Flow Train

There is insufficient power readily available on the UTSI campus to utilize an arc heater as a source of hot air for accelerator research. One could consider using motor generator power supplies for the arc heater as done tor the NASA Langley Accelerator research program. However, most of the needed experimentation can be performed with a combustion gas source. The combustion approach would be to burn in gaseous oxygen either pulverized carbon, solid carbon, or liquid cyanogen. Current plans are based on using pulverized carbon in a combustor similar to the DOE MHD combustor design. Use of liquid cyanogen would give comparable performance with somewhat better operational characteristics of liquid fuel. Use of a carbon fuel cast as a solid with the seed material as in the current UTSI SDI MHD combustor would be possible, but the binder material required for such a cast fuel would contain hydrogen, resulting in the reduction in electrical conductivity from the OH radical. Cyanogen presents a minor safety problem in that it is toxic. Preliminary assessments have been made with pulverized carbon fuel, but cyanogen will be investigated further.

The initial flow train would be a combustor operating at 10 atm (higher would be desirable), a nozzle that expands the gas to 1 atm, a Faraday accelerator consisting of 10 2-cm electrodes, and a diffuser to exhaust to atmospheric pressure.

Projected performance of the experimental accelerator at the base case current density (50 amp/cm^2) is shown in Table C.1.3. These calculations are based on the use of pulverized carbon burned with gaseous oxygen and 2-percent elemental potassium seed.

Table C.1.3. Experimental Accelerator Operating Regime

Property	Entrance	Outlet
Static Pressure	1 atm	0.54 atm
Total Pressure	10 atm	305 atm
Static Temperature	2,808 K	3,095 K
Velocity	1913 m/sec	3813 m/sec
Mach No.	2.16	4.01
Conductivity	53.5 s/m	163 s/m
Cross Sectional Area	25 cm^2	26 cm^2

C.1.4 Instrumentation and Controls

A computer control system will be implemented to control the entire test sequence with manual abort. Control must include regulation of the oxygen and carbon flows and the ignition sequence. Control of the electrical power to the magnet and accelerator will be by on-off switching for this facility. Limit checks will be utilized for safety on all necessary parameters.

Conventional instrumentation will be used to measure the following:

Oxygen and Fuel Flow Rates

Pressures (Combustor, Nozzle, Accelerator, and Diffuser)

Caloriometry on all Components for Heat Flux

Metal Temperatures in Selected Electrodes

All Currents and Voltages

Dynamic Pressure Distribution (via Traversing Pitot Tube to Map the Outlet Velocity)

Advanced diagnostics will include:

Optical Conductivity Measurement at Accelerator Entrance

Potassium Line Reversal Temperature Measurement

Temperature Profile Measurements Via Line Reversal to Include

Resolution Sufficient for Boundary-Layer Profile (If Possible)

Velocity Profile by Laser Doppler Velocimetry

Electrode Surface Temperature and Emissivity Measurements by Two-Color Pyrometry

C.2 RESEARCH PLAN

This section assumes the experimental facility is complete and a checkout test has been successfully completed in which the outlet velocities were mapped. It should be considered preliminary in the sense that additional analysis and planning may result in changes and will certainly identify additional experiments.

Current distribution on the electrodes and in the plasma between the electrodes is a critical issue. To address this issue, some (perhaps all) electrodes will be segmented into small sections in both the (z) and (y) directions. Each segment will have separate leads and connect to the power supply through a small resistor. The resistor must be small enough that the resulting voltage difference does not change the current distribution. Measurement of the voltage drops

across each of these resistors will enable determination of the current to that small segment. These voltage measurements need to be made at high speed to detect variations due to arcing. This will yield directly the current distribution on the electrodes from which some information about uniformity of the current flow in the plasma can be inferred.

The effects of high current density as a function of conductivity can be investigated with the same segmented electrode configuration. The conductivity can be varied by changing combustor temperature. This will be done by mixing nitrogen with the oxygen and keeping the total flow constant. Applied voltage will have to be increased for each reduction in conductivity. Arcing across the channel will be detectable on the segmented electrodes by a rapid increase in current. When this occurs, the power supply circuit will be opened to avoid damage to the accelerator.

Viscous wall losses have been identified as the most significant loss mechanism in the MHD accelerator. The first issue will be to perform experiments from which these losses can be determined for comparison and calculated results. This can be accomplished by measuring the velocity profile in two different regimes - in this case with the MHD acceleration and without it. Subsequently, experiments will be directed toward evaluation of different materials and methods of construction that are smoother and thus lead to less viscous loss.

Electrode segmentation results will be evaluated in all experiments. There are two adverse effects that may occur. Breakdown between electrodes will be apparent from the electrode voltages in all tests. If none occur, wider electrodes should be constructed to establish how high the gap voltage can be for these conditions. Circulating currents can be determined by careful analysis of the electrode current distribution data.

The issue of diffuse condition in the plasma at high pressure cannot be adequately addressed with the combustor gas source, because of pressure limitations. However, the shock tube gas source discussed briefly in Section 5.3 will provide the opportunity to operate the accelerator at higher pressures and repeat the current distribution experiments.

NOMENCLATURE

A   Duct cross-sectional area; reaction rate constant

a   Stoichiometric coefficient of species

B   Magnetic field flux density

b   Backward reaction rates

c   Species concentration

d   Channel width

D   Hydraulic diameter

E   Electric field; activation energy

f   Forward reaction rates

H   Total enthalpy

h   Static enthalpy

J   Current density

K   Channel loading, or degrees Kelvin

kg   Kilogram

kJ   Kilojoules

L   Length

M   Mach number

MJ   Megajoules

$\dot{m}$ Mass flow rate

P	Pressure
Q	Wall specific heat flux
q	Dynamic pressure
q_w	Wall heat transfer
R	Gas constant
R_e	Reynolds number
S	Magnetic force number
s	Entropy
T	Temperature
u	Velocity in x-direction
U	Velocity
V	Total velocity
V_d	Electrical boundary-layer voltage drop
x, y, z	Right-hand coordinates, x in flow direction
∇	Vector operator
γ	Ratio of specific heats
Δ	Electrical boundary-layer loss factor
ϱ	Density
σ	Conductivity
μ_0	Magnetic permeability
T	Stress tensor
τ_w	Wall shear stress
Ω	Hall parameter, $\omega\tau$